3D SEISMIC EVIDENCE FOR MULTIPLE MOVEMENT DIRECTIONS AND DETACHED EXTENSION DURING MESOZOIC RIFTING IN THE JEANNE D'ARC BASIN, OFFSHORE NEWFOUNDLAND, CANADA

by

NATALIE ELIZABETH STIER

A thesis submitted to the

Graduate School–New Brunswick

Rutgers, The State University of New Jersey

In partial fulfillment of the requirements

For the degree of

Master of Science

Graduate program in Geological Sciences

Written under the direction of

Dr. Martha Oliver Withjack

Dr. Roy W. Schlische

And approved by

____

____

____

New Brunswick, New Jersey

January 2016

ABSTRACT OF THE THESIS

3D SEISMIC EVIDENCE FOR MULTIPLE MOVEMENT DIRECTIONS AND DETACHED EXTENSION DURING MESOZOIC RIFTING IN THE JEANNE D'ARC BASIN, OFFSHORE NEWFOUNDLAND, CANADA

By NATALIE ELIZABETH STIER

Thesis Directors:

Dr. Martha O. Withjack and Dr. Roy W. Schlische

The Jeanne d'Arc rift basin formed during the breakup of Pangea from Late Triassic through Early Cretaceous time. My study focuses on the Flying Foam region, which lies east of the NNE-striking, ESE-dipping Mercury fault in the northwestern section of the basin. Multiple phases of deformation, along with the presence of evaporites within the latest Triassic to earliest Jurassic Argo Formation, make it difficult to constrain the timing of tectonic activity and the extension direction in the basin. Using 3D seismic data (donated by WesternGeco). I focused on constraining the slip on faults through time to better understand the evolution of the basin.

Previous 3D seismic studies have identified corrugations subparallel to the slip direction on the surface of a fault. I identified corrugations on the Mercury fault that indicate an ESE-movement direction during the first phase of rifting from the Late Triassic to the earliest Jurassic. During the second phase of rifting (earliest Jurassic – latest Jurassic), a relay ramp formed in the southern part of the study

area, between the basement-involved Mercury and Murre faults, resulting in a northeastward tilt of strata in the hanging wall of the Mercury fault. During the third phase of rifting (latest Jurassic – Early Cretaceous), evaporites within the Argo formation acted as a detachment fault zone. N-directed gravity sliding along the detachment fault zone tilt resulted in NE-oriented extension. Concurrently, the N-striking, basement-involved Flying Foam fault imparted a component of top-to-the east motion on the detachment fault zone. This resulted in geographic and temporal variation in the movement direction on the detachment fault zone from the latest Jurassic through the Early Cretaceous. As the Flying Foam fault propagated southward, the Flying Foam anticline formed above it. Breakup in the northern part of the Jeanne d'Arc basin occurred in the earliest Aptian. However basement-involved faulting with a dip-slip normal component continued through the Aptian, and offset of a late Albian unconformity indicates that NNE-directed detached faulting continued into the Albian.

ACKNOWLEDGMENTS

I would like to thank my advisors, Dr. Martha Withjack and Dr. Roy Schlische for their constant support and assistance during my time at Rutgers and their contribution to this work. Additionally, thank you to my committee member, Dr. Christopher Potter, for his continuous feedback and support throughout this process. I would also like to thank Iain Sinclair from Husky Energy for his input, and Kevin Lyons from Schlumberger for permission to publish seismic and well data. Thank you to WesternGeco, the Canada-Newfoundland Offshore Petroleum Board, and IHS Kingdom for providing the seismic data, well data, and SMT seismic interpretation software, respectively. Thank you to the Department of Earth and Planetary Sciences of Rutgers University and Husky Energy for providing financial support. Finally, thank you to my family, friends, and the faculty from the Earth and Planetary Sciences Department for providing support and encouragement over the past few years.

TABLE OF CONTENTS

LIST OF TABLES

LIST OF APPENDICES

LIST OF ILLUSTRATIONS

1. Introduction

The petroliferous Jeanne d'Arc rift basin is part of the passive margin of eastern North America (Figs. 1 and 2). The basin has a protracted geologic history, and controversy surrounds the number of rifting phases and their extension directions (*e.g.*, Hubbard *et al.*, 1985; Tankard and Welsink, 1987; Hubbard, 1988; Sinclair, 1988; Grant and McAlpine, 1990; McAlpine, 1990; Sinclair and Riley, 1995; Sinclair *et al.*, 1999; Welsink and Tankard, 2012; Withjack *et al.,* 2012; Serrano Suarez, 2013). Reactivation of preexisting zones of weakness during rifting in the Jeanne d'Arc basin (Enachescu, 1987; Tankard and Welsink, 1989; Withjack and Schlische, 2005) makes determining the slip on faults difficult. During fault reactivation, slip on the preexisting structure depends on the angle between the extension direction and the strike of the preexisting structure (*e.g.*, Ratcliffe and Burton, 1985; Henza *et al.,* 2010). Therefore, the strike of a fault is an unreliable indicator of the slip direction during reactivation. Unfortunately, more reliable slip indicators, such as slickenlines, are below seismic resolution.

The presence of the ductile, latest Triassic – earliest Jurassic Argo Formation (Fig. 3) adds another complication to the Jeanne d'Arc basin (Tankard and Welsink, 1987; Withjack and Callaway, 2000; Withjack and Schlische, 2005; Serrano Suarez, 2013). Ductile units decouple deep deformation from shallow deformation, possibly resulting in contrasting structural styles in overlying and underlying strata (*e.g.,* Withjack *et al*., 1990; Withjack and Callaway, 2000). Closely examining fault-surface topography, along with interpretation of growth packages and secondary structures, provides a way of determining the slip on faults in the Jeanne d'Arc basin while taking the effects of a ductile unit (*i.e.,* the Argo Formation) into consideration.

2. Background information

2.1 The eastern North American rift system

The eastern North American rift system extends from northern Florida to the Grand Banks of Canada, and formed in the Mesozoic during the break up of Pangea when eastern North America separated from northwestern Africa and Iberia (Fig. 1 inset) (*e.g.*, Louden, 2002; Seton *et al.*, 2012; Withjack *et al.*, 2012a). Rifting was underway along the entire rift system by the Late Triassic. Magnetic anomalies in oceanic crust and the age of preserved syn-rift strata indicate that the rift/drift transition was diachronous, beginning in the latest Triassic in the south and the Early Cretaceous in the north (Withjack *et al.*, 1998; Schlische *et al.*, 2002; Withjack and Schlische, 2005; Withjack *et al.*, 2012a). Withjack *et al*. (2005) divided the rift system into the southern, central, and northern geographic segments, based on the inferred timing of breakup (Fig. 1).

Previous studies divided rifting in the Jeanne d'Arc basin, part of the northern segment of the eastern North American rift system (Figs. 1 and 2), into multiple tectonic phases:

1) active rifting from the Late Triassic to the earliest Jurassic;

2) tectonic quiescence with thermal subsidence from the earliest Jurassic to the latest Jurassic;

3) active rifting from the latest Jurassic to the Early Cretaceous

(*e.g.*, Hubbard *et al.*, 1985; Tankard and Welsink, 1987; Hubbard, 1988; Sinclair, 1988; Grant and McAlpine, 1990; McAlpine, 1990; Sinclair and Riley, 1995; Sinclair *et al.*, 1999; Welsink and Tankard, 2012; Withjack *et al.,* 2012). However, Serrano Suarez (2013), using 3D seismic data from the Flying Foam region of the Jeanne d'Arc basin, concluded that rifting in the basin was continuous from the Late Triassic through the Early Cretaceous (Fig. 3). She identified growth beds within Upper Triassic through Lower Cretaceous strata indicating syn-rift deposition.

2.2 Flying Foam region of the Jeanne d'Arc Basin

The Flying Foam region is in the northwestern part of the Jeanne d'Arc basin (Fig. 2). Several basement-involved normal faults were active in the Flying Foam region during the breakup of Pangea from Late Triassic through Early Cretaceous time (*e.g.,* Enachescu, 1987; Driscoll *et al*, 1995; Serrano Suarez, 2013). The NNE-striking, ESE-dipping Mercury fault bounds the Flying Foam region in the west (Figs. 2, 4c, and 5). The N-striking, E-dipping Murre fault is only present in the southeastern part of the basin (Figs. 2 and 4c). Several other NNW-striking, ENE-dipping basement-involved faults are present between the Murre and Mercury faults in the southern part of the study area (Fig. 4c). Another NNE-striking, ESE-dipping, basement-involved fault, the Flying Foam fault, underlies the Flying Foam anticline (Fig. 5) (*see section 7.3 for further discussion*). Additionally, a set of approximately E-striking, N-dipping minor detached normal faults is present between the Mercury fault and the Flying Foam anticline (Fig. 4c).

The Flying Foam anticline developed above the sub-salt basement-involved Flying Foam fault (Fig. 5) (*see section 7.2 for further discussion*). It is both an extensional forced fold and an extensional fault-bend fold (Withjack and Callaway, 2000; Serrano Suarez, 2013). After running scaled experimental models with both sand and clay, Withjack and Callaway (2000) concluded that in the presence of a ductile layer, movement on a basement-involved fault will likely fold the cover layer, producing a forced fold (Fig. 6). The ductile unit decouples deep, faulted strata from shallow, folded strata as it does in the southern Rhine graben and the Suez rift (*e.g.*, Laubscher, 1982; Withjack *et al.,* 1990; Maurin, 1995). The fault-bend fold (*e.g.*, Xiao and Suppe, 1992; Schlische, 1995) formed because of movement of the lower Jurassic and younger cover strata above the non-planar detachment fault zone between the Mercury fault and Flying Foam fault concurrent with displacement on the Flying Foam fault. Withjack and Callaway (2000) and Serrano Suarez (2013) describe the development of the Flying Foam anticline in greater detail.

2.3 Strain state in the Jeanne d'Arc basin

Some studies suggest that the extension direction in the Jeanne d'Arc basin changed through time (Sinclair, 1995a,b; Sinclair *et al.,* 1999; Tankard and Welsink, 1987; Withjack and Schlische, 2005); these studies used the strike of basement-involved faults, the orientation of dykes and secondary faults, and growth patterns within syn-rift strata. However, this conclusion is suspect given the likely presence of preexisting zones of weakness and a ductile layer that likely decoupled the deep and shallow deformation.

Identifying the sense and direction of slip on faults would improve our understanding of the strain state, but determining slip on faults is especially difficult when using seismic data because slip indicators, such as slickenlines, are below seismic resolution. Previous studies have documented fault-surface undulations with axial traces parallel or sub-parallel to the slip direction on faults in natural exposures and experimental models (Fig. 7) (Marchal *et al.,* 1998 and 2003; Granger, 2006; Granger *et al.*, 2008; Fossen, 2010; Withjack *et al.,* in prep). In this thesis, I call undulations that parallel the slip direction fault-surface corrugations. Large-scale fault-surface corrugations likely result from linkage of originally isolated fault segments (Marchal *et al.,* 1998, 2003). If two faults with sub-parallel strikes are propagating radially, they can link up and create a larger undulating fault (Fig. 8) (Marchal *et al.,* 1998, 2003).

Granger (2006) conducted scaled experimental clay models with a known extension direction. She observed small faults linking together as the model progressed resulting in a larger, undulating fault surface. These undulations had axial traces sub-parallel to the slip direction, and to the extension direction. Therefore, by definition, these undulations were fault-surface corrugations (Fig 9). Withjack *et al.* (in prep) also observed the formation of fault surface-corrugations in scaled experimental clay models with two phases of non-coaxial extension. Small and large-scale corrugations trending parallel to the slip direction formed during the first phase of extension. During the second phase of extension small-scale corrugations were overprinted, but the large-scale corrugations, which formed during fault-linkage, were mostly preserved (Fig. 8).

I am not the first to use large-scale undulations to define slip direction. Lohr *et al.* (2008) inferred slip on a fault in the Northwest German Basin using large-scale undulations on the fault surface. Lohr *et al.* (2008) mapped the fault using 3D seismic data and then created a 3D rendering of the fault surface. They then inferred the slip direction using the principal orientation of the axial traces of the undulations by assuming that the undulations were actually corrugations. Although not every axial trace is continuous along the fault surface, they calculated a slip direction with an overall trend of 089° (Fig. 10).

2.4. Tectonostratigraphic packages defined by Serrano Suarez (2013)

Serrano Suarez (2013) studied the spatial and temporal evolution of the Flying Foam region using 3D seismic and well data. She divided the strata in the study area into tectonostratigraphic packages A-E based on previously defined phases of rifting (*e.g.*, Hubbard *et al.*, 1985; Tankard and Welsink, 1987; Hubbard, 1988; Sinclair, 1988; Grant and McAlpine, 1990; McAlpine, 1990; Sinclair and Riley, 1995; Sinclair *et al.*, 1999; Welsink and Tankard, 2012) (Fig. 3). Serrano Suarez (2013) then studied the characteristics of the reflections within each package and the 3D geometry of the packages. She concluded that rifting in the Jeanne d'Arc basin was not episodic as suggested in many previous studies. Instead, she determined that rifting was continuous from the Late Triassic through the Early Cretaceous, because she observed growth beds within the Upper Triassic through Lower Cretaceous strata. Following are interpretations of each package from Serrano Suarez (2013):

Package A – pre-rift basement rock

Package B – syn-rift strata deposited during the first phase of rifting from the Late Triassic to the earliest Jurassic

Package C – syn-rift strata deposited during the second phase of rifting from the earliest Jurassic to the latest Jurassic

Package D – syn-rift strata deposited during the third phase of rifting from the latest Jurassic through the Aptian

Package E – post-rift strata deposited from the Albian to the present

Additionally, Serrano Suarez (2013) concluded, because the top of package B behaved ductilely and decoupled the deep deformation from the shallow deformation, that both basement-involved and detached structures formed in the study area. My study uses the same 3D seismic survey studied by Serrano Suarez (2013) in the Flying Foam region of the Jeanne d'Arc basin. After my own detailed analysis of this data set, I concur with Serrano Suarez's major conclusions. However, I made several changes to her interpretations (*see section 3.2*) and divided package E into subpackages E1 and E2 (*see section 7.3*). Table 1 and Figure 3 give the formations included in each package.

3. Data and methodology

3.1 3D seismic data

The 3D seismic data from the Flying Foam region, interpreted in this study, consist of 1532 E-W inlines, 3150 N-S crosslines, and 2250 time slices acquired by WesternGeco in 1995. Table 2 lists the main seismic-acquisition parameters, and

Appendix 1 gives the seismic processing report (Schlumberger and Geco-Prakla, 1996). Inlines and crosslines are seismic profiles, or cross sections, from a 3D seismic volume. Inlines are parallel to the movement direction of the ship during data acquisition, and crosslines are perpendicular to the inlines. A time slice is a horizontal slice through the 3D seismic volume at a given two-way travel-time. The inlines and crosslines from the Flying Foam seismic survey are 39 km long with interpretable lengths of approximately 30 km and 36 km, respectively. Therefore, the interpretable area of the 3D survey is approximately 1080 km^2.

3.2 Seismic interpretation and methodology

The seismic interpretation and methodology included the following:

1) interpreting the surfaces that divide the study area into tectonostratigraphic packages A-E2 modified from Serrano Suarez (2013) (Table 1);

2) mapping the basement-involved faults and detached faults throughout the study area;

3) generating contour maps of two-way travel time to the Mercury fault surface and to the top of the detachment fault zone in in order to analyze the fault surfaces;

4) identifying growth packages to constrain timing of deformation.

Figure 4b gives the locations of the six fully interpreted seismic profiles presented in this study (Figs. 11-16). All seismic profiles are displayed at 1:1 using a velocity of 4.0 km/s. Velocity analyses from line HBV83-195, located near seismic line B, support this average velocity (Serrano Suarez, 2013) (Appendices 2 and 3).

Serrano Suarez (2013) constructed time-depth functions for the West Flying Foam I-13 and Flying Foam L-23 wells (Fig. 4b) to tie the well data to the seismic data in two-way time by using velocity data from line HBV83-195 (Appendices 2 and 3). I used formation tops from these wells to identify and trace the base Paleogene, late Albian, Aptian and Tithonian unconformities throughout the study area (Fig. 12b) (Appendix 4) (McAlpine,,1990; CNLOPB, 2012). No wells in the study area reached the basement or the Argo Formation. A high-amplitude reflection separates package B and package C in the northwestern part of the study area (Figs. 11-16). In other parts of the study area, the position of this horizon was less clear because of problems with data quality and the nature of seismic imaging of ductile units. Tying inlines, crosslines, and time slices and interpreting arbitrary lines (seismic profiles with orientations other than that of the inlines and crosslines) helped define surfaces in areas of uncertainty.

Interpreted faults include the Mercury fault, Murre fault, Flying Foam fault, and detached faults. Some faults produce high-amplitude fault-surface reflections on seismic profiles and time slices; other faults were interpreted based on offset strata. The Mercury fault is well imaged on inlines and time slices (Figs. 4 and 11-14). The Mercury fault has several per-leg multiples; therefore, I interpreted the first high-amplitude reflection encountered as the fault surface (Fig. 17). The Murre fault is well imaged on time slices (Fig. 4). Therefore, I loop tied the fault from time slices to seismic profiles, making sure not to mistake high-amplitude reflections from package B, which overlies the Murre fault, as the fault surface (Figs. 4 and 14). The Flying Foam fault is poorly imaged in the study area. Although the exact location of the fault is unknown, I interpreted the tip of the fault to lie approximately beneath the bisector of the two limbs of the Flying Foam anticline, and assumed a dip magnitude similar to other basement-involved faults in the study area. My interpretation of the Flying Foam fault is similar to that of Withjack and Callaway (2000), who interpreted the fault location using the results of experimental models involving basement-involved faulting beneath a ductile unit. Detached faults are well imaged in the study area (Figs. 4 and 15). The numerous detached faults made mapping individual faults throughout the study area difficult. I chose two particularly well-imaged detached faults, labeled 1 and 2, and mapped them throughout the study area (Figs. 4c and 15b).

Figure 18 compares the interpretation of line B from Serrano Suarez (2013) to line B from my study, at the same location in both studies. I divided package E into package E1 and E2. In my interpretation, the base-Paleogene is stratigraphically higher based on my interpretation of the base-Paleogene unconformity. Additionally, I interpreted a suprasalt, detached fault offsetting the Flying Foam anticline after observing offset strata in the crest of the anticline. I also placed the Flying Foam fault (called the Murre fault in Serrano Suarez (2013) and Withjack and Callaway (2000)) closer to the Mercury fault. My interpretation is similar to the interpretation of Withjack and Callaway (2000).

After interpreting the faults in the 3D seismic data, I generated structure-contour maps for the Mercury fault and the top of the detachment fault zone (top of package B), which allowed for detailed analysis of the fault surfaces (Figs. 19-22). Construction of these maps involved placing traces from seven time slices, from 2 s to 5 s in 0.5 s intervals of two-way travel time, on the same map. Filling in topographic lows and highs on the fault surfaces with blue and red, respectively, highlighted any undulations or irregularities. To decrease uncertainty in my structure-contour map of the top of the detachment fault zone, I did not include the part of the study area east of the Flying Foam fault, because of poor imaging of the top of the detachment fault zone in that part of the study area. Undulations on uncertain contours on the detachment fault zone (dotted black lines) are not highlighted with red or blue. In this study, I refer to any undulation, or irregularity on a fault surface, with potential kinematic significance as a corrugation.

While corrugations assist in constraining the slip direction on a fault (Marchal *et al.,* 1998 and 2003; Granger, 2006; Granger, 2008; Fossen, 2010), growth beds provide information on the timing of deformation. For example, reflections within hanging-wall strata deposited during faulting diverge toward the fault, whereas fold-related growth beds thin toward the crest of antiforms (*e.g.* Withjack *et al.,* 2002).

4. Mercury fault

All six tectonostratigraphic packages are present on the downthrown side of the Mercury fault, but only packages A and E are present on the footwall (Figs. 11-14). Because normal separation on the Mercury fault juxtaposed packages B through D in the hanging wall against package A (basement) in the footwall, it is a basement-involved fault. The Mercury fault has an irregular trace (Fig. 4c), but it generally strikes NNE and dips ESE. With the seismic section plotted at 1:1 assuming a velocity of 4 km/s, the Mercury fault dips about 25° at 6 s two-way travel time, and 50-60° at 2 s two-way travel time (Fig. 11-14). Using a higher or lower velocity would increase or decrease the dips, respectively. However, velocity analyses from line HBV83-195 support an average velocity of 4 km/s (Serrano Suarez, 2013) (Appendices 2 and 3). The dip of the deep segments of the Mercury fault are anomalously low for a normal fault (*e.g.,* Anderson, 1951). The Murre fault, present in the southern part of the Flying Foam region (Figs. 4c and 14), also has an anomalously low dip for a normal fault. Previous studies proposed that the Murre fault is a reactivated Paleozoic thrust fault to explain its low dip (Enachescu, 1987; Tankard and Welsink, 1989; Withjack and Schlische, 2005). This reasoning likely also explains the anomalously low dip of the Mercury fault.

The structure-contour map of the surface of the Mercury fault shows undulations on the fault surface (Figs. 19 and 20). The wavelengths of the undulations generally decrease up-dip and to the south. Similar to the fault surface interpreted by Lohr *et al.* (2008) (Fig. 10), not all undulations are continuous along the entire fault surface (Fig. 20b). Overall, continuous ESE-trending axial-traces connect the longer wavelength undulations (Fig. 20b). Although not quite as continuous, axial traces connecting the shorter wavelength undulations still trend ESE (Fig. 20b). With the exception of a topographic low and high on the northeastern part of the fault surface, the undulations are fairly low amplitude (Fig. 20).

5. Detachment fault zone

The evaporites within the Argo Formation, deposited during the first phase of rifting, acted as a detachment fault zone during the third phase of rifting (Serrano Suarez, 2013). The strike of the top of the detachment fault zone parallels the strike of the Mercury fault, NNE, in the northwestern part of the study area. The strike becomes NW to ESE in the south. Finally, it becomes parallel to the strike of the Flying Foam fault, NNE, in the northeastern part of the study area (Fig. 4c). The structure-contour map of the top of the detachment fault zone shows that these changes in strike occur farther north at deeper levels because the surface tilts toward the NE (Figs. 21 and 22). The shaded structure-contour map illustrates the trough-shaped surface of the detachment fault zone resulting from this NE tilt and the changes in strike (Fig. 23). Short-wavelength, low-amplitude undulations are present on the surface of the detachment fault zone (Fig. 22a). In the southern part of the study area, fairly continuous NE-trending axial surfaces connect the undulations (Fig. 22b). Sharp irregularities on the surface of the detachment fault zone in the northeastern part of the study area are associated with detached faults (Fig. 22b).

Stratigraphic patterns within package D, in the hanging wall of the detachment fault zone, vary from north to south (Figs. 11-13 and 24). On line A, the reflections within package D diverge toward the detachment fault zone below the late Albian unconformity and above the Tithonian unconformity and converge toward the crest of the Flying Foam anticline (Figs. 11 and 24). On line B, reflections between the Aptian and late Albian unconformities diverge toward the detachment fault zone and converge toward the Flying Foam anticline (Figs. 12 and 24), whereas reflections below the Aptian unconformity are sub-parallel (Figs. 12 and 24). On line C, reflections within the strata below the Aptian unconformity diverge toward the Flying Foam anticline (Figs 13 and 24). Some shallow reflections toward the top of the strata between the Aptian and late Albian unconformities likely diverge toward the detachment fault zone, but are obscured by peg-leg multiples from the base Paleocene unconformity (Figs. 13 and 24).

On line E, reflections within package D terminate against the top of the detachment fault zone in the southern part of the study area (Fig. 15). Termination of reflections is either due to onlap or faulting. In this case, onlap implies unrealistically deep water (almost 4 km assuming a velocity of 4 km/s) for the deposition of the lithologies that compose package D (Deptuck, *et a.,* 2003; CNLOPB, 2012) (Fig. 1). Therefore, faulting likely resulted in the southward termination of reflections against the top of the detachment fault zone.

6. Detached faults

A set of approximately E-striking, N-dipping normal faults are present in the study area between the Mercury fault and the Flying Foam anticline (Figs. 4c and 15b). They are slightly curved in map view and mostly planar in cross-sectional view (Fig. 4c and 15b). Most detached faults have an apparent dip of approximately 60° in a N-oriented seismic section. However, several faults dip only 30° (Fig. 15b), which is possibly a result of fault rotation. Faults 1 and 2, two representative detached faults, offset the late Albian, Aptian and Tithonian unconformities and the top of package B before detaching within ductile package B (Fig. 15b). Offsets of the top of package B associated with these detached faults are visible on the contour map of the detachment fault zone (Fig. 22b). None of the faults offset the basement (Fig. 15b).

Normal offset on the detached faults is consistent for most affected reflections (Fig. 15b). Thus, the faults formed after deposition of these reflections. Strata in package E1, above the late Albian unconformity, clearly thicken across detached fault 2 on line E (Fig. 25). No obvious growth related to the detached faults is present within the section between the Aptian and late Albian unconformities even though the thickness of this unit varies slightly (Figs. 15b and 25). Because the late Albian unconformity is an angular unconformity, erosion likely explains these thickness changes.

7. Discussion

7.1 When was the Mercury fault active? What was the movement direction on the Mercury fault?

I propose that ESE-trending undulations on the surface of the Mercury fault (Fig. 20b) are corrugations reflecting fault slip during the first phase of rifting for the following reasons:

1) The geometry of these undulations resembles corrugations formed during fault linkage in experimental models of normal faulting (Fig. 8);

2) The geometry of these undulations resembles those observed on fault surfaces defined by 3D seismic data (Fig. 10);

3) This ESE-movement direction during the first phase of rifting is consistent with previous literature on the Jeanne d'Arc basin (Tankard and Welsink, 1987; Sinclair, 1995a; Sinclair *et al.*, 1999) and the strain state during intrusion of the earliest Jurassic, NE-striking Avalon dyke exposed in Newfoundland (Pe-Piper *et al.,* 1992; Sinclair, 1995a; Pe-Piper and Piper, 1999) (Fig. 1).

Breaching of relay-zones during fault linkage produces an undulating fault surface with topographic lows and highs similar to those present on the Mercury fault (Fig. 8). For example, on the northern part of the fault surface a prominent topographic low lies between two topographic highs (Fig. 20). Three overlapping fault segments with similar strikes possibly existed during initial faulting, but the center fault was slightly farther to the west than the other faults (Fig. 20c). Formation of relay ramps between the fault segments and subsequent breaching of these relay ramps likely resulted in this topographic low (Fig. 20c). Experimental models show that even though many faults link during extension, the linkages perpendicular to the slip direction have the best chance of preservation (Withjack *et al.,* in prep). If these undulations formed during fault linkage, then they are corrugations, and indicate an ESE-movement direction on the Mercury fault when the corrugations formed (Fig. 20b).

Why were the corrugations not overprinted during subsequent extension? Package B is a ductile syn-rift unit (Serrano Suarez, 2013). In addition to decoupling the basement from the cover layer, the evaporites preferentially accumulated or were preserved in the topographic low areas on the Mercury fault (Fig. 26). I hypothesize that the evaporites prevented overprinting of the corrugations during later phases of rifting by not allowing the cover layer to come into direct contact with the basement. Additionally, experimental models show large-scale corrugation formed during fault linkage are not completely overprinted during a second phase of deformation (Fig. 8) (Withjack *et al.,* in prep).

Although the Mercury fault is likely a reactivated Paleozoic structure, these corrugations are probably not preserved Paleozoic features for the following reason. A shallowly-dipping reflection possibly related to an old Paleozoic thrust fault exists beneath the reflection of the Mercury fault (Fig. 27) and appears to merge with the Mercury fault at about 6 s TWT. This is similar to the extensional reactivation of a preexisting thrust, with a new normal fault splaying off the thrust, as described by Morley (2014). The branchpoint for the splay occurs at 6 s TWT, but the structure-contour map (showing the ESE-trending corrugations) only covers the interval between 2s and 5 s TWT (Figs. 19 and 20). Thus, the structure-contour map likely only represents features on the new normal fault, not the reactivated thrust.

Relay ramps, present between adjacent normal faults that overlap in map view, produce inclined zones between overlapping faults (*e.g.,* Peacock and Sanderson, 1991, 1994). The northeastward tilt of strata in the hanging wall of the Mercury fault (Fig. 15), along with northward diverging reflections within package C (Fig. 16 and 28), reflect the formation of a relay ramp between the overlapping Mercury and Murre faults in the southern part of the study area during the second phase of rifting (Fig. 29). Formation of this relay ramp provides evidence for continued movement on the Mercury fault during the second phases of rifting from the earliest Jurassic to the latest Jurassic. However, without slip indicators, determining an exact movement direction on the Mercury fault during the second phase of rifting is not possible.

7.2 When did the Flying Foam fault form?

Lack of a thickness change in package C across the Flying Foam fault (Figs. 11-13 and 24) indicates this fault was not active until deposition of package D during the third phase of rifting. Previous studies refer to this fault as the northern extent of the Murre fault (Withjack and Callaway, 2000; Serrano Suarez, 2013) but, in this study, I refer to it as the Flying Foam fault because it appears it moved independently of the Murre fault. Movement on the detachment fault zone in the northern part of the study area was likely coupled with movement on the Flying Foam fault (*see section 7.3 for further discussion)*.

7.3 When was the detachment fault zone active? What was the slip direction on the detachment fault zone?

Formation of the relay ramp between the Mercury and Murre fault tilted strata in the hanging wall of the Mercury fault to the NE during the second phase of rifting (Fig. 29). Tilted strata included the ductile Argo Formation, which acted as the detachment fault zone during the third phase of rifting from the latest Jurassic to the Albian. The northeastward tilt of the detachment fault zone possibly resulted in gravity-driven, NE-directed movement on the detachment fault zone throughout deposition of package D. On line E (Fig. 15), faulting with a normal dip-slip component likely resulted in the southward termination of reflection against the top of the detachment fault zone in the southern part of the study area. Additionally, if the undulations with NE-trending axial traces present on the surface of the detachment fault zone in the southern part of the study area are corrugations, they support NE-directed movement on the detachment fault zone during the third phase of rifting on the southern part of the detachment fault zone (Fig. 22b). As top-to-the northeast movement occurred on the detachment fault zone in the southern part of the study area package D filled the available accommodation space.

Westward diverging growth beds within package D indicate an E-directed component of movement on the detachment fault zone beginning in the northern part of the study area, concurrent with NE-directed movement on the detachment fault zone in the south (Fig. 24). As movement began on the Flying Foam fault in the north, non-planar movement with an E-directed component began on the detachment fault zone. An extensional forced fold, the Flying Foam anticline, developed above the Flying Foam fault as movement on the detachment fault zone and the sub-salt Flying Foam fault progressed (Fig. 30) (Withjack and Callaway, 2000; Serrano Suarez, 2013). As the Flying Foam anticline developed, the flanks of the structure were down-dropped relative to the crest, producing the trough-shaped detachment fault zone (Fig. 31).

Movement with an E-directed component on the detachment fault zone beginning in the north, concurrent with movement on the Flying Foam fault and formation of the Flying Foam anticline, explains why the westward divergence of reflections within package D involves younger parts of the section toward the south

(Figs. 24). The E-directed component of movement on the detachment fault zone beginning in the north also explains why strata beneath the Aptian unconformity on line C thicken toward the Flying Foam anticline (Fig. 24), indicating that at the time of their deposition, this area was a low. This means that E-directed movement on the underlying basement-involved fault had not started this far south, and motion on the detachment fault zone only had a NE-directed component.

7.4 When were the detached faults active?

The offset of the late Albian unconformity, along with growth within package E2 (Fig. 25), indicates active faulting occurred during late Albian time, and ended sometime after the deposition of the beds above the unconformity. Additionally, because these detached faults strike approximately E-W (Fig. 8) and are N-dipping (Fig. 4c and 15b), their slip had a northward component. Because the detached, normal faults are not reactivated faults, their strike is likely to be perpendicular to the slip direction (*i.e.,* N-S). Offset from detached faults 1 and 2 are visible on the structure-contour map of the top of the detachment fault zone (Fig. 22b). These offsets are not corrugations, and would give an incorrect movement direction if interpreted as such.

7.5 How are faults in the Flying Foam region of the Jeanne d'Arc basin related to each other temporally?

7.5.1 Late-Triassic – earliest Jurassic (phase 1)

Syn-rift deposition of package B and ESE-oriented corrugations suggest mostly normal slip and ESE extension on the Mercury fault during the first phase of rifting (Figs. 32 and 33). The Flying Foam fault, previously referred to as the northern Murre fault, was likely not active in the study area during the first phase of rifting (Edwards, 1989; Sinclair, 1995a). Additionally, the detachment fault zone was not active during the first phase of rifting.

7.5.2 Earliest Jurassic – Tithonian (phase 2)

Stratigraphic patterns in package C indicate movement on the Mercury fault continued during the second phase of rifting (Figs. 28 and 34a) (Serrano Suarez, 2013). A relay ramp developed between the overlapping parts of the Mercury and Murre faults in the southern part of the study area during the second phase of rifting (Fig. 34b). The development of this relay ramp produced a northward tilt of all the strata in the hanging wall of the Mercury fault, including the Argo Formation that later acted as the detachment fault zone (15 and 34a). Without any slip indicators, the exact movement direction during this phase of rifting is unknown. Most previous literature labels this a period of thermal subsidence without active faulting (Hubbard *et al.*, 1985; Tankard and Welsink, 1987; Hubbard, 1988; Tankard *et al.*, 1989; Grant and McAlpine, 1990; Sinclair, 1995a; Sinclair and Riley, 1995; Sinclair *et al.*, 1999), and therefore, those authors did not specify a movement direction.

7.5.3 Tithonian – Aptian (phase 3)

Movement on the detachment fault zone occurred during phase three of rifting, and the movement direction varied geographically through time (Figs. 15, 22, 24 and 32). Tilting of package B during the second phase of rifting resulted in NE-directed movement on the detachment fault zone during the third phase of rifting, possibly due to gravity sliding (Fig. 15, 32 and 34) (Tankard and Welsink, 1987). NE-trending corrugations on the surface of the detachment fault zone, along with the termination of reflections, likely due to faulting, between the detachment fault zone and the top of package D in the southern part of study area, support this NE-oriented movement of the detachment fault zone in the southern part of the study area (Figs. 15, 24, and 32).

Growth beds in package D indicate movement on the detachment fault zone had an E-directed component in the northern part of the study area, concurrent with the NE-directed movement in the south (Fig. 24 and 32). Once extension with an E-directed component began on the Flying Foam fault, top-to-the east movement began on the non-planar detachment fault zone, and the Flying Foam anticline developed above the Flying Foam fault (Fig. 32 and 35a). Growth beds in package D indicate that this component of E-directed movement on both the Flying Foam fault and the detachment fault zone, along with the development of the Flying Foam anticline, began in the north and propagated southward. This resulted in temporal and spatial variation in the movement direction on the detachment fault zone throughout the third phase of rifting (Fig. 32 and 35b).

Magnetic anomalies give the age of the oldest oceanic crust adjacent to the continent-ocean boundary. Magnetic anomaly 0 (M-0), in oceanic crust directly adjacent to the northeastern Grand Banks (Fig. 1), suggests that breakup in this region began in the early Aptian (Fig. 1) (*e.g.*, Driscoll *et al.*, 1995; Srivastava *et al.*, 2000; Shipboard Scientific Party, 2003; Withjack and Schlische, 2005). Usually breakup implies the end of tectonic activity. However, my work shows basement-involved movement on the Flying Foam fault with a dip-slip normal component continued through the Aptian (Fig. 35).

7.5.4 Albian – Present (post-rift)

By late Albian time drifting was underway (*e.g.*, Driscoll *et al.*, 1995; Srivastava *et al.*, 2000; Shipboard Scientific Party, 2003; Withjack and Schlische, 2005) and basement-involved had ceased in the northern part Jeanne d'Arc basin. Therefore, the detached faults indicate that minor faulting in the basin continued after rifting ended. Post-rift strata make up all of package E, but growth beds and offset of the late Albian unconformity indicate deposition of package E1 occurred during small-magnitude, approximately NNE-oriented detached extension (Figs. 25, 32, and 36). In contrast, deposition of package E2 occurred during tectonic quiescence (Serrano Suarez, 2013).

Detached faults are likely related to either post-rift salt movement (Tankard and Welsink, 1987; Withjack and Schlische, 2005) or separation of northern Canada from Greenland (Tankard and Welsink, 1987; Foster and Robinson, 1993; Sinclair, 1995b; Withjack and Schlische, 2005). If the faults reflect deep-seated extension related to separation of northern Canada from Greenland, then a basement-involved normal fault, accommodating a component of N-directed extension, must lie outside of the study area.

8. Conclusions

In an extensional basin with reactivated faults, fault slip need not be perpendicular to the strike of the faults. Additionally, the presence of a ductile unit complicates structural development by decoupling deep structures from shallow structures. Thus, strata above a ductile unit may move and deform independently from strata beneath the ductile unit. Interpretation of fault-surface topography, growth packages, and secondary structures provides a way of constraining slip direction and timing.

ESE-oriented corrugations on the surface of the Mercury fault, most likely formed during linkage of smaller fault segments, indicate ESE-oriented movement during the first phase of rifting in the Jeanne d'Arc basin (Late Triassic – earliest Jurassic). These corrugations provide a slip indicator independent of the strike of the fault. The upper part of package B, deposited during this first phase of rifting, is a highly ductile evaporitic unit and acted to decouple the basement and cover layer, thus preserving the corrugations.

Northward tilting of strata in the hanging wall of the Mercury fault in the southern part of the study area, along with northward diverging reflections in package C, indicates the formation of a relay ramp between the Mercury and Murre faults in the southern part of the study area during the second phase of rifting (earliest Jurassic – latest Jurassic). Formation of this relay ramp indicates movement continued movement on the Mercury fault; it also tilted package B, which later acted as a detachment fault zone.

Detached extension, with a geographically and temporally varied movement direction, occurred on the detachment fault zone during the third phase of rifting. Possible gravity sliding along the NE-dipping detachment fault zone resulted in NE-oriented detached extension. Concurrently, as movement with an east-side-down component began on the southward propagating Flying Foam fault, westward-diverging growth beds within package D indicate the detachment fault zone also gained a component of top-to-the east motion. The southward decrease in age of these westward-diverging growth beds indicate that, as the Flying Foam fault propagated southward, a component of E-oriented movement on the detachment fault zone affected areas farther south. Also, as the Flying Foam fault propagated southward, the Flying Foam anticline, an extensional forced fold and extensional fault-bend fold, formed above it. M-0 indicates breakup in the Jeanne d’Arc basin occurred in the earliest Aptian. However, this study indicates basement-involved faulting continued through the Aptian.

Basement-involved faulting had ended and drifting was underway by the late Albian, but growth above the late Albian unconformity indicates detached faulting continued into the Albian. Detached faulting either relates to post-rift salt movement or separation of Greenland from northern Canada or both.

References

Anderson, E.M. (1951), The dynamics of faulting and dyke formation with applications to Britain: Oliver and Boyd, Edinburg, 206.

CNLOPB (2012), www.cnlopb.nl.ca/well_alpha.shtml.

Deptuck, M. E., MacRae, A., Shimeld, J. W., Williams, G., and Fensome, R. A. (2003), Revised Upper Cretaceous and lower Paleogene lithostratigraphy and depositional history of the Jeanne d'Arc Basin, offshore Newfoundland, Canada, *AAPG Bulletin*, *87*(9), 1459 - 1483.

Driscoll, N.W., Hogg, J. R., Christie-Blick, N., and Karner, G. D. (1995), Extensional tectonics in the Jeanne d'Arc Basin, offshore Newfoundland: implications for the timing of break-up between Grand Banks and Iberia, *Geological Society, London, Special Publication, 90*(1), 1-28.

Edwards, A. (1989), Seismic studies of the Jeanne d'Arc Basin. Geological Survey of Canada, Open File, 2098.

Enachescu, M. E. (Ed.) (1987), *Tectonic and structural framework of the northeast Newfoundland continental margin*, 117-146 pp., Canadian Society of Petroleum Geologist.

Fossen, H. (2010), Structural Geology. Cambridge New York: Cambridge University Press. Print.

Foster, D.G., and A.G. Robinson (1993), Geological history of the Flemish Pass basin, offshore Newfoundland: AAPG Bull., v. 77, p. 588-609.

Granger, A.B. (2006). Influence of basal boundary conditions on normal-fault systems in scaled physical models. Masters thesis, Rutgers University.

Granger, A.B., Withjack, M.O., Schlische, R.W. (2008), Fault surface corrugations: insights from scaled experimental models of extension. In: ‘‘Fault Zones: Structure, Geomechanics, and Fluid Flow’’ Conference, Abstracts Volume. Geological Society of London, page 38.

Grant, A. C., and McAlpine, K. D. (1990), The continental margin around Newfoundland, in *Geology of the continental margin of Eastern Canada*, edited by Keen, M. J. and Williams, G. L., pp. 241-292.

Henza, A. A., Withjack, M. O., and Schlische, R. W. (2010), Normal-fault development during two phases of non-coaxial extension: An experimental study, *Journal of Structural Geology, 32(11)*, 1656-1667.

Hubbard, R. J. (1988), Age and Significance of Sequence Boundaries on Jurassic and Early Cretaceous Rifted Continental Margins, *AAPG Bulletin*, *72*(1), 49-72.

Hubbard, R. J., Pape, J., and Roberts, D. G. (1985), Depositional sequence mapping to illustrate the evolution of a passive continental margin, in *Seismic Stratigraphy II*, edited by Berg, O. R. and Woolverton, D. G., pp. 79-115.

Lohr, T., Krawczyk, C. M., Oncken, O., David C. Tanner, D.C. (2008), Evolution of a fault surface from 3D attribute analysis and displacement measurements: Journal of Structural Geology, v. 30, p. 690-700

Louden, K. (2002), Tectonic evolution of the East Coast of Canada, *Canadian Society of Exploration Geophysicist - Recorder*, *2*, 37-48.

Laubscher, H. P. (1982), Die Südostecke des Rheingrabens—ein kinematisches und dynamisches Problem: Eclogae Geologicae Helvetiae, v. 75, p. 101–116.

Magoon, L. B., Hudson, T. L., and Peters, K. E. (2005), Egret-Hibernia(!), a significant petroleum system, northern Grand Banks area, offshore eastern Canada, *AAPG Bulletin*, *89*(9), 1203-1237.

Marchal D., Guiraud, M., Rives, T., and Van den Driessche, J. (1998), Space and time propagation processes of normal faults, in Jones, G., Fisher, Q.J., and Knipe, R.J., eds., Faulting, Fault Sealing, and Fluid Flow in Hydrocarbon Reservoirs: Geological Society, London, Special Publication 147, p. 51-70.

Marchal, D., Guiraud, M., and Rives, T. (2003), Geometric and morphological evolution of normal fault planes and traces from 2D to 4D data: Journal of Structural Geology, v. 25, p. 135-158.

Maurin, J.-C. (1995), Drapage et décollement des séries jurassiques sur la faille de détachement majeure du rift rhénan sud: implications sur la géométrie des dépôts syn-rifts oligocenes: Comptes Rendus Académie des Sciences Paris, v. 321, p. 1025–1032.

McAlpine, K. D. (1990), Mesozoic stratigraphy, sedimentary evolution, and petroleum potential of the Jeanne d'Arc Basin, Grand Banks of Newfoundland, *Geological Survey of Canada*, *paper 89-17*, 1-50.

Morley, C.K. (2014). The widespread occurrence of low-angle normal faults in a rift setting: Review of examples from Thailand, and implications for their origin and evolution. Earth-Science Reviews, 133, 18-42.

Olsen, P.E. (1997), Stratigraphic record of the early Mesozoic breakup of Pangea in the Laurasia-Gondwana rift sys- tem: Annual Reviews of Earth and Planetary Science, v. 25, p. 337-401.

Peacock, D.C.P., and Sanderson, D.J. (1991), Displacements, segment linkage and relay ramps in normal fault zones: Journal of Structural Geology, v. 13, p. 721–733.

Peacock, D. C. P., and Sanderson, D. J. (1994), Geometry and development of relay ramps in normal fault systems, *AAPG Bulletin, 78*(2), 147-165.

Pe-Piper, G., Jansa, L.F., Lambert, R.S.J. (1992), Early Mesozoic magmatism of the Eastern Canadian margin; petrogenetic and tectonic significance, *in* J.H. Puffer and P.C. Ragland, eds., Eastern North American Mesozoic Magmatism: Geological Society of America Special Paper 268, p. 13-36.

Pe-Piper, G., and Piper, D.J.W. (1999), Were Jurassic tholeiitic lavas originally widespread in southeastern Canada?: a test of the broad terrane hypothesis, Canadian Journal of Earth Sciences 36, no. 9 (1999): 1509-1516.

Ratcliffe, N.M., and Burton, W.C., 1985, Fault reactivation models for the origin of the Newark basin and studies related to U.S. eastern seismicity: U.S. Geological Survey Circular 946, p. 36-45.

Schlische, R. W. (1995), Geometry and origin of fault-related folds in extensional settings, *AAPG Bulletin*, *79*(11), 1661-1678.

Schlische, R. W., Withjack, M. O., and Olsen, P. E. (2002), Relative Timing of CAMP, Rifting, Continental Breakup, and Basin Inversion: Tectonic Significance, in *The Central Atlantic Magmatic Province*, edited by Hames, W. E., McHone, G. C., Renne, P. and Ruppel, C., American Geophysical Union Monograph.

Schlumberger and Geco-Prakla (1996), 1995/6 Marine 3D survey Newfoundland Grand Banks. Final processing report for Exploration Services Geco-Prakla, 51 pp, Houston.

Serrano Suarez (2013), Evolution of the Jeanne d'Arc basin, offshore Newfoundland, Canada: 3D seismic evidence for >100 million years of rifting, Masters thesis, Rutgers University.

Seton, M., Muller, R. D., Zahirovic, S., Gaina, C., Torsvik, T., Shephard, G., Talsma, A., Gurnis, M., Turner, M., Maus, S., and Chandler, M. (2012), Global continental and ocean basin reconstructions since 200 Ma, *Earth-Science Reviews*, *113*, 212- 270.

Shipboard Scientific Party (2003), Leg 210 Preliminary Report. ODP Preliminary Report 110 [Online], http:// www-odp.tamu.edu/publications/prelim/ 210_prel/210PREL.PDF.

Sinclair, I. K. (1988), Evolution of Mesozoic-Cenozoic sedimentary bains in the Grand Banks area of Newfoundland and comparison with Falvey's (1974) rift model, *Bulletin Canadian Petroleum Geology*, *36*(3), 255-273.

Sinclair, I. K. (1995)a, Transpressional inversion due to episodic rotation of extensional stresses in Jeanne d'Arc Basin, offshore Newfoundland, in *Basin Inversion*, edited by Buchanan, J. G. and Buchanan, P.G., pp. 249-271, Geological Society Special Publication 88.

Sinclair, I.K., (1995)b, Sequence stratigraphic response to Aptian-Albian rifting in conjugate margin basins: A comparison of the Jeanne d'Arc basin, offshore New- foundland, and the Porcupine basin, offshore Ireland, *in* R.A. Scrutton, M.S. Stoker, G.B. Shimmield, and A.W. Tudhope, eds., The Tectonics, Sedimentation and Paleooceanography of the North Atlantic Region: Geo- logical Society Special Publication no. 90, p. 29-49.

Sinclair, I. K., and Riley, L. A. (1995), Separation of Late Cimmerian rift and post-rift megasequences: comparison of the Jeanne d'Arc Basin, Grand Banks and the Outer Moray Firth, North Sea, in *Sequence Stratigraphy on the Northwest European Margin*, edited by Steel, R. J. e. a., pp. 347-363, Elsevier, Amsterdam.

Sinclair, I. K., Evans, J. E., Albrechtsons, E. A., and Sydora, L. J. (1999), The Hibernia Oilfield - effects of episodic tectonics of stuctural character and reservoir compartmentalization, in *Petroleum Geology of Northwest Europe: Proceedings of the 5th Conference*, edited by Fleet, A. J. and Boldy, S. A. R., pp. 517-528.

Srivastava, S.P., Sibuet, J.C., Cande, S., Roest, W.R., and Reid, I.D. (2000), Magnetic evidence for slow seafloor spreading during the formation of the Newfoundland and Iberian margins: Earth and Planetary Science Let- ters, v. 182, p. 61-76.

Tankard, A. J., and Welsink, H. J. (1987), Extensional tectonics and stratigraphy of Hibernia oil field, Grand Banks, Newfoundland, *AAPG Bulletin*, *71*, 1210-1232.

Tankard, A. J., and Welsink, H. J. (1989), Mesozoic Extension and Styles of Basin Formation in Atlantic Canada, in *Extensional Tectonics and Stratigraphy of the North Atlantic Margins*, AAPG Memoir, 46, pp. 175-195

Tankard, A. J., Welsink, H. J., and Jenkins, W. A. M. (1989), Structural styles and Stratigraphy of the Jeanne d'arc basin, Grand Banks of Newfounland, in *Extensional Tectonics and Stratigraphy of the North Atlantic Margins*, AAPG Memoir, 46, pp. 265-282.

Welsink, H. J., and Tankard, A. J. (2012), Extensional tectonics and stratigraphy of the Mesozoic Jeanne d'Arc basin, Grand Banks of Newfoundland, in *Regional* *geology and tectonics: Phanerozoic passive margins, cratonic basins and global tectonic maps*, edited by Roberts, D. G. and Bally, A. W., pp. 337-381, Elsevier, New York.

Whipp, P.S., Jackson, C.A.L., Schlische, R.W., Withjack, M.O., Gawthorpe, R.L. (2015), Spatial distribution and evolution of fault-segment boundary types in rift systems; observations from experimental clay models: *Geological Society of London Special Publication,* in press*.*

Withjack, M. O., Olson, J., and Peterson, E. (1990), Experimental-Models of Extensional Forced Folds, *AAPG Bulletin*, *74*(7), 1038-1054.

Withjack, M. O., Schlische, R.W., and Olsen, P.E. (1998), Diachronous rifting, drifting, and inversion on the passive margin of Central Eastern North America: An analog for other passive margins, *AAPG Bulletin*, *82*(5A), 817-835.

Withjack, M. O., and Callaway, S. (2000), Active normal faulting beneath a salt layer: An experimental study of deformation patterns in the cover sequence, *AAPG Bulletin*, *84*(5), 627-651.

Withjack, M. O., Schlische, R. W., and Olsen, P. E. (2002), Rift-basin Structure and its Influence on Sedimentary Systems, in *Sedimentation in Continental Rifts*, edited by Ranaut, R. W. and Ashley, G. M., pp. 57-81. SEPM Special Publication 73.

Withjack, M. O., and Schlische, R.W. (2005), A review of tectonic events on the passive margin of eastern North America, in *Petroleum Systems of Divergent Continental Margin Basins: 25th Bob S. Perkins Research Conference*, edited by Post, P.J., pp. 203-235, Gulf Coast Section of SEPM.

Withjack, M. O., and Schlische, R.W. (2006), Geometric and experimental models of extensional fault-bend folds, in *Analogue and Numerical Modelling of Crustal-Scale Processes*, edited by Buiter, S. J. H. and Schreurs, G., Geological Society of London, Special Publication 253.

Withjack, M. O., Schlische, R.W., and Olsen, P.E. (2012), Development of the passive margin of Eastern North America, in *Phanerozoic Rift Systems and Sedimentary Basins*, edited by Roberts, D. G. and Bally, A. W., pp. 300-335, Elsevier, New York.

Withjack, M.O., Henza, A.A., and Schlische, R.W. (in prep), 3D fault geometries and interactions during multiphase extension: An experimental modeling study.

Xiao, H., and Suppe, J. (1992), Origin of rollover, *AAPG Bulletin*, *76*(4), 509-529.

Table 1. Summary of the tectonostratigraphic units present in the Flying Foam area, Jeanne d'Arc basin, offshore eastern Canada. Modified from Serrano Suarez (2013).

Packages and Horizons	Seismic-reflection geometries	Unit, lithology, and age
Package E2 (post-rift)	Continuous, sub-parallel, low- to high-amplitude reflections	Banquereau Fm. (shales); Paleogene - Recent (Paleogene – present) (CNLOPB, 2012; Deptuck, *et al*., 2003)
base-Paleogene unconformity	Erosional truncation surface	Early Paleogene
Package E1 (post-rift)	Continuous, mostly sub-parallel, low- amplitude reflections	Dawson Canyon Fm. (shales, limestones), Wyandot Fm. (chalks and marlstones) and Otter Bay Fm. (sandstones) (Late Cretaceous) (CNLOPB, 2012; Deptuck, *et al*., 2003)
late Albian unconformity	Inferred unconformity	Late Cretaceous
Package D (syn-rift)	Continuous, low- to high-amplitude reflections; the geometry of the reflections varies from north to south and from west to east.	Ben Nevis Fm. (shales and some sandstones), Nautilus Fm. (calcareous shales). Avalon Fm. (sandstones), Whiterose Fm. (shales and limestones), Catalina Mb. (sandstones), Hibernia Fm. (sandstones), Fortune Bay Fm. (shales) and Jeanne d'Arc Fm. (sandstones); Late Jurassic – Early Cretaceous (CNLOPB, 2012; McAlpine, 1990; Sinclair, 1999)
Tithonian unconformity	Inferred unconformity	Late Jurassic
Package C (syn-rift)	Continuous, mostly sub-parallel, low- to high-amplitude reflections	Rankin Fm. (limestones), Downing Fm. (shales with interbedded limestones) and Iroquois Fm. (dolomites and limestones); Early to Late Jurassic (?) (McAlpine, 1990; Sinclair *et al*., 1999)

top of salt	Relatively high-amplitude reflection	earliest Jurassic
Package B (syn-rift)	Chaotic and locally grading to low- to moderate-amplitude parallel reflections	Eurydice Fm. (continental red beds) and Argo Fm. (mainly salt); Late Triassic – Early Jurassic (?) (McAlpine, 1990; Sinclair *et al.*, 1999)
top of basement	Inferred angular unconformity; poorly imaged	Late Triassic
Package A (pre-rift)	No primary reflections	Pre-Triassic strata and basement (Sinclair *et al.*, 1999)

Table 2. Main parameters of the 3D seismic data set from the Flying Foam area.

Number of inlines (E-W orientation)	1532
Number of crosslines (N-S orientation)	3150
Inline spacing	25 m
Crossline spacing	12.5 m
Processing record length	9 s
Processing sample interval	4 ms
Nominal fold	32

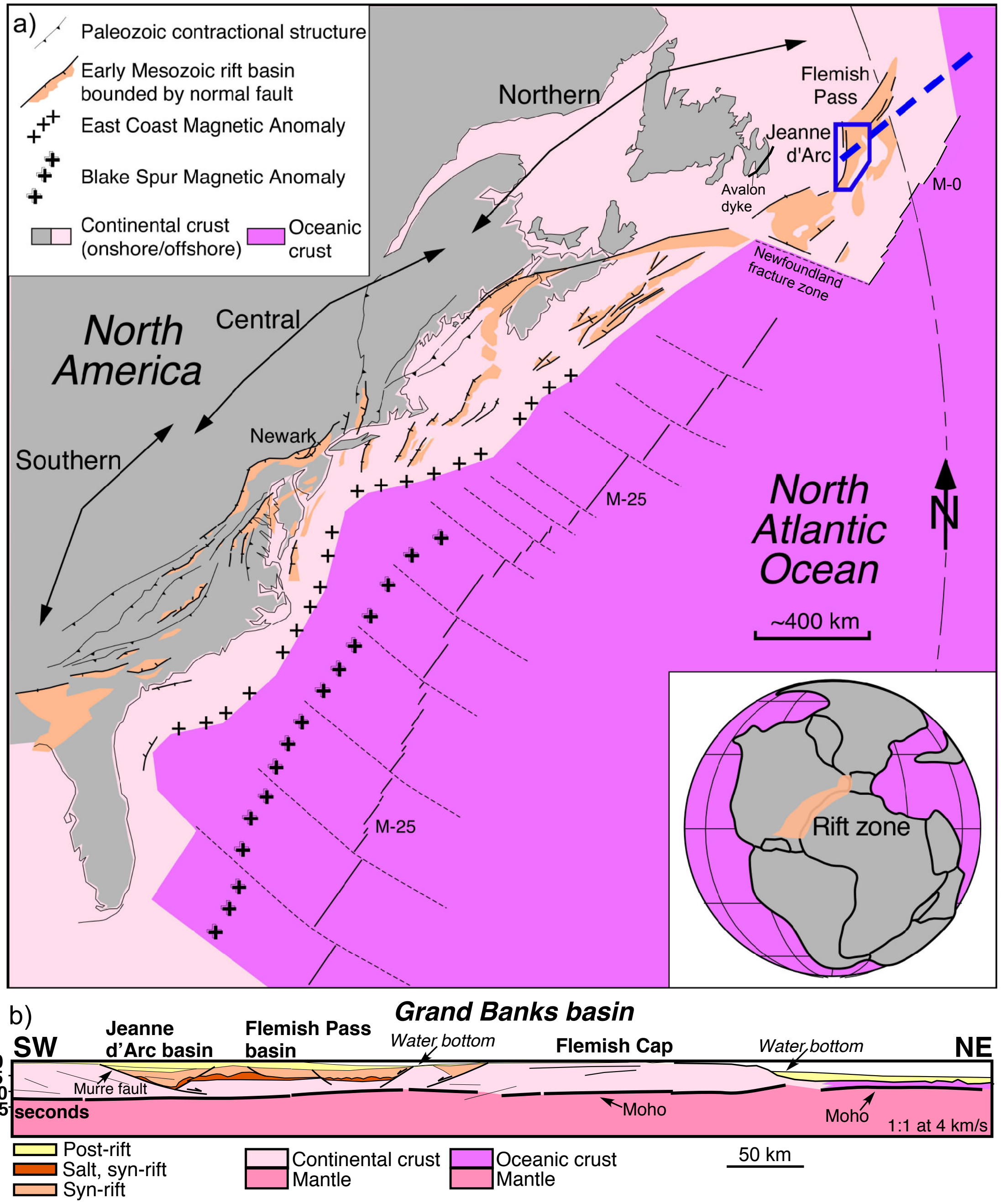

Figure 1. Tectonic setting of Jeanne d'Arc basin. a) Map of the passive margin of eastern North America showing Mesozoic rift basins (modified from Withjack et al., 2012). Locations of M-0 and the Avalon dyke are from Shipboard Science Party (2003) and Pe-Piper and Piper (1999), respectively. The ages of M-0 and M-25 are approximately125 my and 155 my, respectively. See Figure 2 for an enlargement of the area in the blue polygon. Inset shows Pangea during Late Triassic time (Olsen, 1997) and highlights the rift zone between eastern North America and northwest Africa and Iberia. b) Regional transect from offshore Canada (location given by dashed line in part a) showing tectonostratigraphic features of the Grand Banks basin (modified from Withjack et al., 2012).

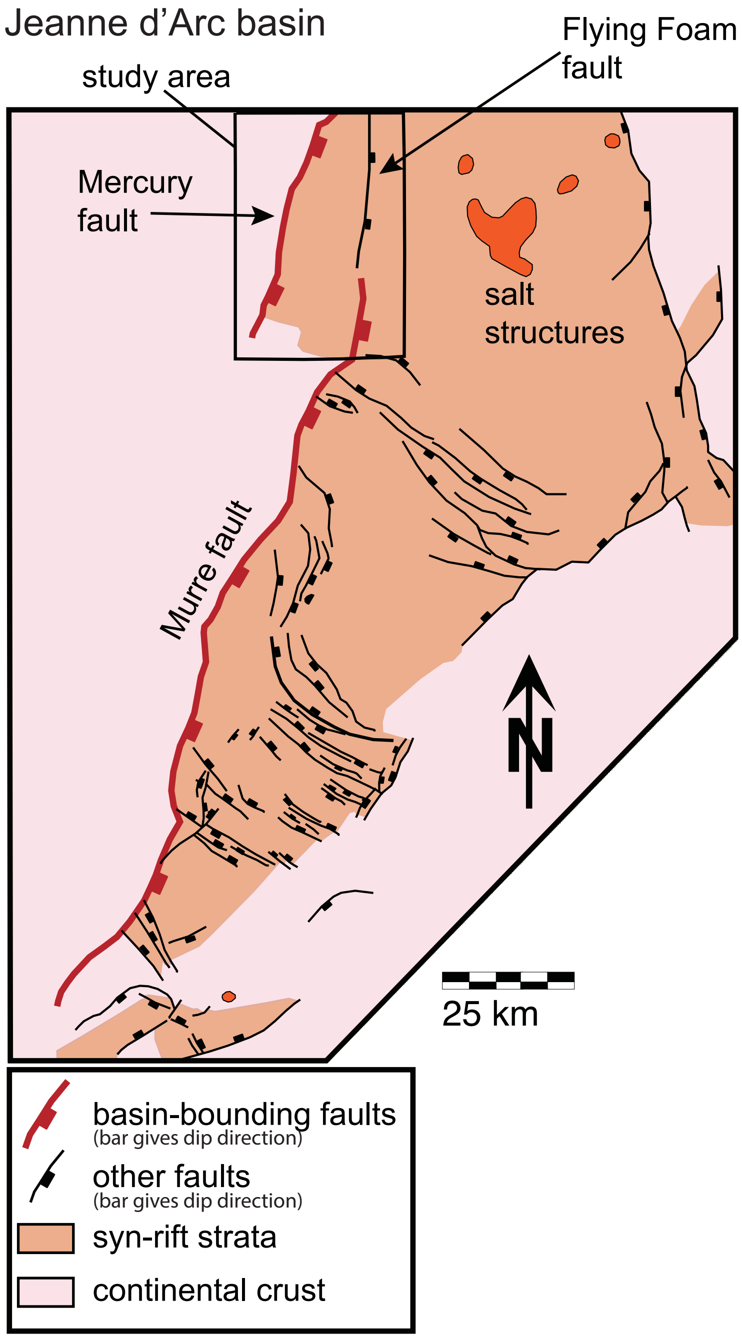

Figure 2. Map of the Jeanne d'Arc basin highlighting the Flying Foam study area. The Flying Foam fault was named in this study. Southern part of map shows faults cutting prominent Middle Jurassic reflection, and northern part shows faults cutting Aptian/Albian sequence (modified from Sinclair, 1995b; Withjack and Schlische, 2005).

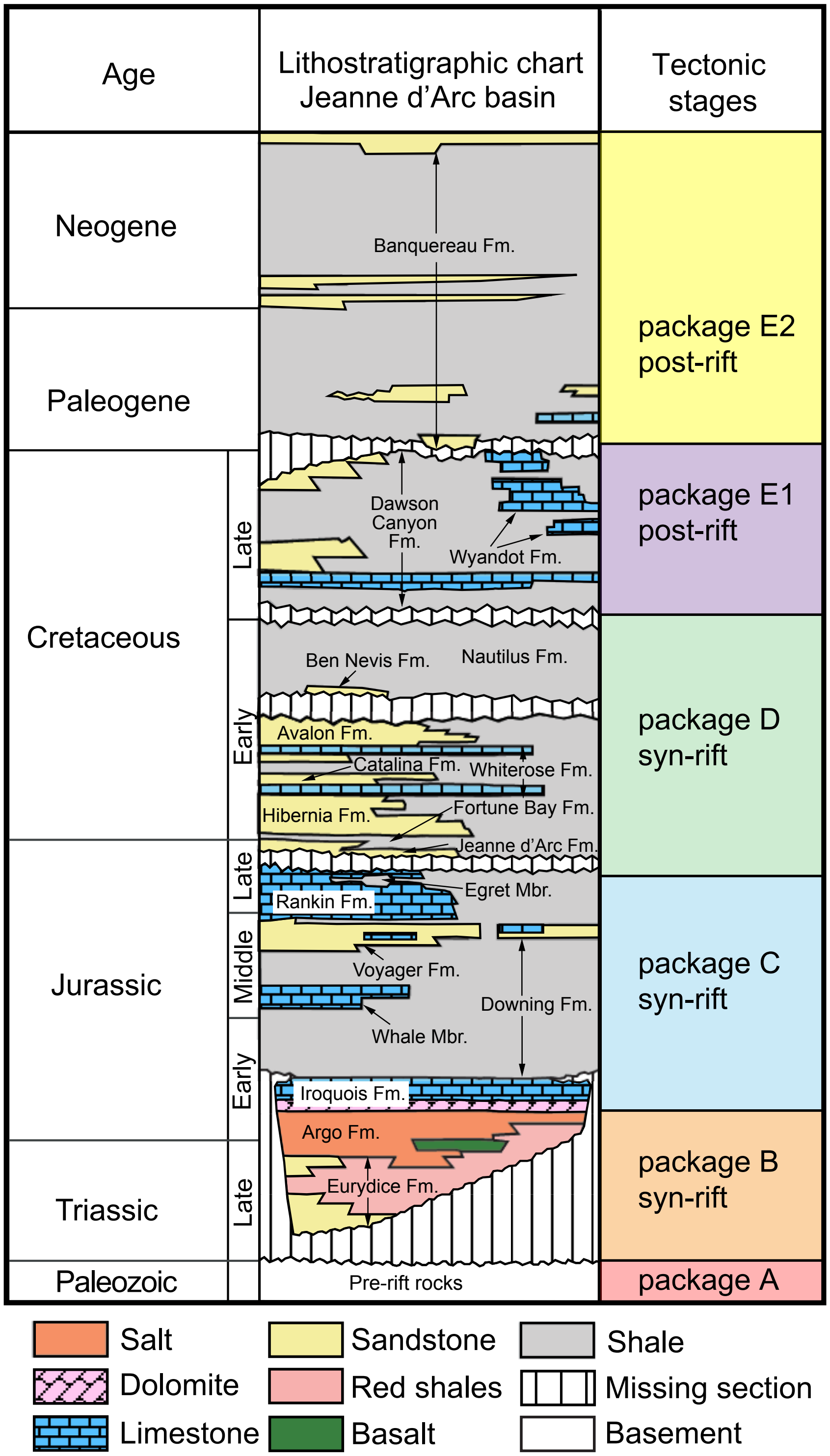

Figure 3. Lithostratigraphic chart of the Jeanne d'Arc basin highlighting tectonostratigraphic packages and tectonic stages defined by Serrano Suarez (2013). This color scheme applies to all subsequent figures. The subdivision of package E into E1 and E2 is new to this study. Modified from Sinclair et al. (1999), Magoon et al. (2005), and Serrano Suarez (2013).

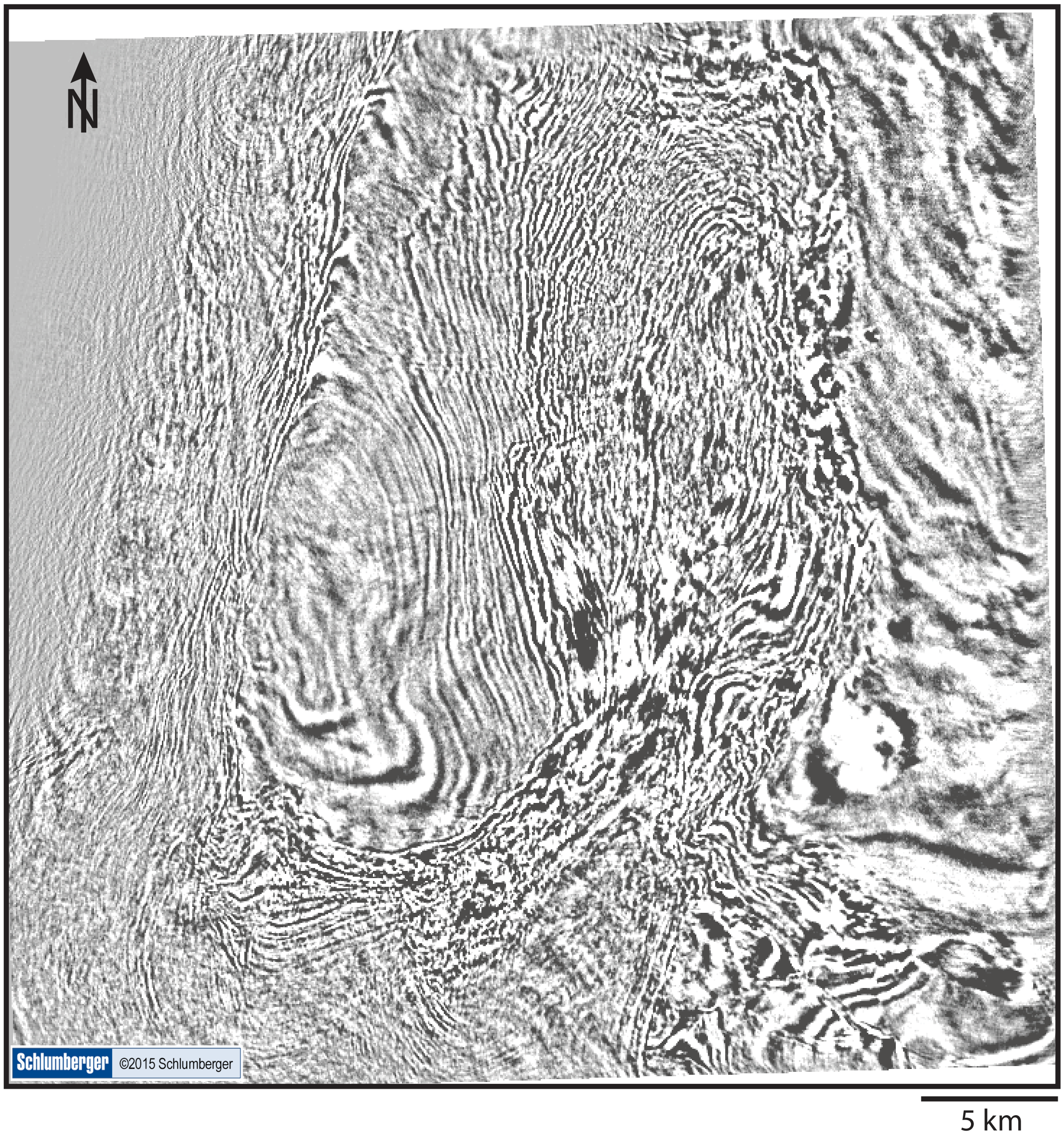

Figure 4a. Uninterpreted time slice at 3.5 s in two-way travel time.

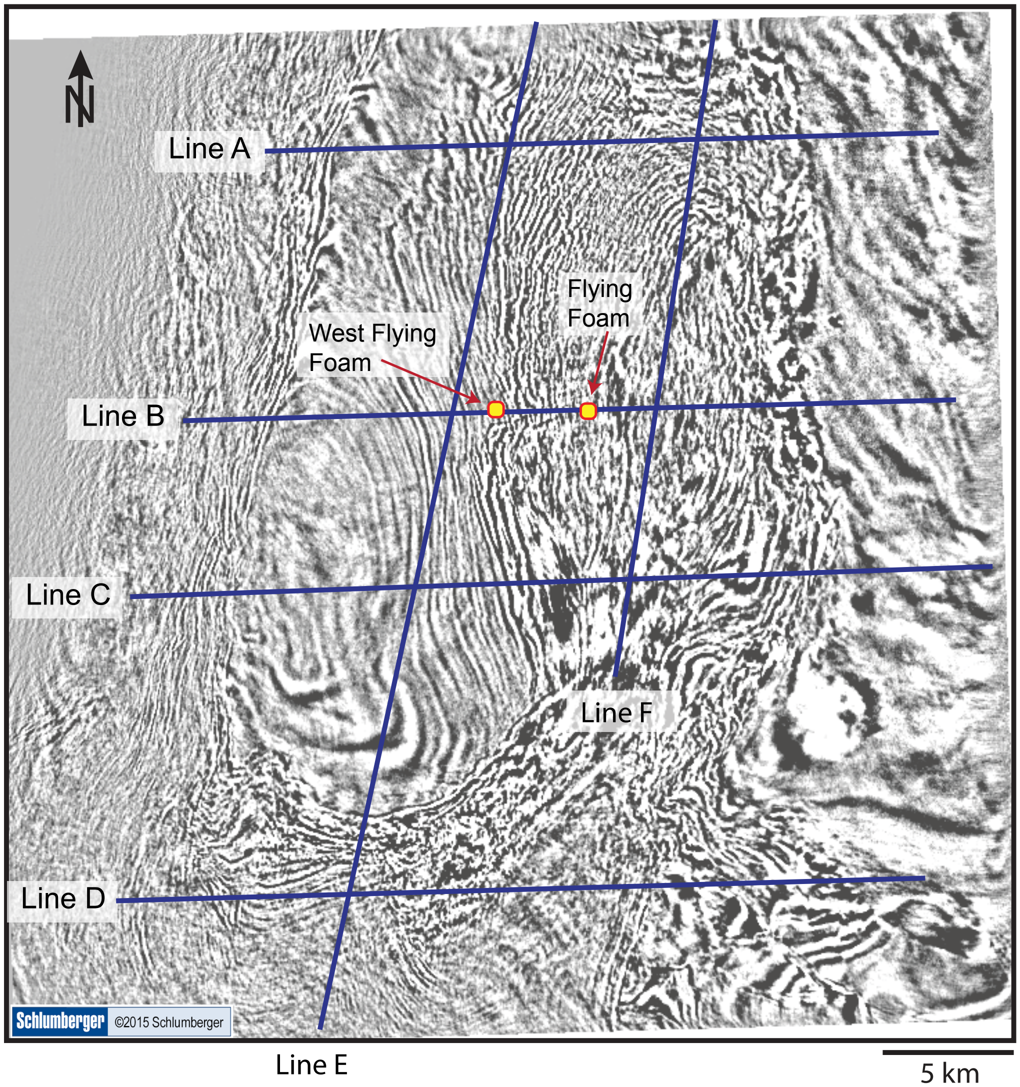

Figure 4b. Time slice at 3.5 s in two-way travel time showing locations of seismic sections presented in this study. Yellow squares are locations of two exploration wells.

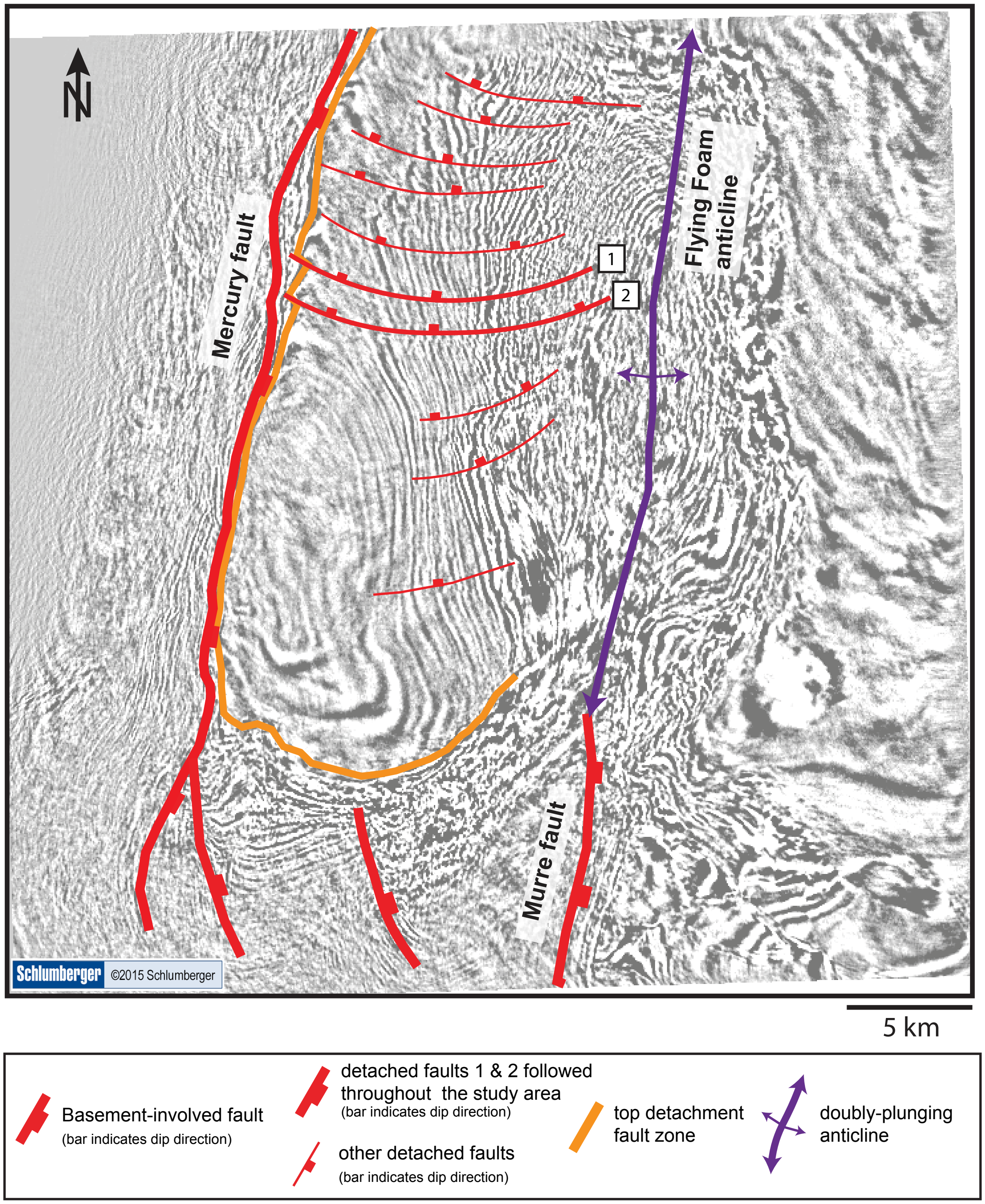

Figure 4c. Interpreted time slice at 3.5 s in two-way travel time showing faults discussed in this study and the Flying Foam anticline.

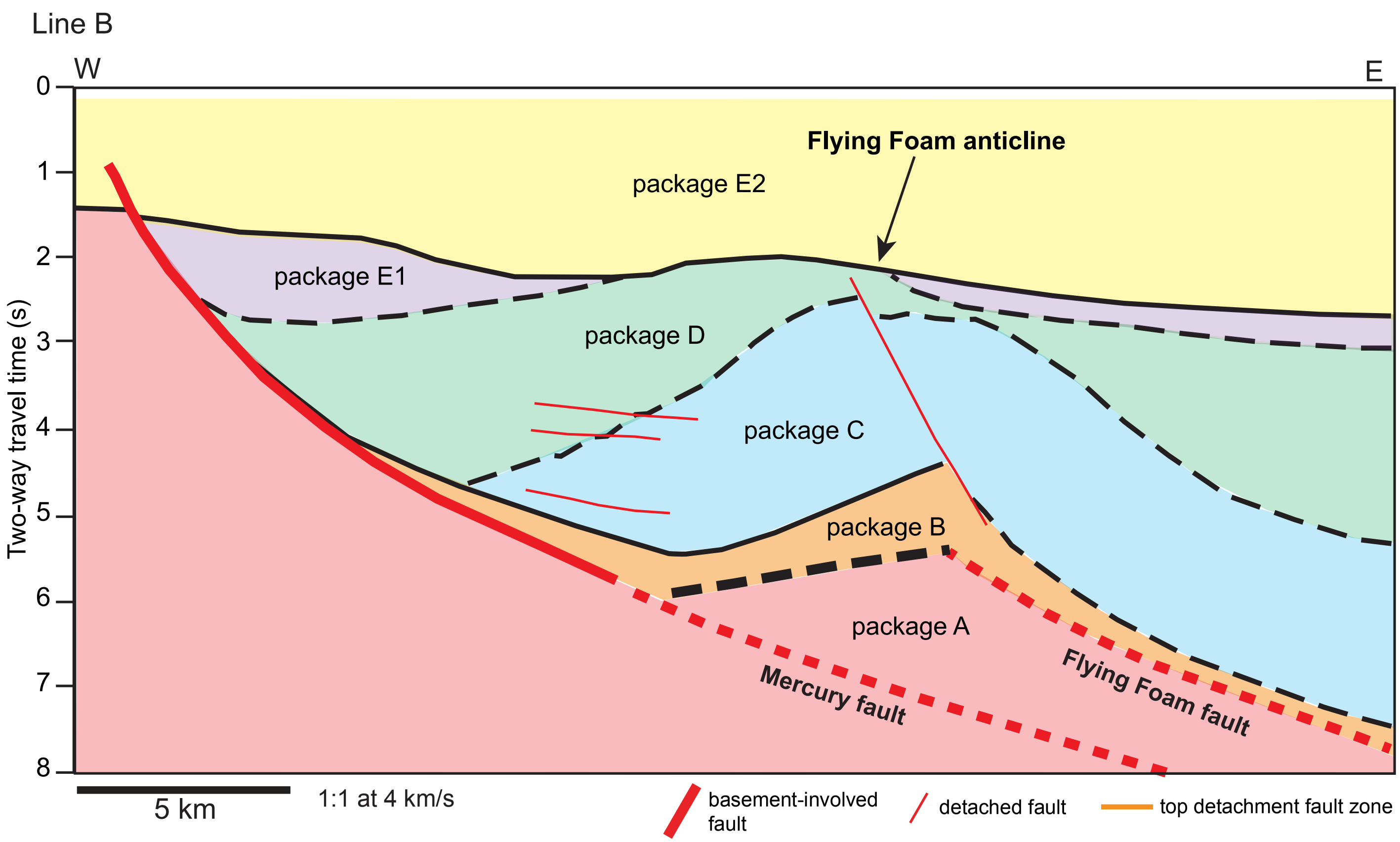

Figure 5. Line drawing of seismic line B showing the six tectonostratigraphic packages, the Mercury fault, the Flying Foam fault, and the Flying Foam anticline. Dashed lines indicate uncertainty. See line location in Figure 4b or uninterpreted line and fully interpreted line in Figure 12.

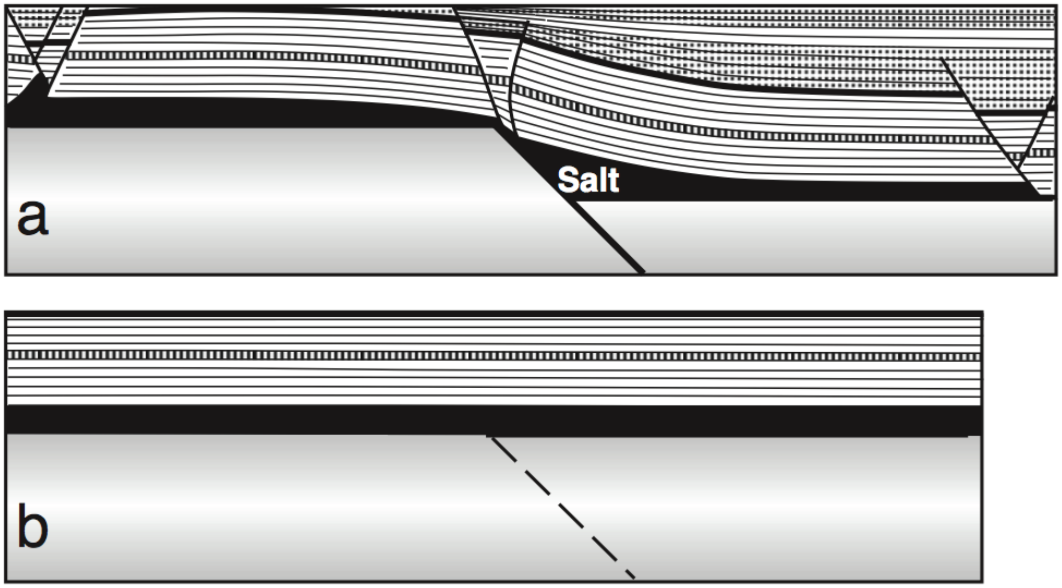

Figure 6. Example of an extensional forced fold based on a scaled experimental model (from Withjack and Callaway, 2000). a) Geometry after movement on subsalt fault. b) Geometry prior to faulting. In the presence of a ductile unit (salt), movement on a fault will fold the cover layer rather than propagating through it, producing an extensional forced fold.

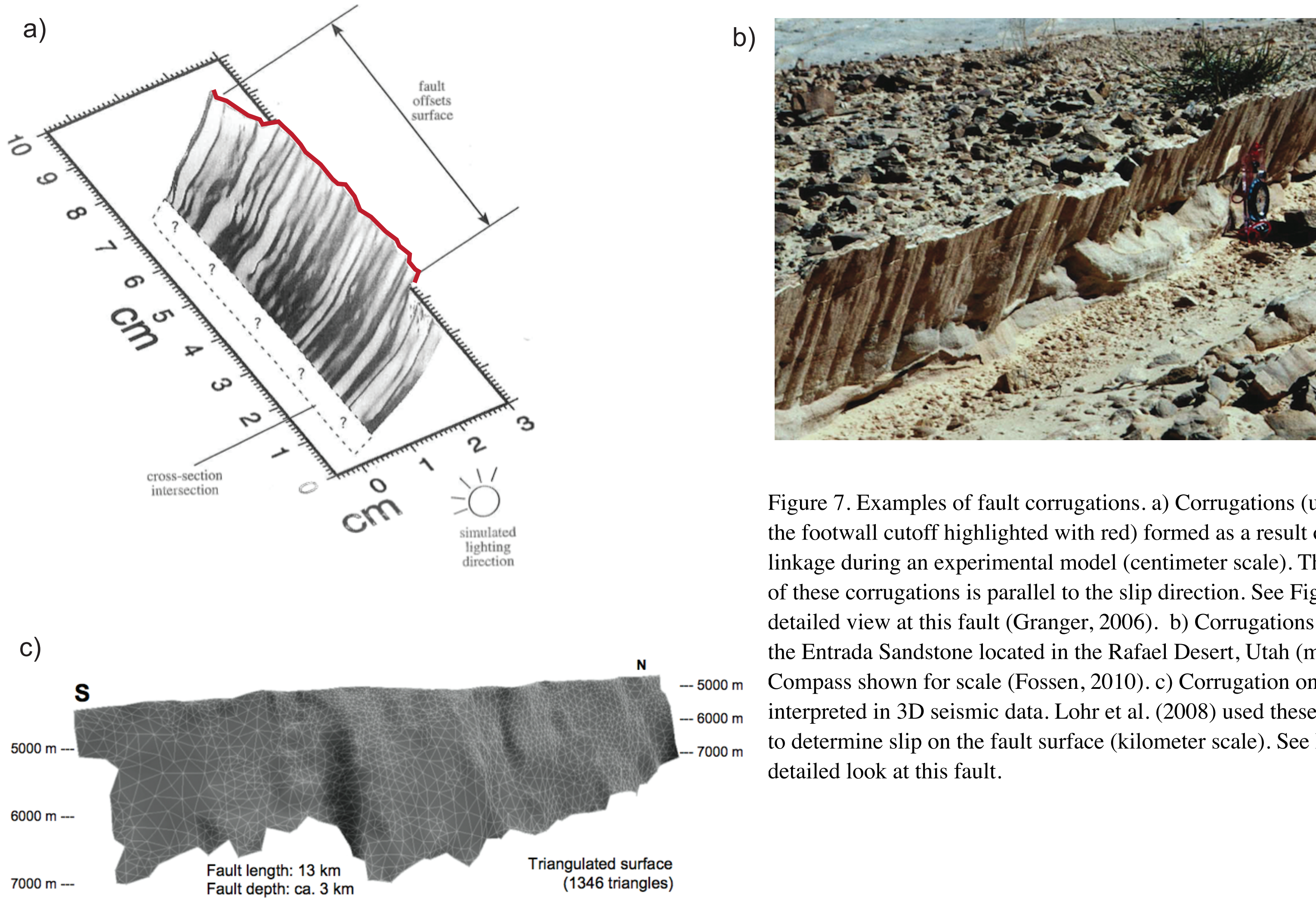

Figure 7. Examples of fault corrugations. a) Corrugations (undulations in the footwall cutoff highlighted with red) formed as a result of fault linkage during an experimental model (centimeter scale). The axial trace of these corrugations is parallel to the slip direction. See Figure 9 for detailed view at this fault (Granger, 2006). b) Corrugations in outcrop in the Entrada Sandstone located in the Rafael Desert, Utah (meter scale). Compass shown for scale (Fossen, 2010). c) Corrugation on fault surface interpreted in 3D seismic data. Lohr et al. (2008) used these corrugations to determine slip on the fault surface (kilometer scale). See Figure 10 for detailed look at this fault.

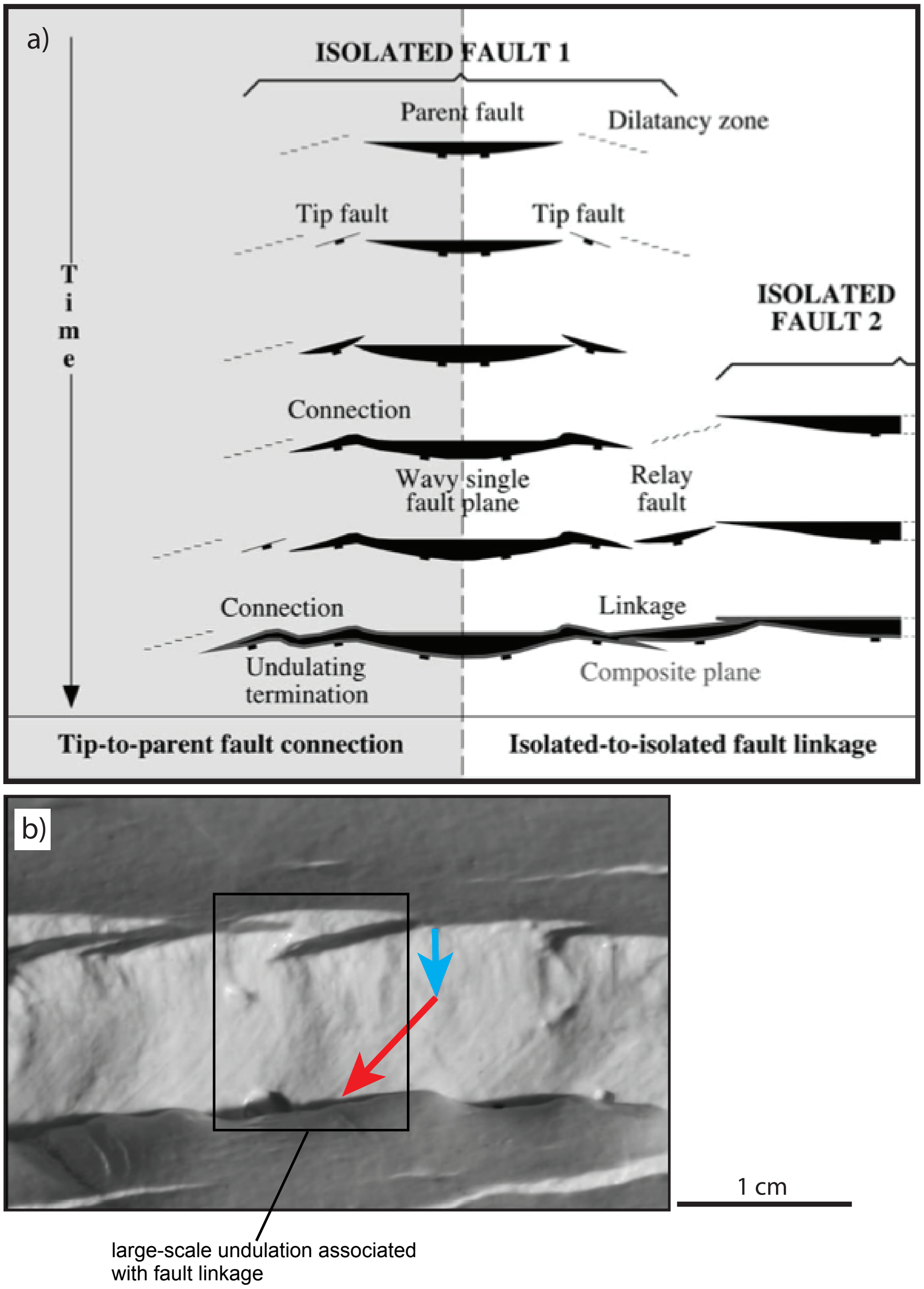

Figure 8. Examples of fault linkages resulting in an undulating fault surface. a) General model of normal-fault propagation and linkage (Marchal et al., 2003). As two faults propagate radially, they eventually overlap, form a relay fault, and then link. This process of linkage produces large-scale corrugations on the fault surface oriented parallel or sub-parallel to the slip direction. This model is based on experimental sand models. b) Example of an undulating fault surface formed during an experimental clay model with two phases of non-coaxial deformation (from Withjack et al., in prep). Breaching of relay ramps between overlapping fault segments resulted in fault linkage and formation of an undulating fault surface. Large-scale corrugations, formed during fault linkage, parallel the slip direction during the first phase of extension (blue arrow). These large-scale corrugations were mostly preserved during the second phase of extension. Small-scale corrugations that formed during the first phase of extension were overprinted during the second phase of extension (red arrow).

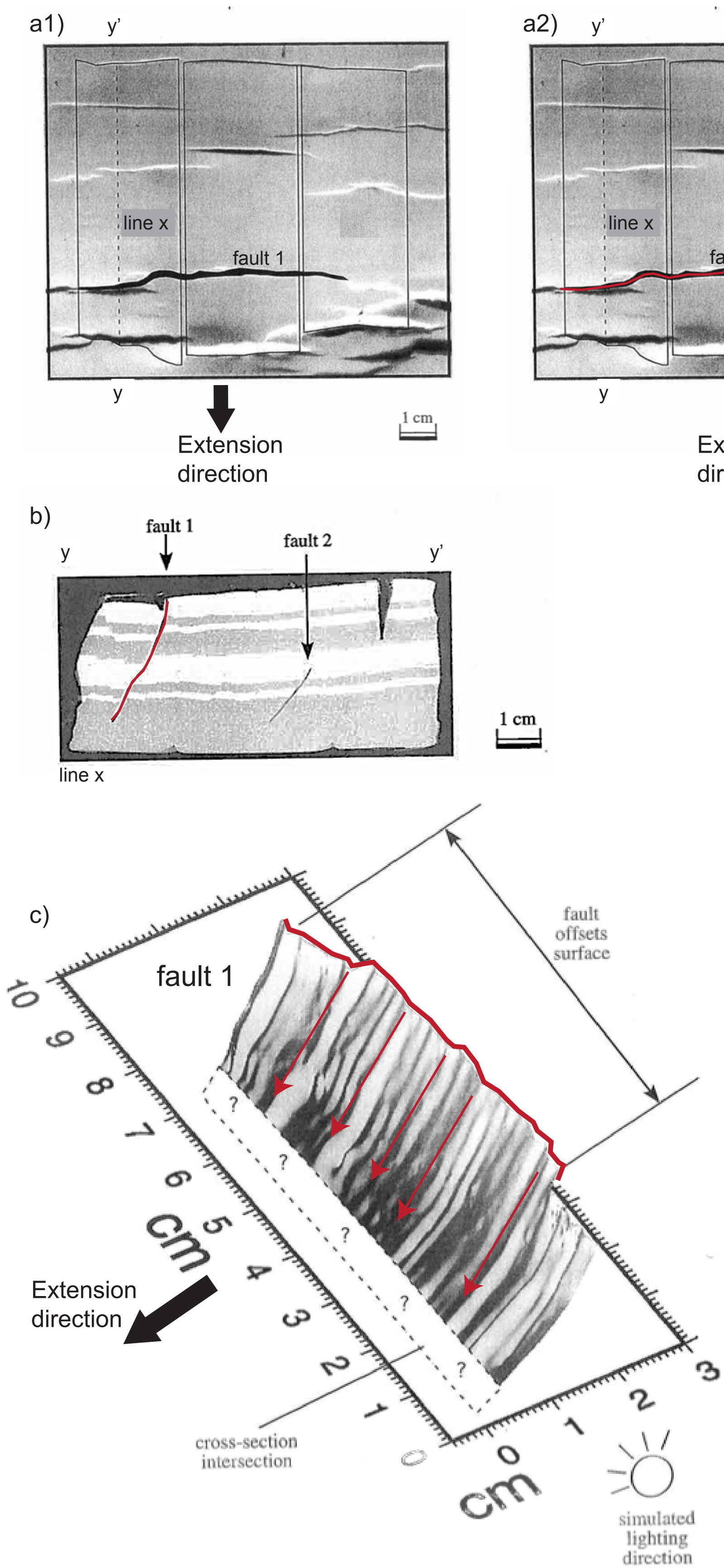

Figure 9. Corrugated normal fault formed during an experimental clay model (modified from Granger, 2006). a1) Uninterpreted map view of the experimental model showing the extension direction. a2) Map view of the model highlighting the undulating trace of fault 1. b) Cross section from y to y' with the location of fault 1 highlighted. c) Fault 1 with axial traces of main corrugations highlighted with red arrows. Corrugations formed parallel to the slip direction (red arrows), the horizontal component of which is parallel to the extension direction.

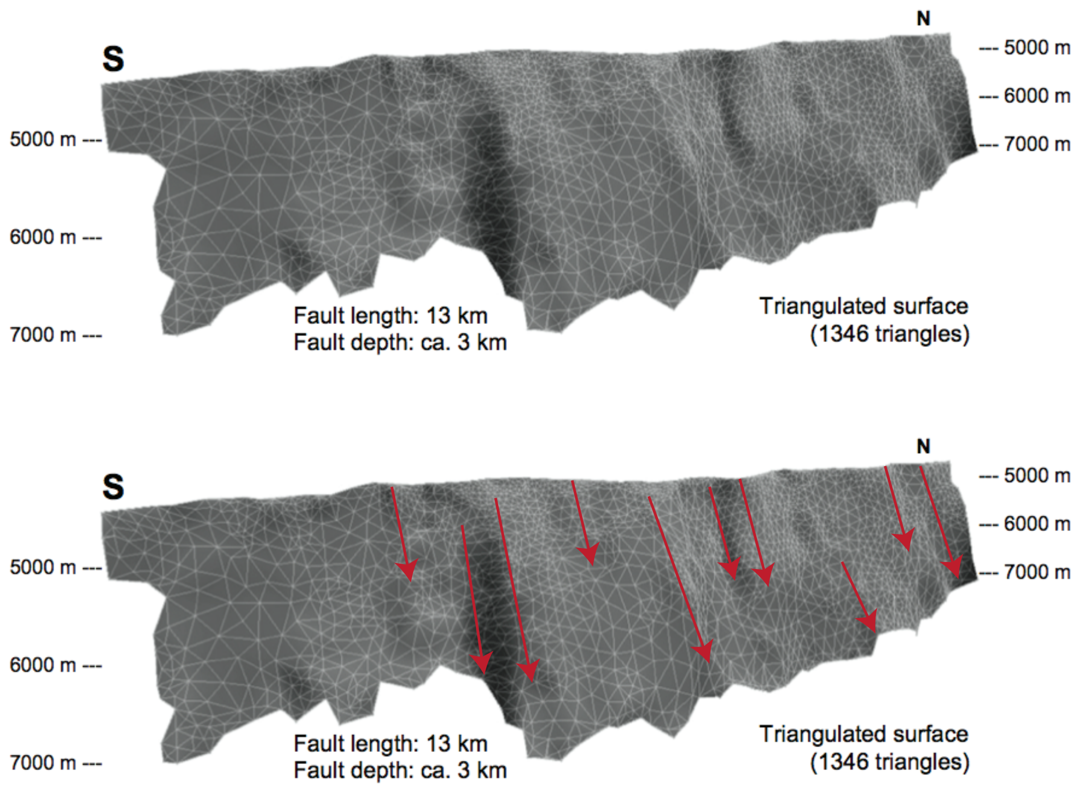

Figure 10. 3D rendering of a normal fault from the Northwest German basin (modified from Lohr et al., 2008). Lohr et al. (2008) determined the slip direction of the fault using the orientation of fault-surface undulations that they assumed to be corrugations (highlighted with red arrows). The axial traces of the corrugations do not necessarily extend the entire way down the fault surface, but overall, their rake is 89°.

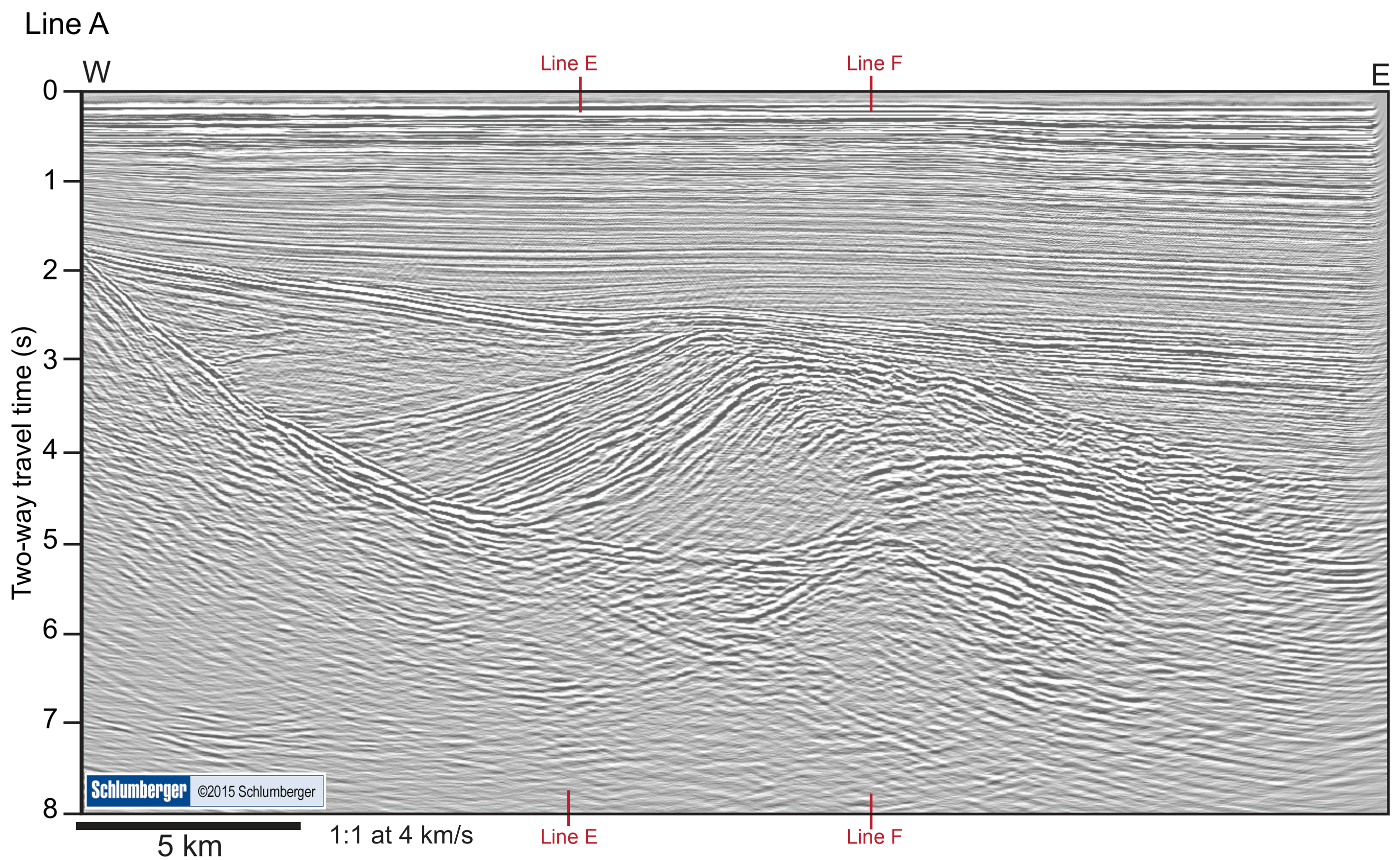

Figure 11a. Uninterpreted seismic line A. See line location in Figure 4b.

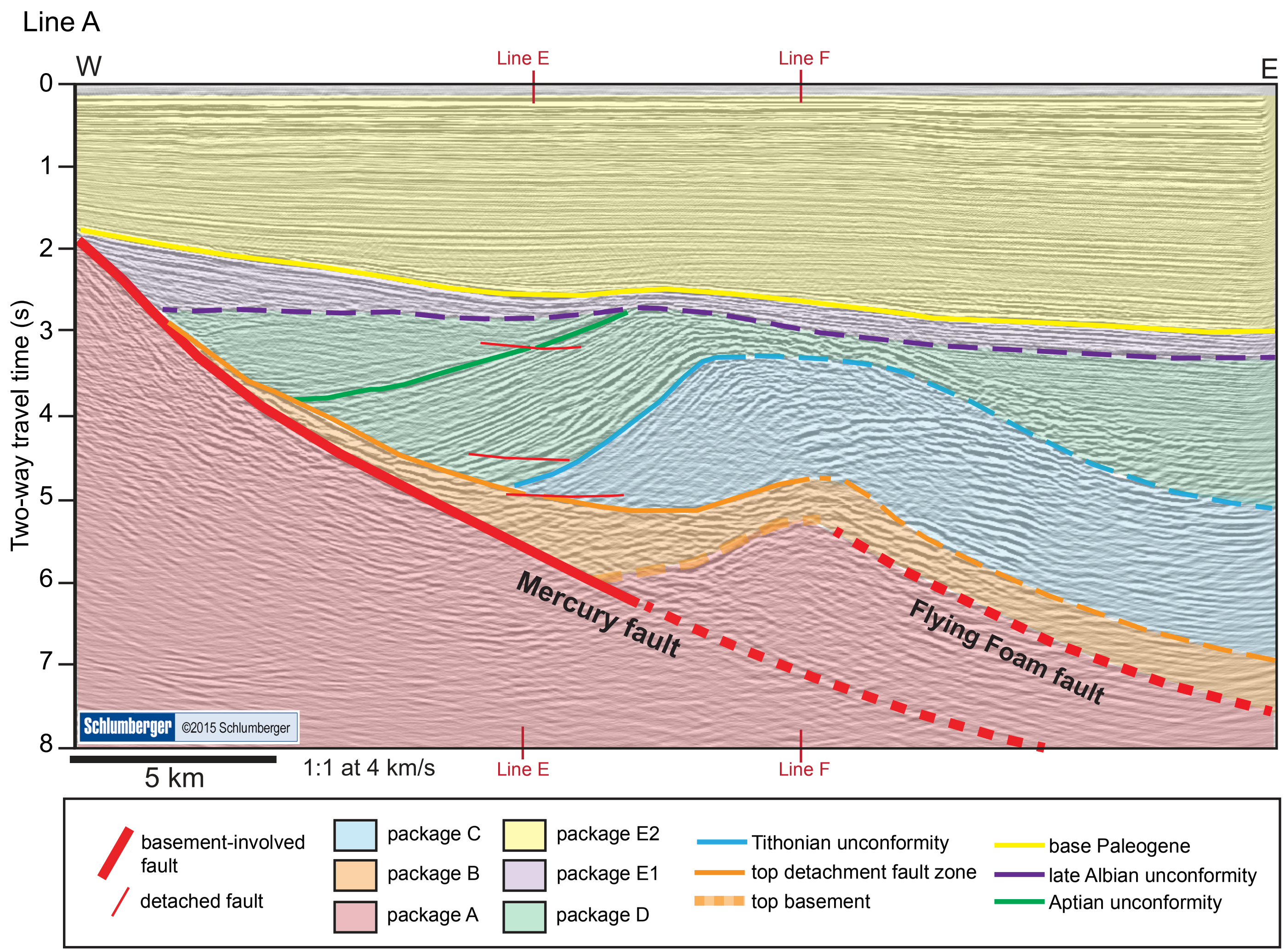

Figure 11b. Interpreted line A showing major faults and six tectonostratigraphic packages. Dashed lines indicate uncertainty of interpreted faults and horizons. See line location in Figure 4b.

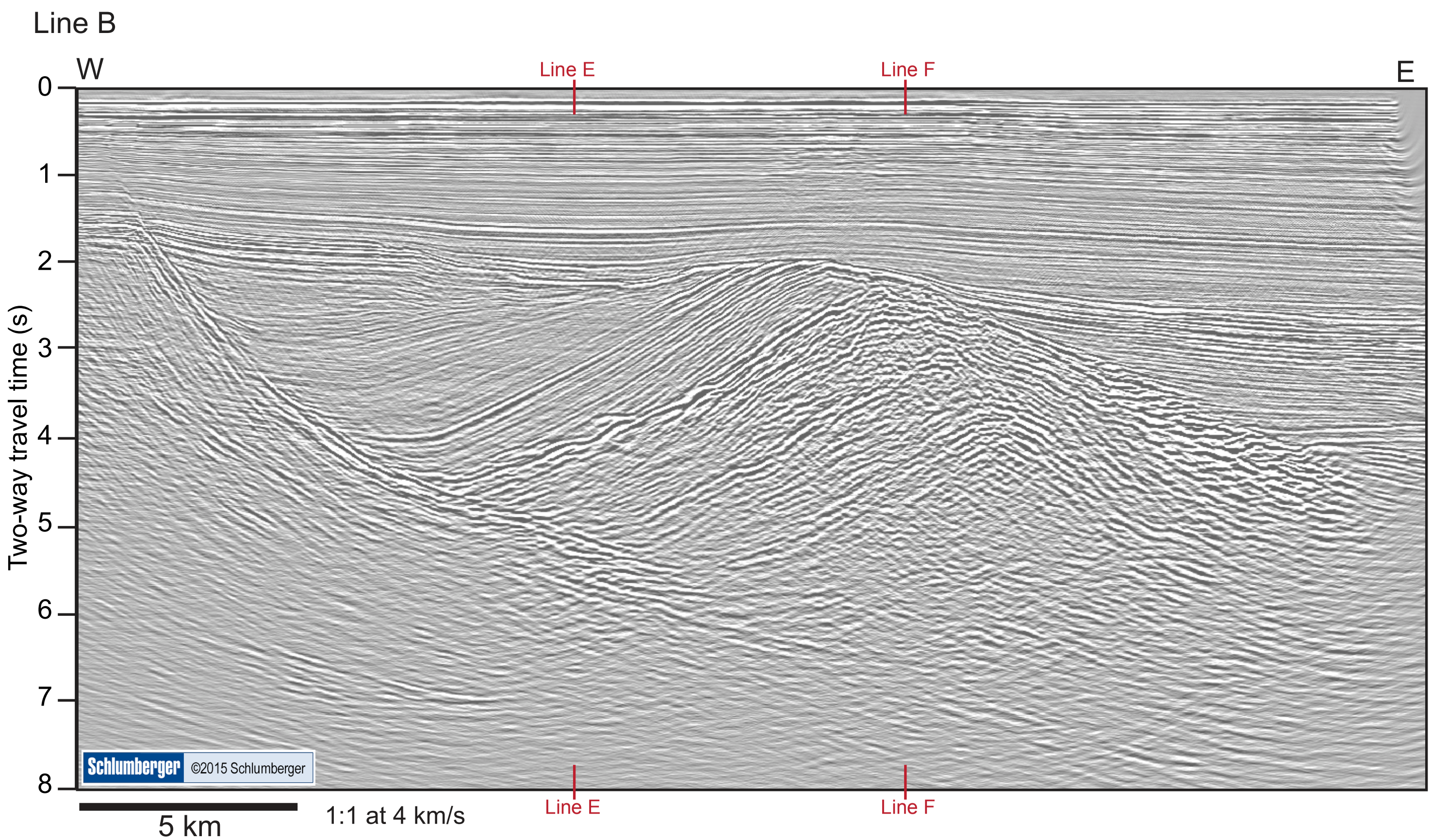

Figure 12a. Uninterpreted seismic line B. See line location in Figure 4b.

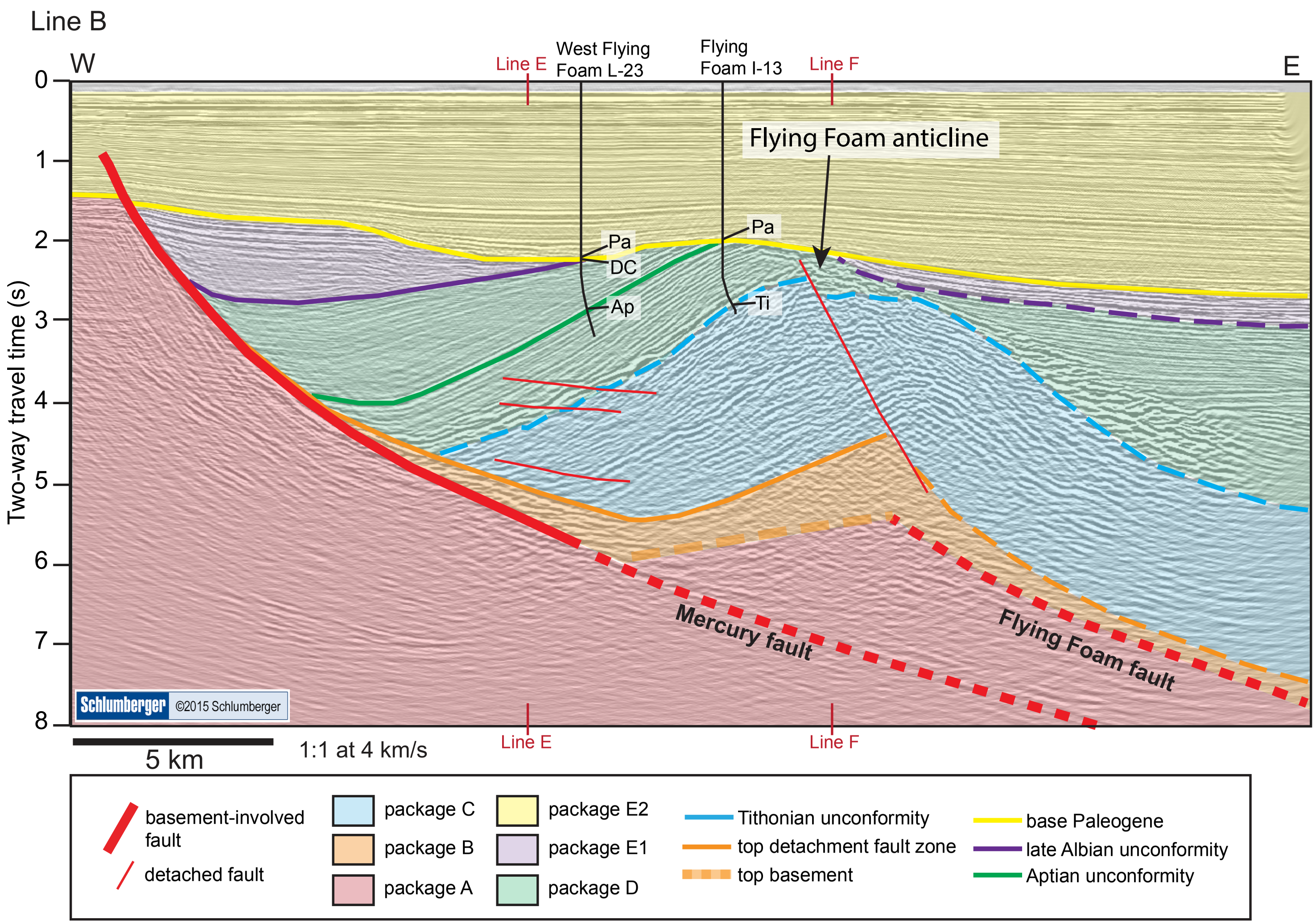

Figure12b. Interpreted line B showing major faults and six tectonostratigraphic packages. Tops of horizons used to tie well data to seismic data are: Pa-base-Paleogene, DC- base Dawson Canyon Formaion, Ap-Aptian unconformity, Ti-Tithonian unconformity. The base of the Dawson Canyon Formation correlates with the late Albian unconformity (Fig. 3). Dashed lines indicate uncertainty of interpreted faults and horizons. See line and well locations in Figure 4b.

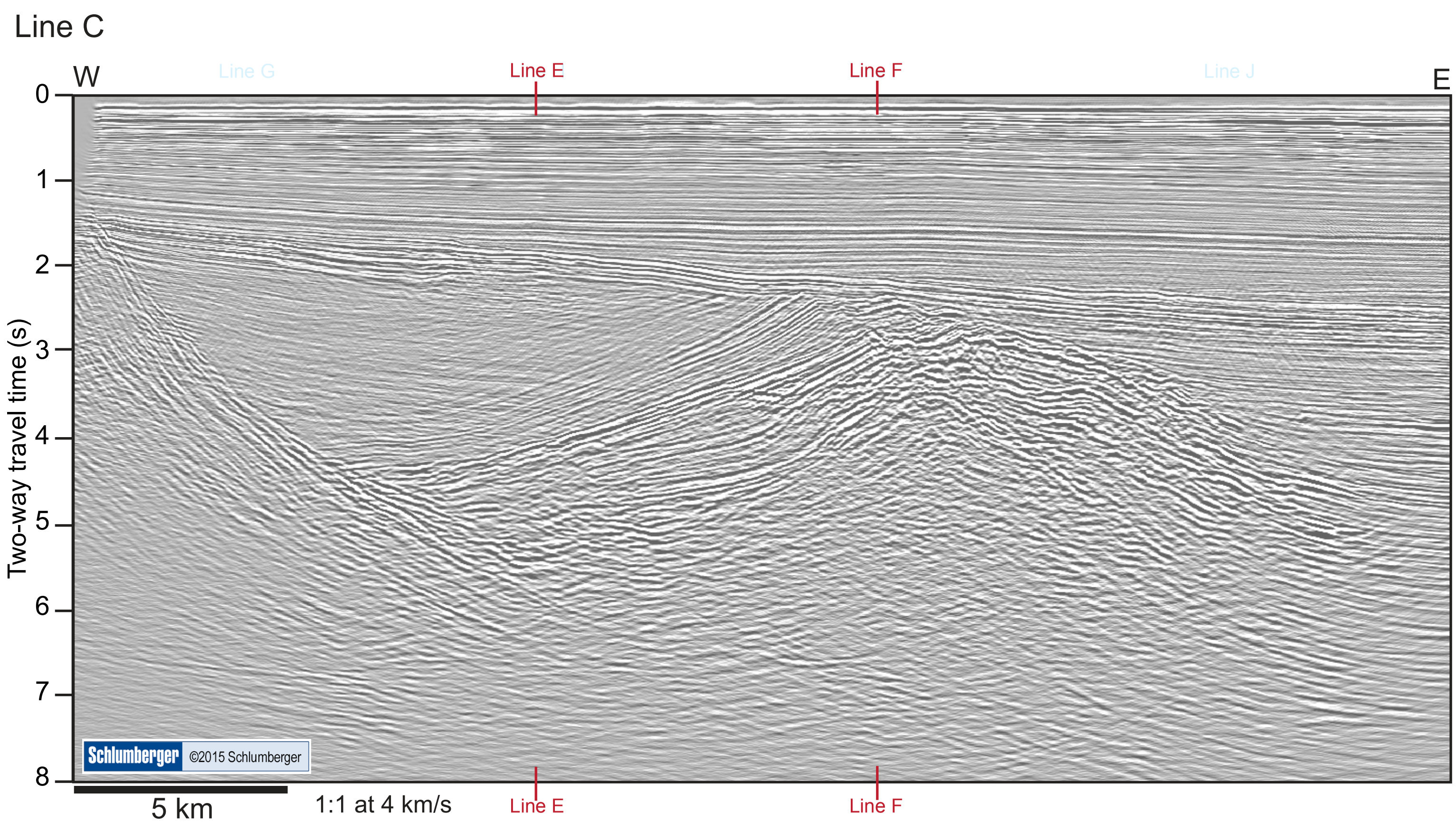

Figure 13a. Uninterpreted seismic line C. See line location in Figure 4b.

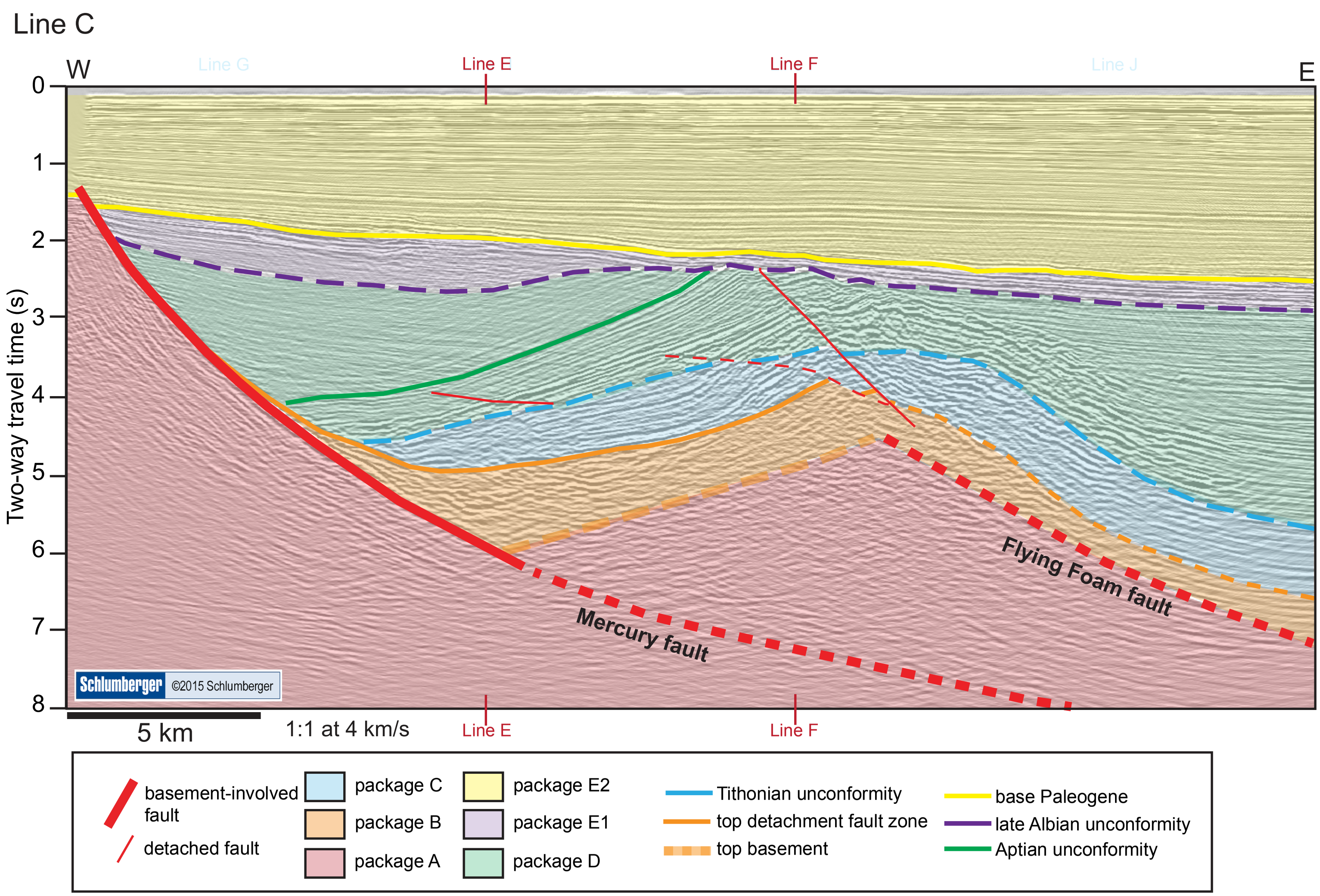

Figure 13b. Interpreted line C showing major faults and six tectonostratigraphic packages. Dashed lines indicate uncertainty of interpreted faults and horizons. See line location in Figure 4b.

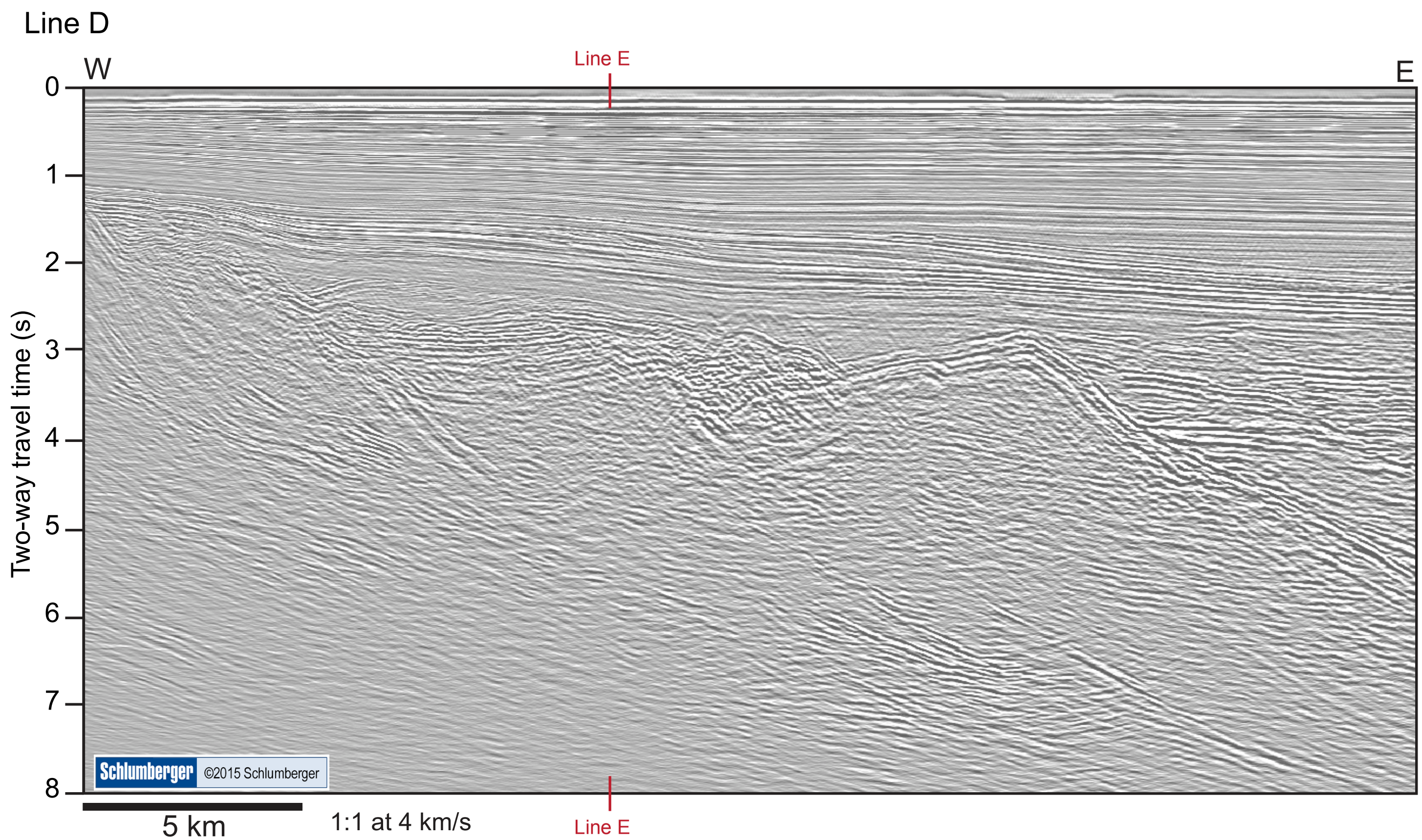

Figure 14a. Uninterpreted seismic line D. See line location in Figure 4b.

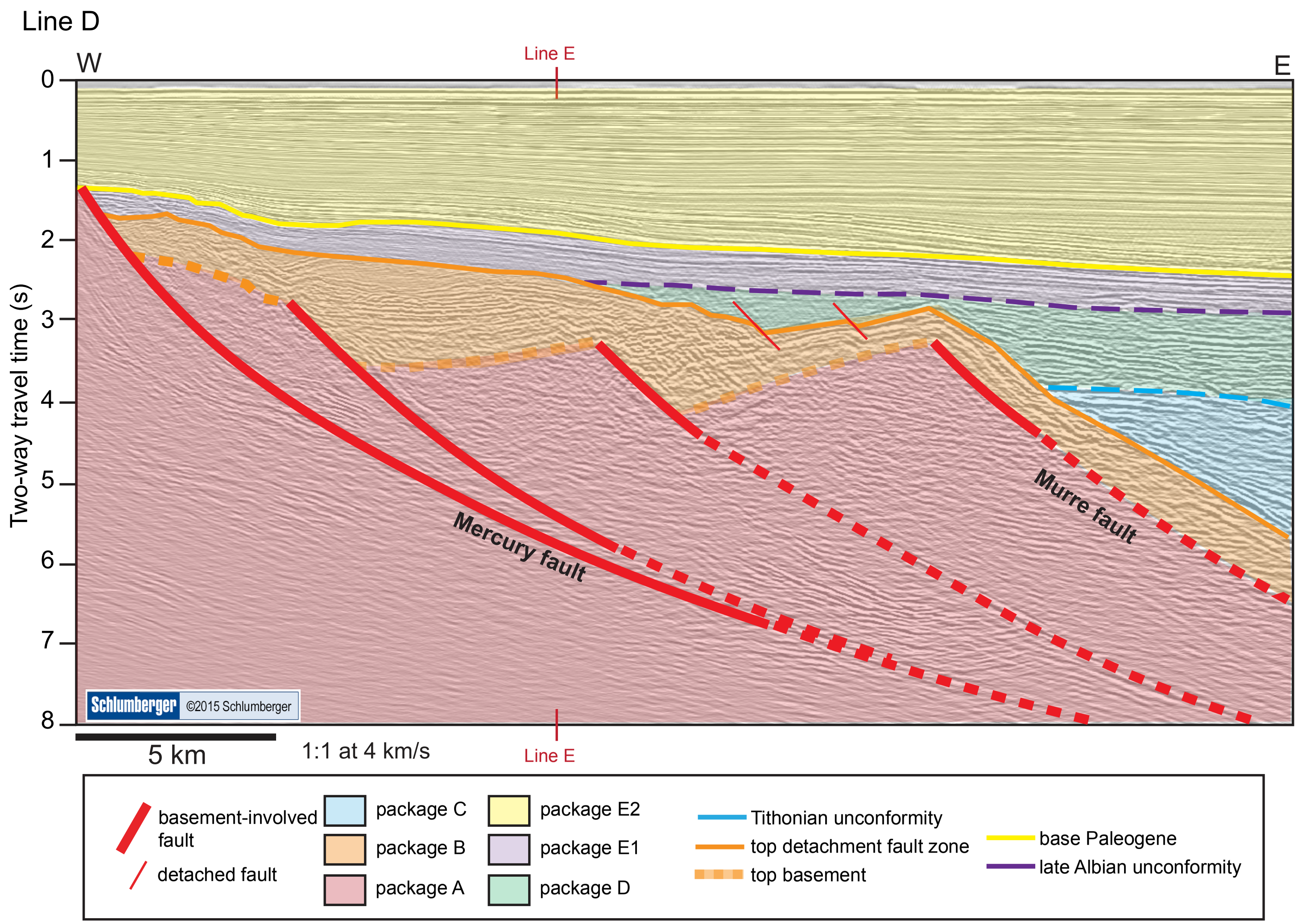

Figure 14b. Interpreted line D showing major faults and six tectonostratigraphic packages. Dashed lines indicate uncertainty of interpreted faults and horizons. See line location in Figure 4b.

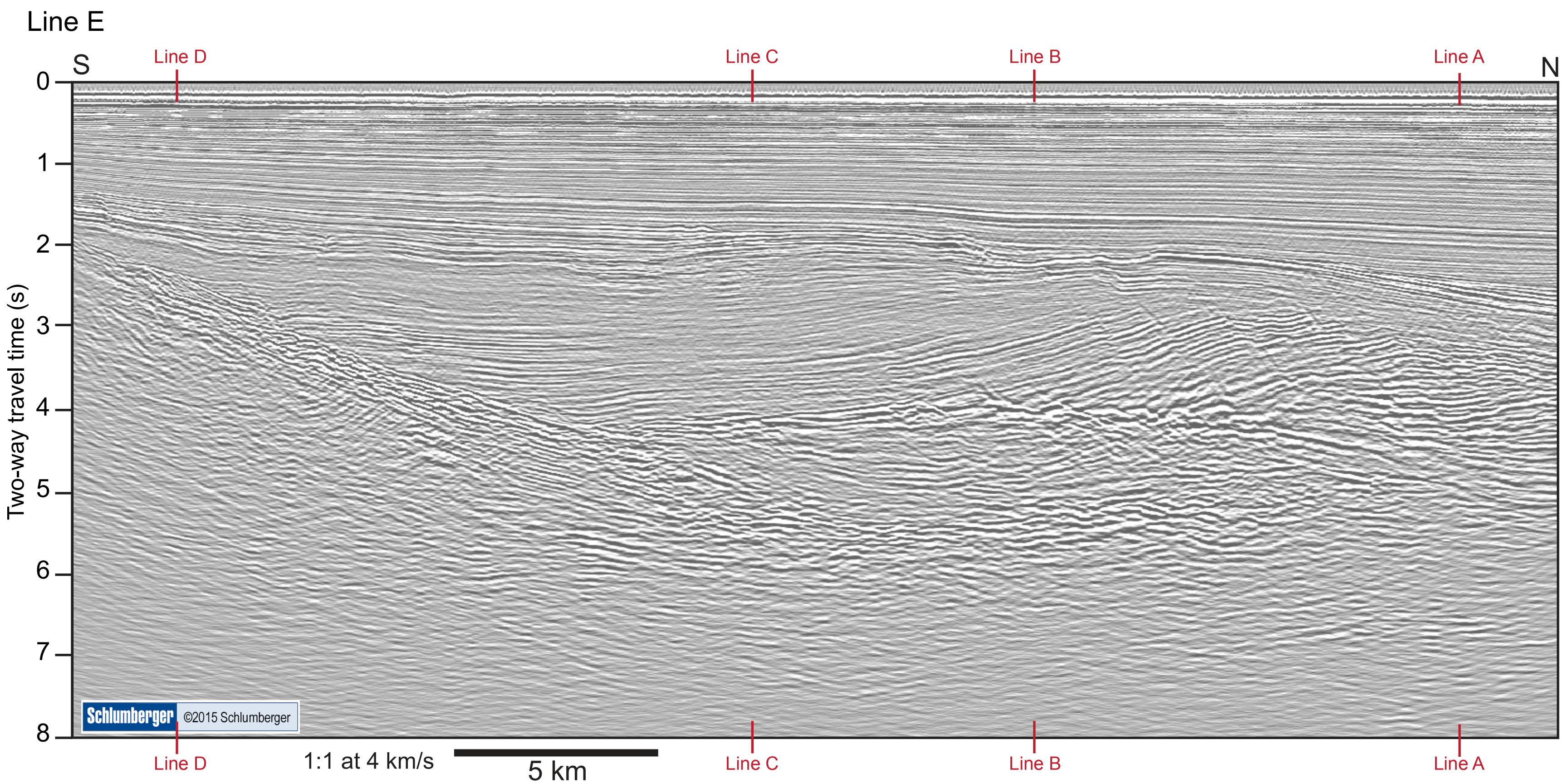

Figure 15a. Uninterpreted seismic line E. See line location in Figure 4b.

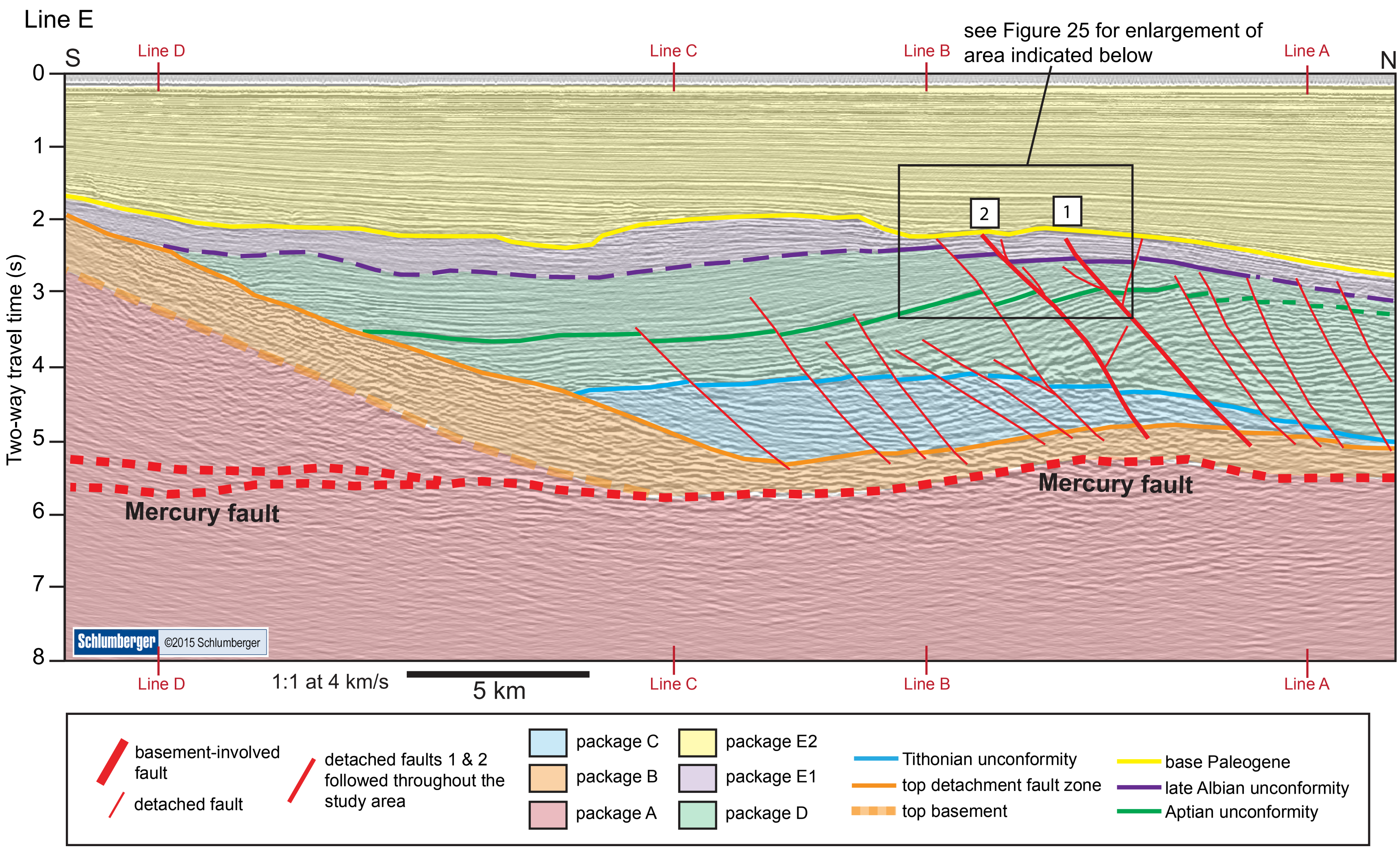

Figure 15b. Interpreted line E showing major faults and six tectonostratigraphic packages. Dashed lines indicate uncertainty of interpreted faults and horizons. See line location in Figure 4b.

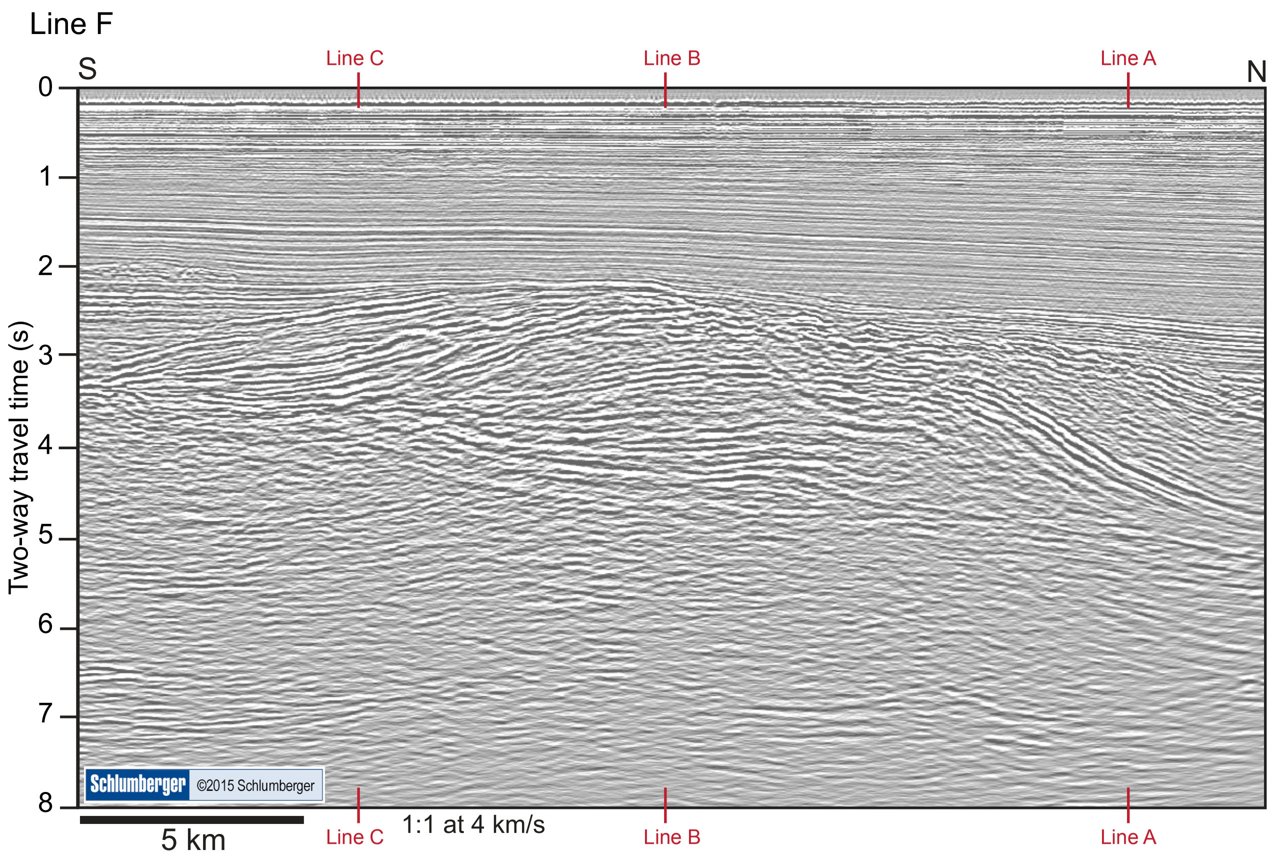

Figure 16a. Uninterpreted seismic line F. See line location in Figure 4b.

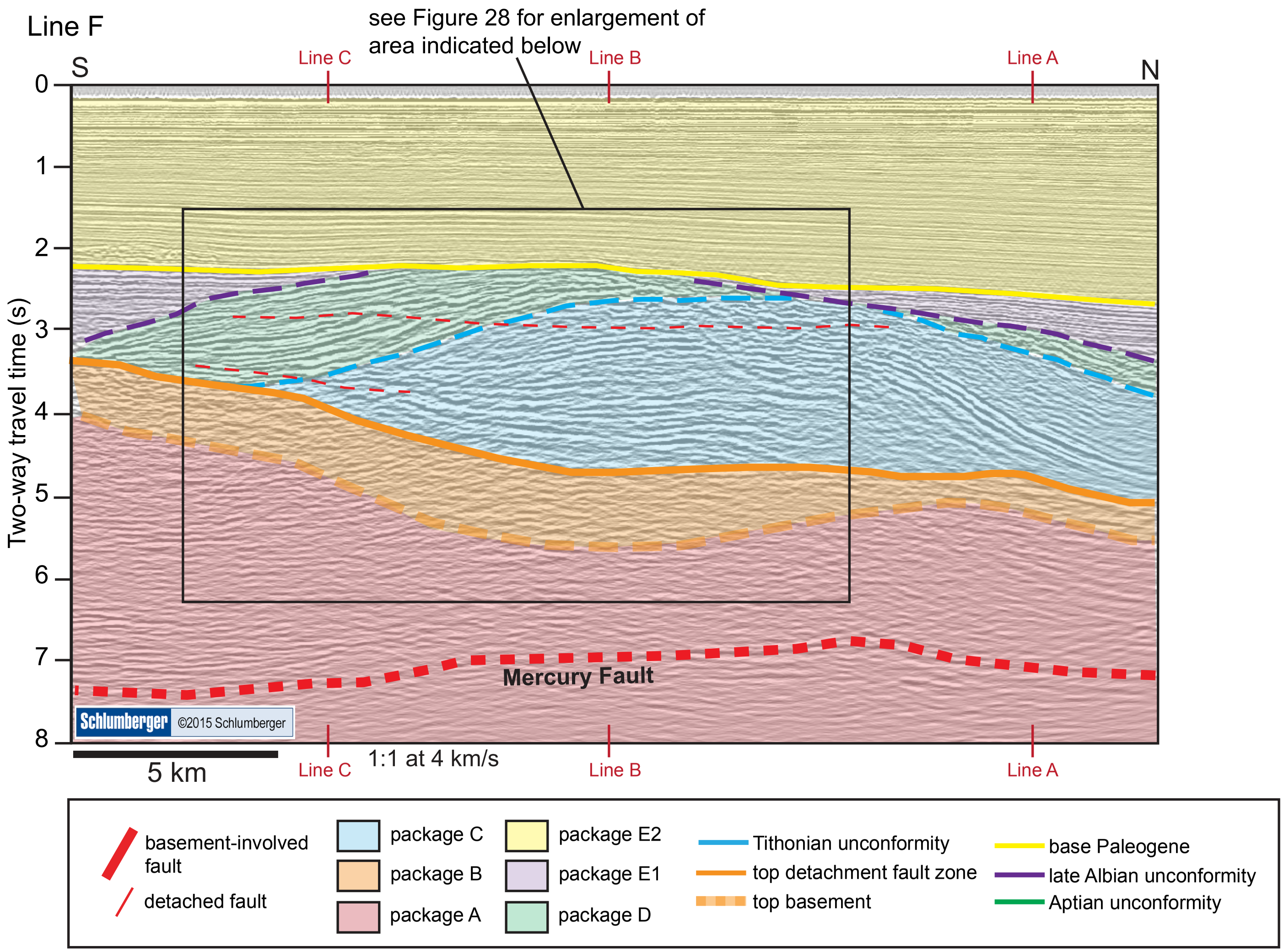

Figure 16b. Interpreted line F showing major faults and six tectonostratigraphic packages. Dashed lines indicate uncertainty of interpreted faults and horizons. See line location in Figure 4b.

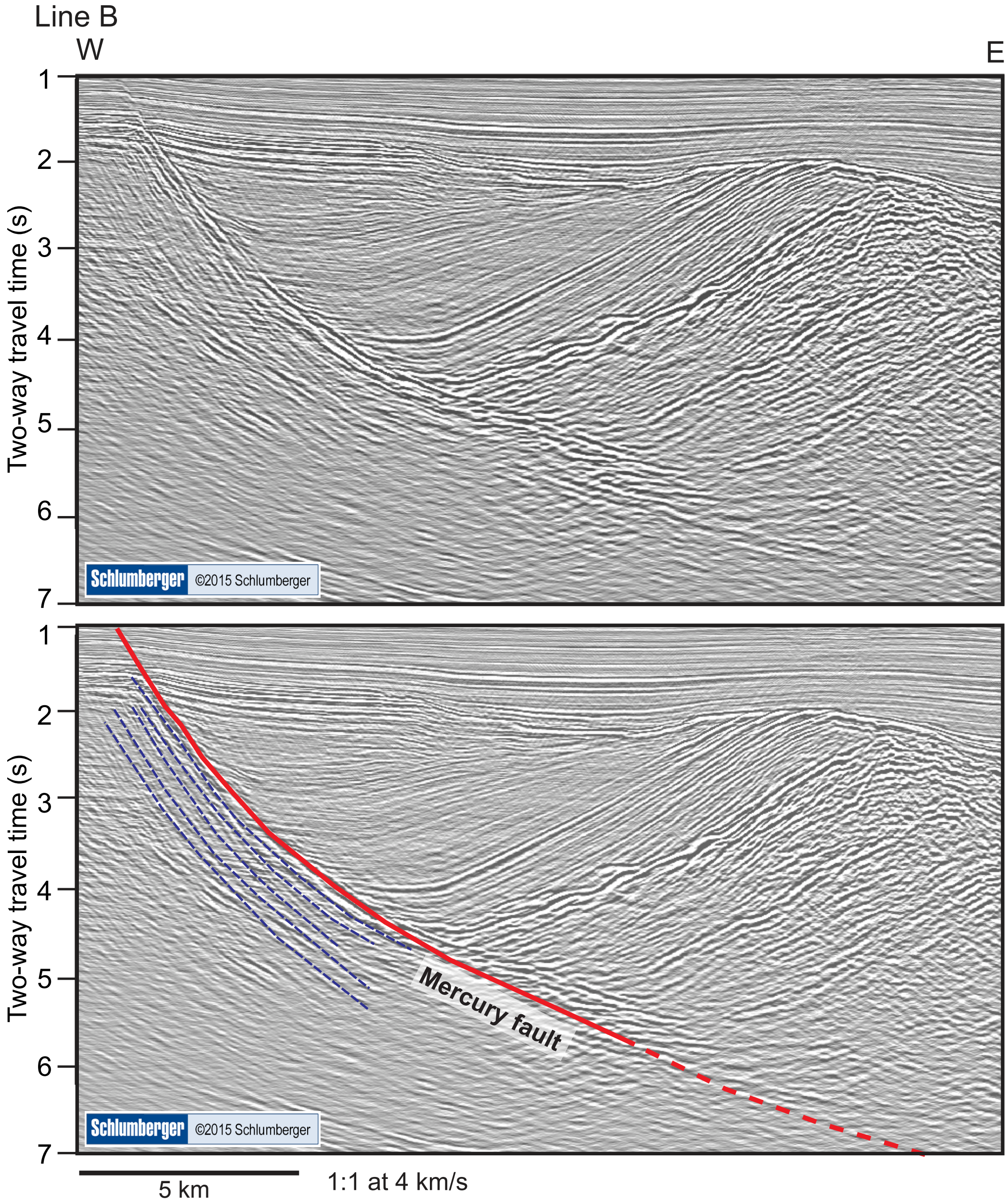

Figure 17. Section of seismic line B showing the the Mercury fault (red line) and peg-leg multiples of the Mercury fault (blue dashed lines). See complete line in Figure 12 and line location in Figure 4b.

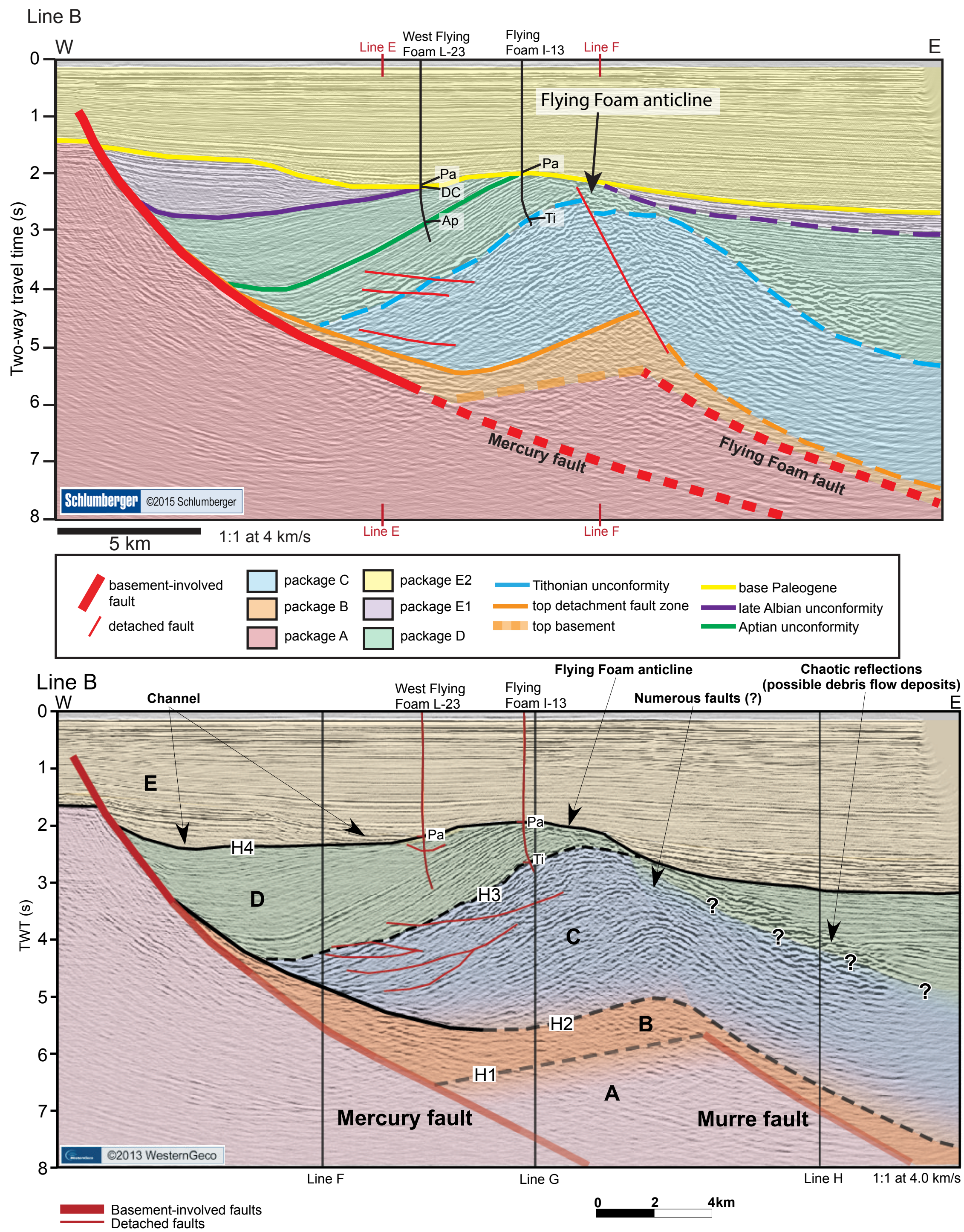

Figure 18. Comparison of the interpretation of line B in this study (top) to the interpretation by Serrano Suarez (2013)(bottom). H1, H2, H3, and H4 in the interpretation by Serrano Suarez (2013) correlate with the top of basement, the top of the detachment fault zone, the Tithonian unconformity, and the base-Paleogene, respectively. See line location in Figure 4b and an uninterpreted line B in Figure 12a.

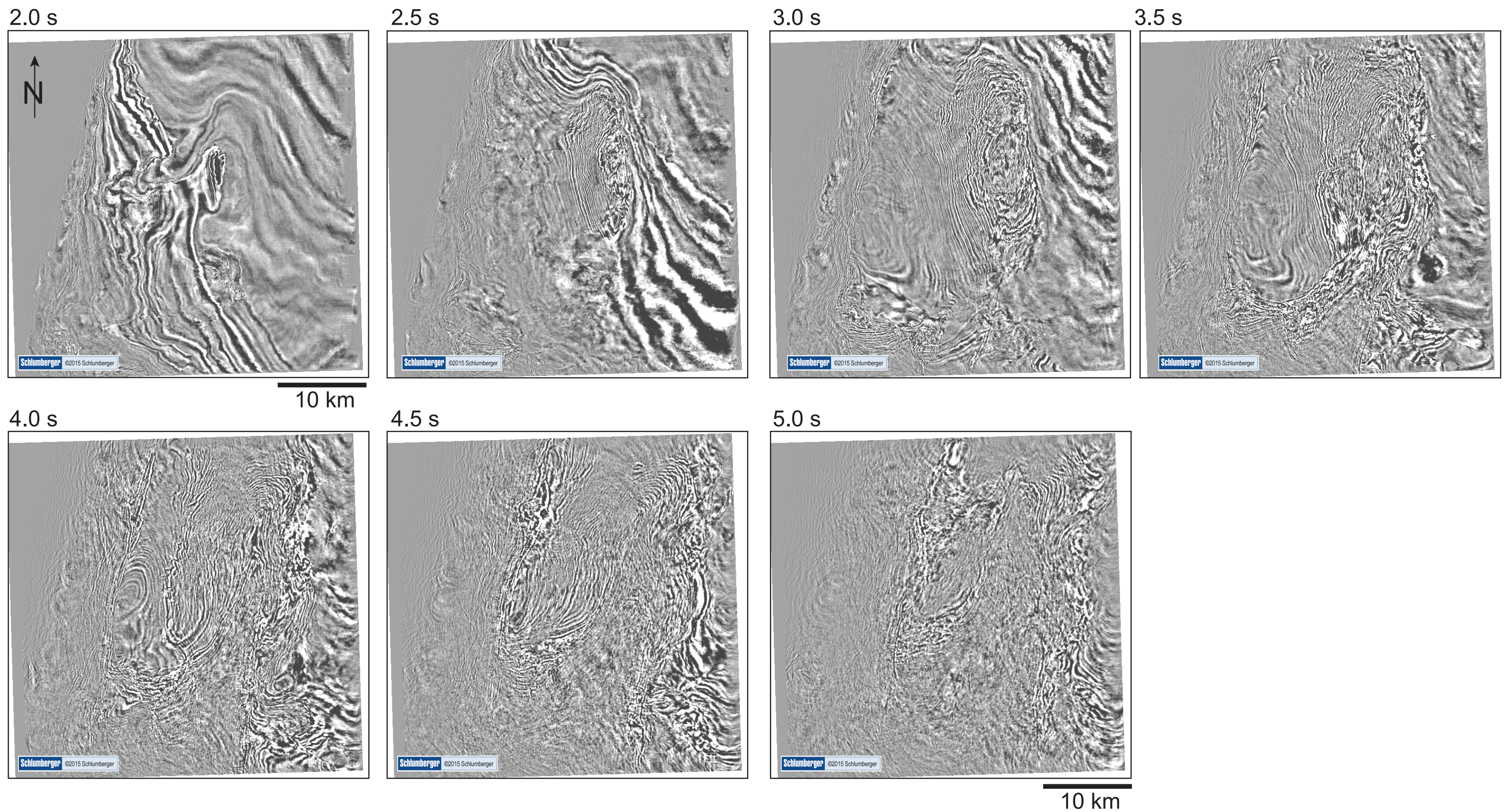

Figure 19a. Seven uninterpreted time slices from 2 s to 5 s in 0.5 s intervals of two-way travel time.

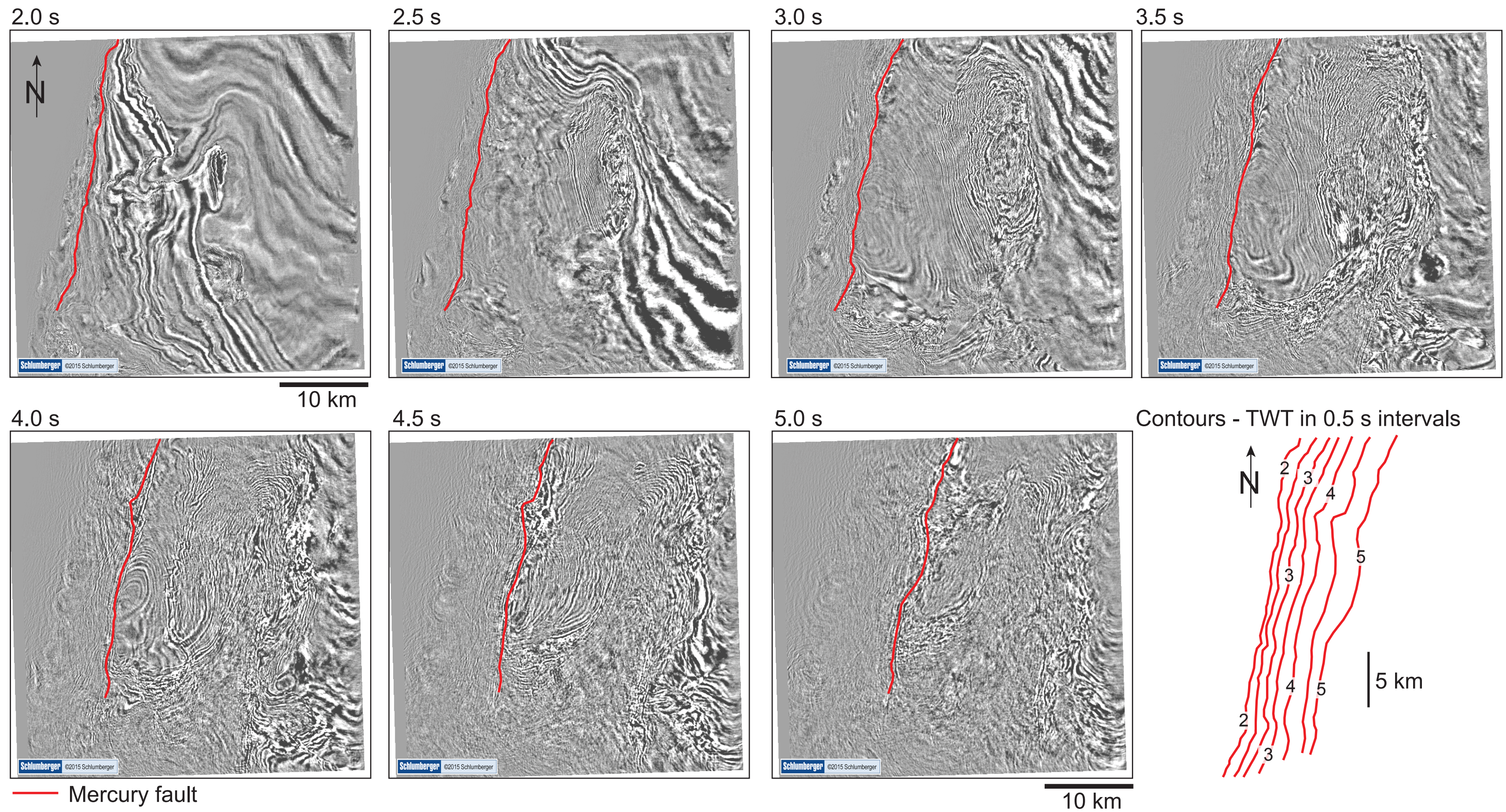

Figure 19b. Trace of the Mercury fault on seven time slices. Placing all traces in the same map generates a structure-contour map of the fault surface. See Figure 20 for detailed analysis of the contour map.

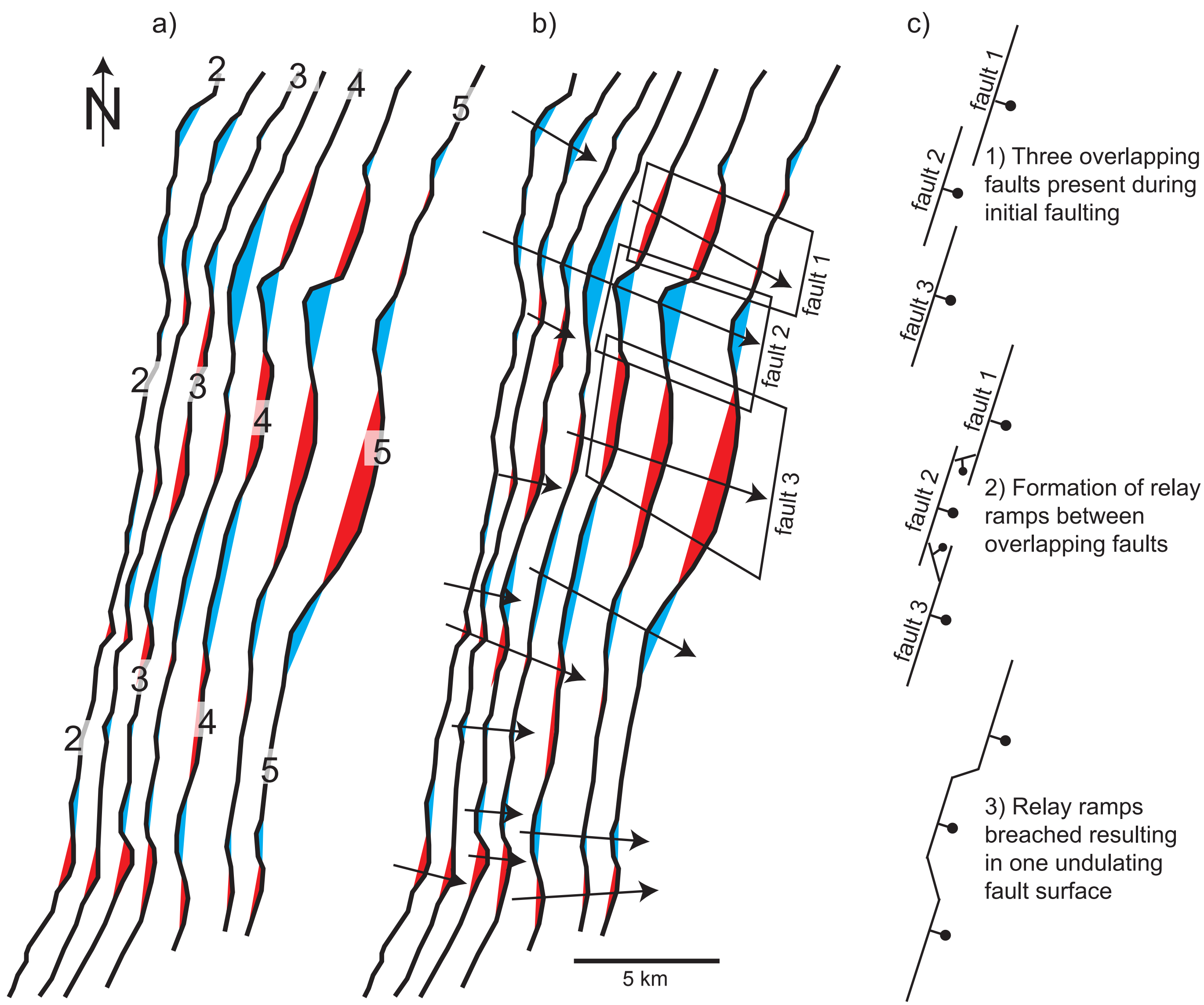

Figure 20. Structure-contour map of the Mercury fault.
a) Black lines are contours of two-way travel time in 0.5 s intervals, and red and blue fill in topographic highs and lows, respectively.
b) Axial traces of continuous topographic highs and lows have an overall trend of ESE. Black boxes highlight possible locations of faults 1, 2, and 3 (shown in part c) during initial faulting.
c) Schematic example of the linkage of faults 1, 2, and 3 during the the first phase of rifting resulting in the topographic low on the northern part of the fault surface.

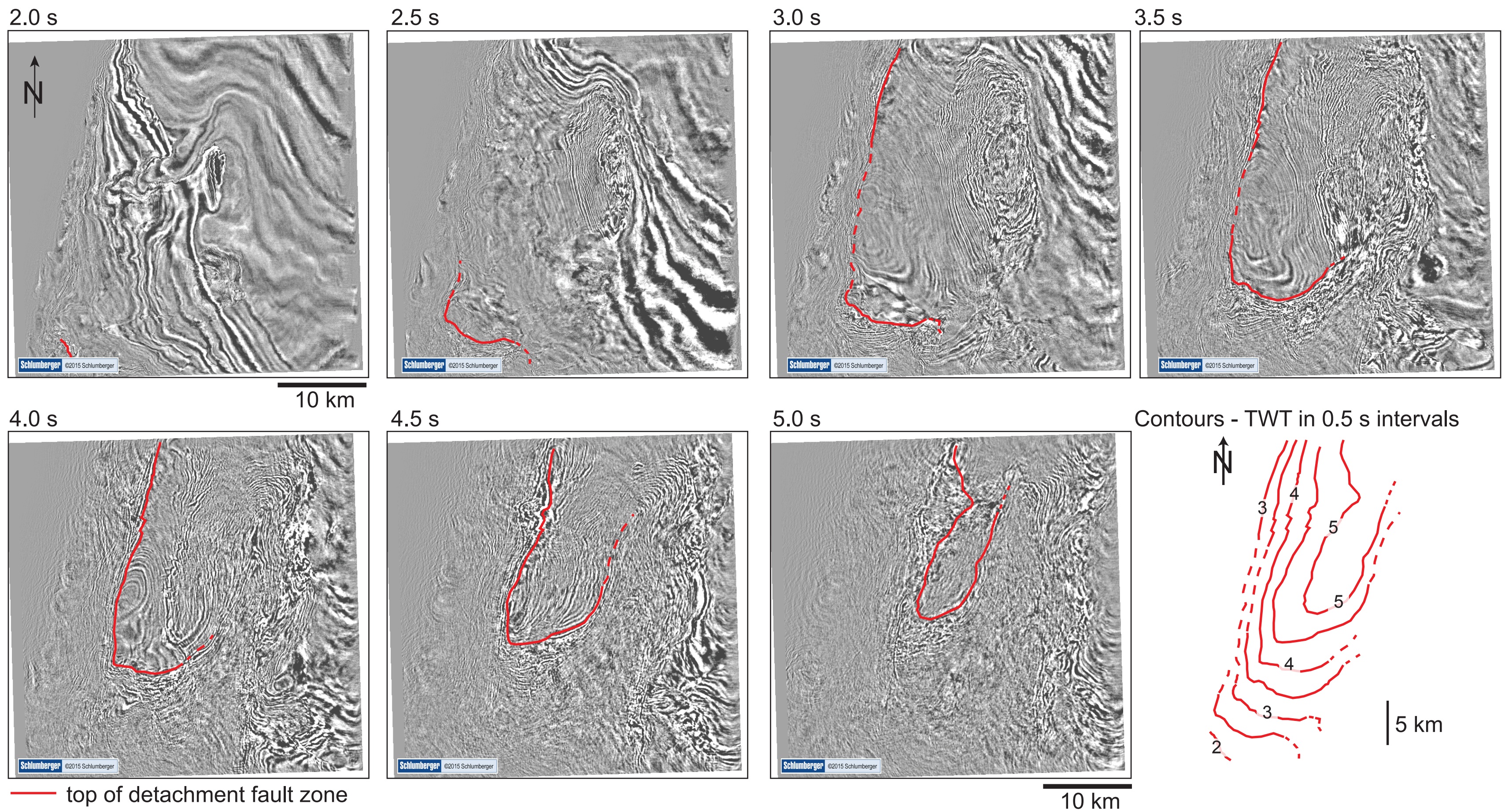

Figure 21. Trace of the top of the detachment fault zone on seven time slices. Placing all traces in the same map generates a structure-contour map of the fault surface. Dashed lines indicate uncertainty. See Figure 19a for uninterpreted time slices. See Figure 22 for detailed analysis of the contour map.

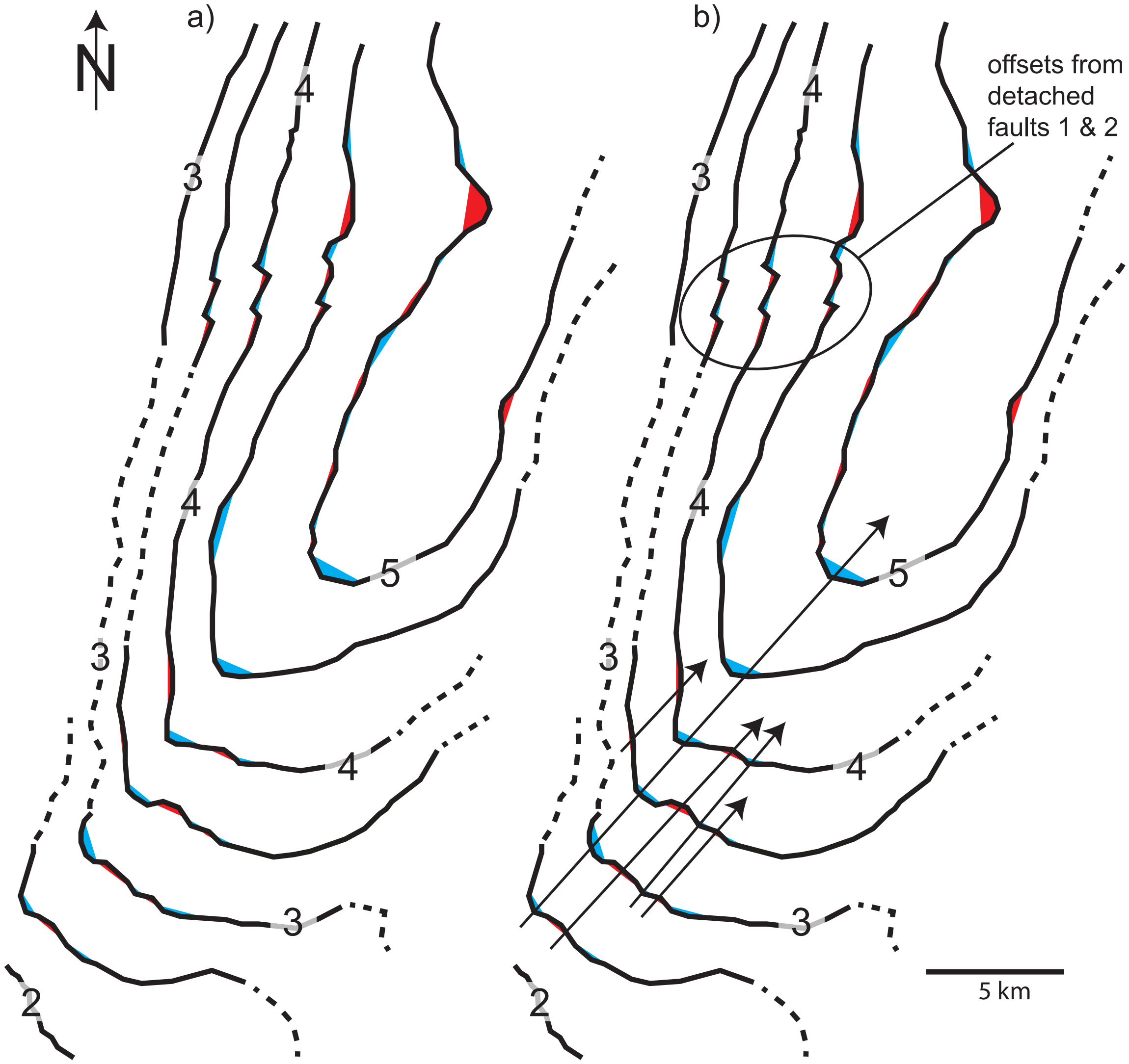

Figure 22. Structure-contour map of the top of the detachment fault zone. a) Black lines are contours of two-way travel time in 0.5 s intervals, and red and blue fill in topographic highs and lows, respectively. Undulations on uncertain contours on the detachment fault zone (dotted black lines) are not highlighted with red or blue. The fault zone strikes NNE in the northern part of the study area and ESE in the southwestern part. This change in strike occurs farther north at deeper levels, which is a result of the northwestward tilt of the detachment fault zone. Dashed lines indicate uncertainty. b) Detached faults offset the top of the detachment fault zone and produce alignments in bends in the contour lines. Undulations on the southern part of the top of the detachment fault zone have axial traces trending NE. These are not undulations related to fault linkage.

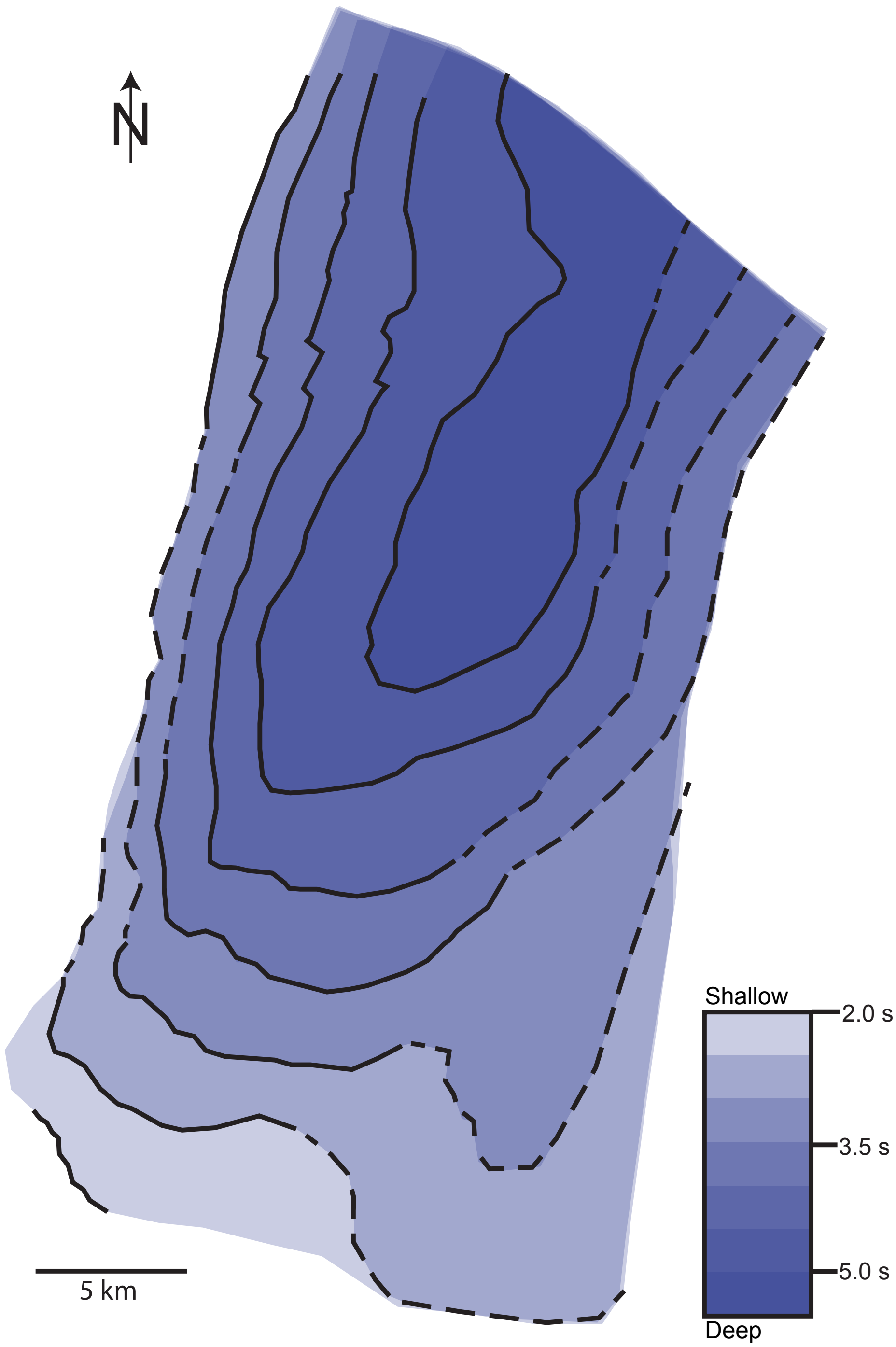

Figure 23. Shaded structure-contour map of the top of detachment fault zone illustrating the trough shape of the fault surface. Dashed lines indicate uncertainty.

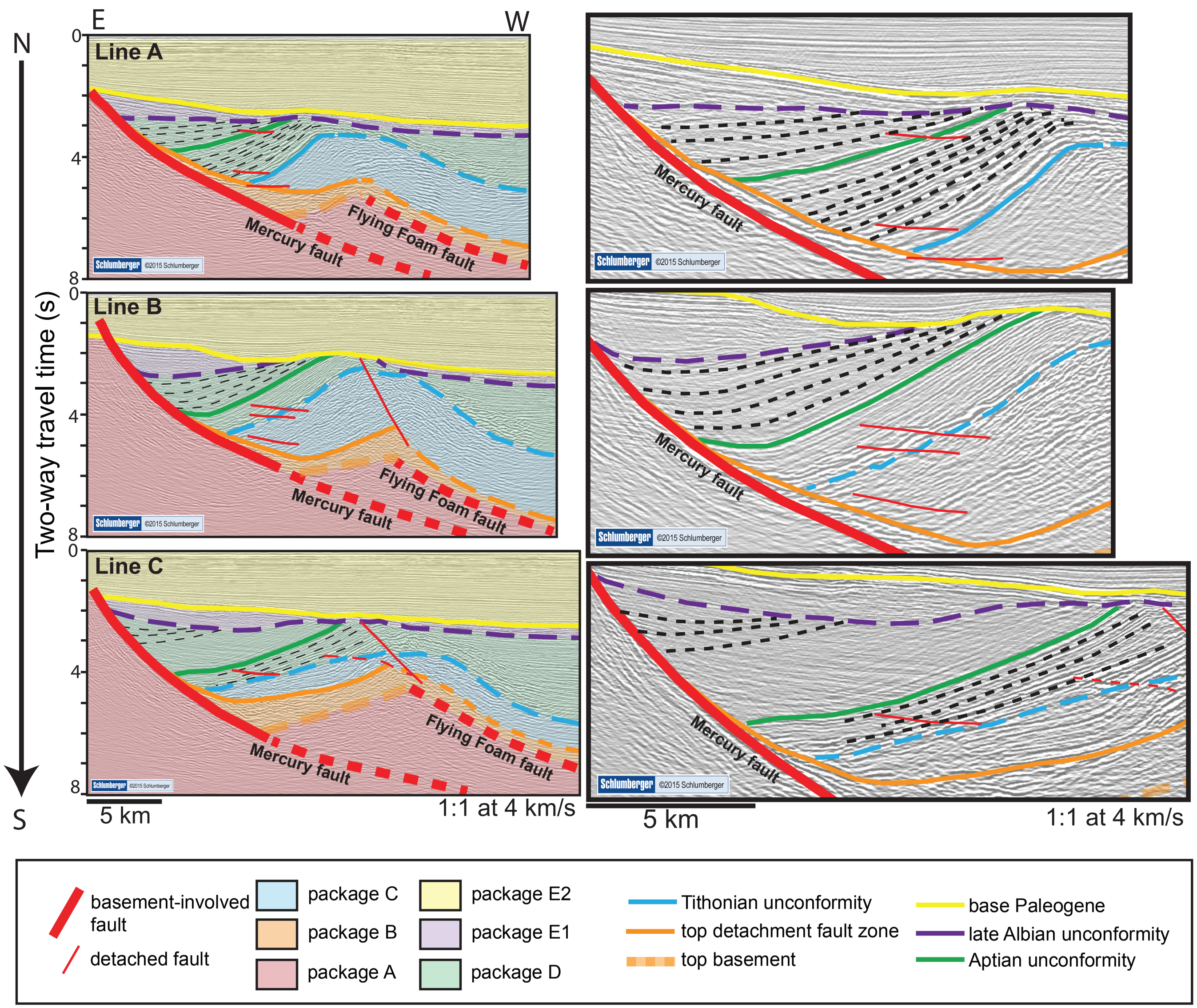

Figure 24. Lines A-C with enlarged view of package D (green unit between the late Albian (purple) and Tithonian (blue) unconformities). Green line is the Aptain unconformity. Black dashed lines highlight diverging reflections within package D. The age of the oldest westward diverging reflections decreases southward, indicating that a component of E-directed movement on the detachment fault zone (orange) began in the north and propagated southward. Reflections beneath the Aptian unconformity on line C thicken toward the crest of the Flying Foam anticline, indicating that the Flying Foam anticline had not yet formed here during depositions. See Figure 4b for location of lines, and Figures 11-13 for uninterpreted lines.

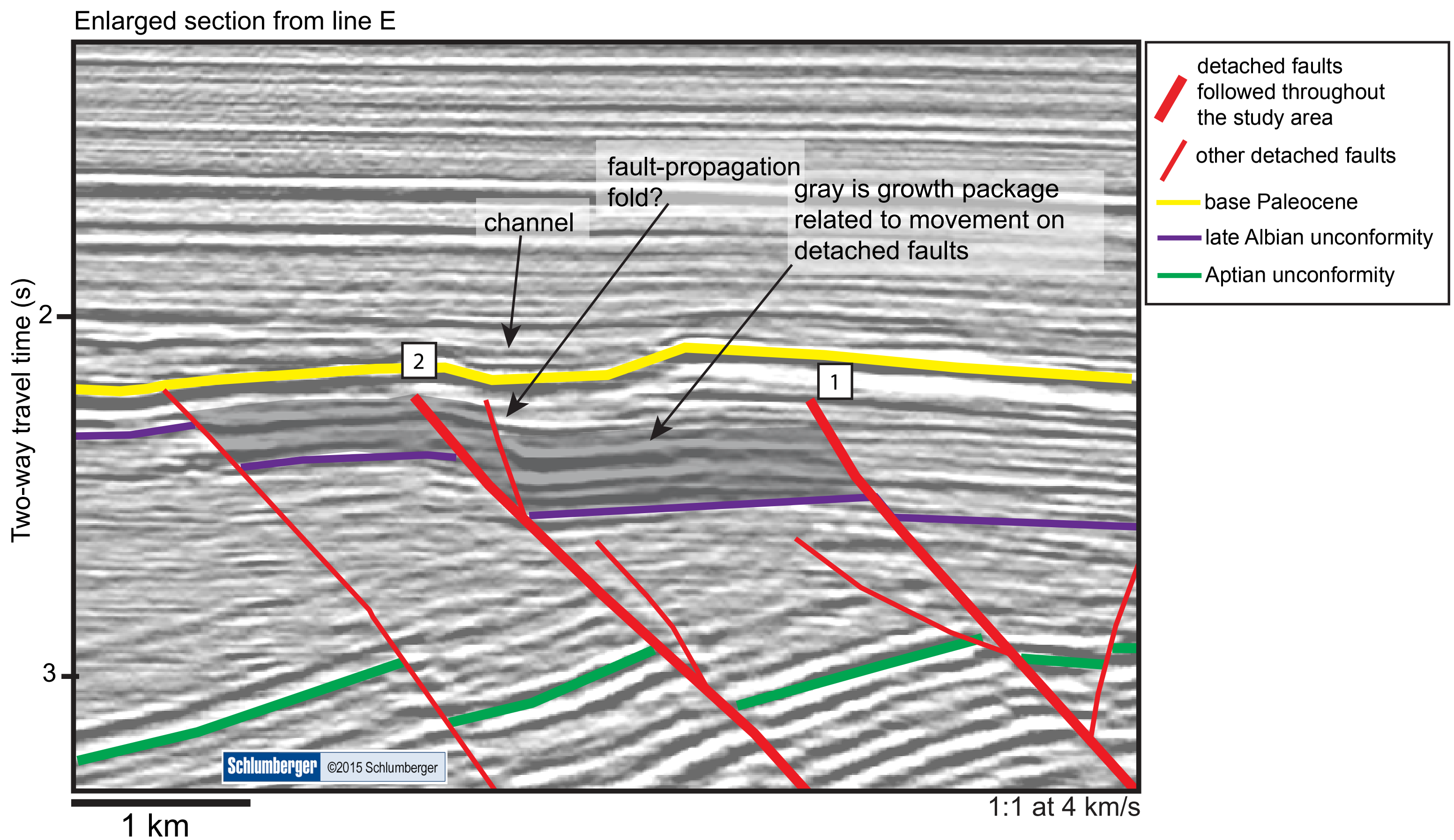

Figure 25. Interpreted, enlarged section of line E. See Figure 15 for location. The gray unit is thicker in the hanging wall than the footwall of fault 2. Therefore, the gray package is a growth package and indicates movement on the detached faults after formation of the late Albian unconformity. No clear growth strata are present between the Aptian and late Albian unconformities, but growth packages may have undergone erosion during formation of the late Albian unconformity. Dashed lines indicate uncertainty.

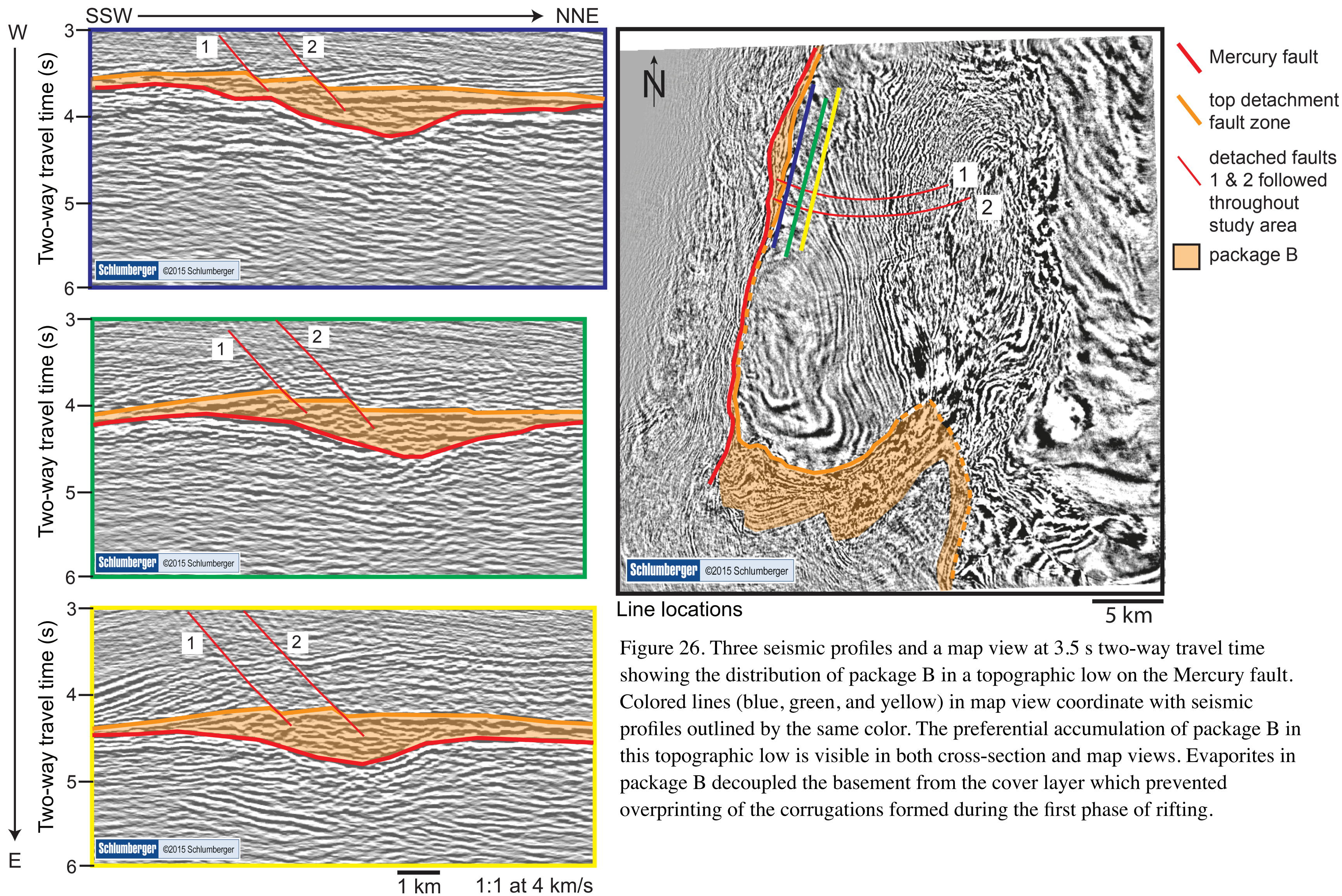

Figure 26. Three seismic profiles and a map view at 3.5 s two-way travel time showing the distribution of package B in a topographic low on the Mercury fault. Colored lines (blue, green, and yellow) in map view coordinate with seismic profiles outlined by the same color. The preferential accumulation of package B in this topographic low is visible in both cross-section and map views. Evaporites in package B decoupled the basement from the cover layer which prevented overprinting of the corrugations formed during the first phase of rifting.

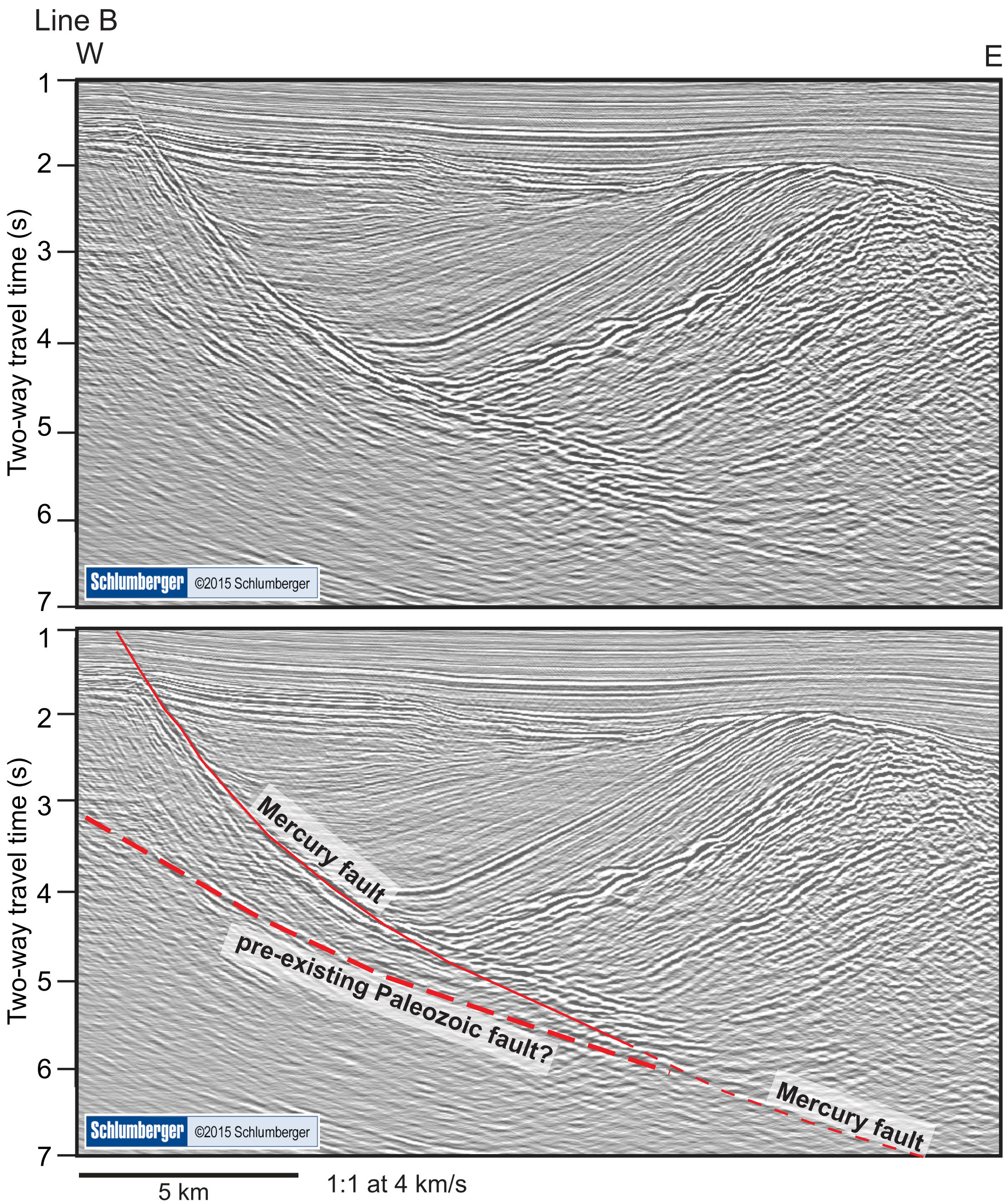

Figure 27. Part of seismic line B showing the present day Mercury fault and the location of the inferred pre-existing Paleozoic thrust fault. Reactivation may have occurred on this pre-existing zone of weakness at depth during rifting, and the present day Mercury fault splayed from the pre-existing fault at shallow levels. See complete line in Figure 12 and line location in Figure 4b.

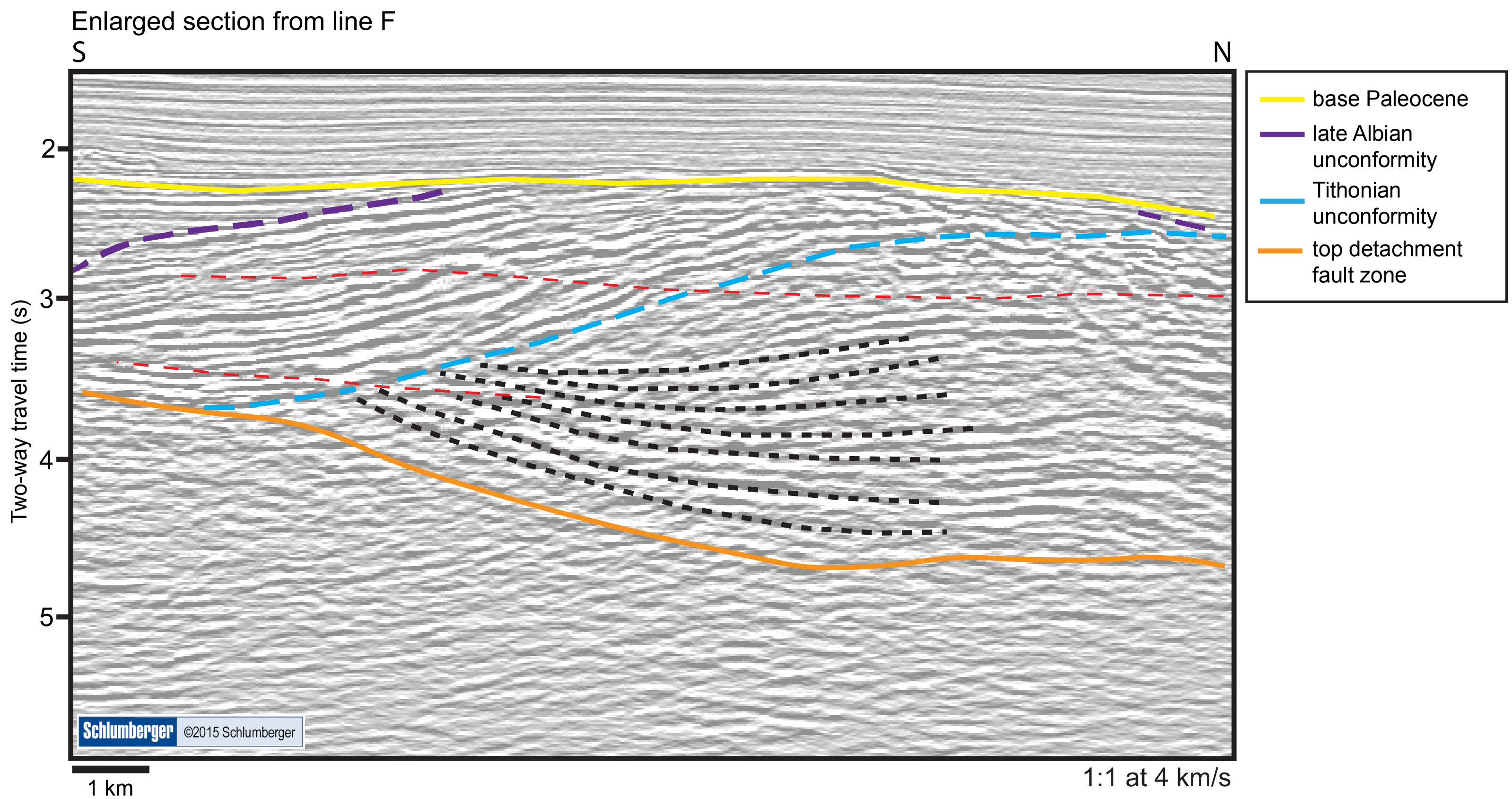

Figure 28. Enlarged section of line F. See Figure 16 for location. Between the top of the detachment fault zone and the Tithonian unconformity (package C), reflections (black dashed lines) diverge to the north, indicating syn-rift deposition of package C. This growth reflects a greater amount of fault displacement and subsidence in the northern part of the line; therefore, differential slip occurred on the Mercury fault during the deposition of package C.

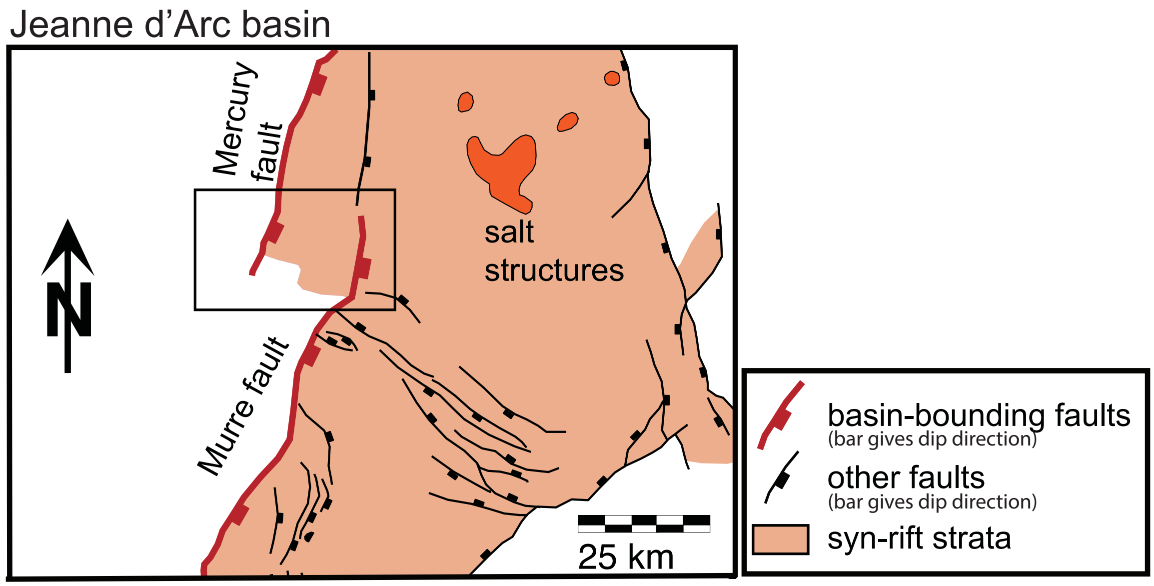

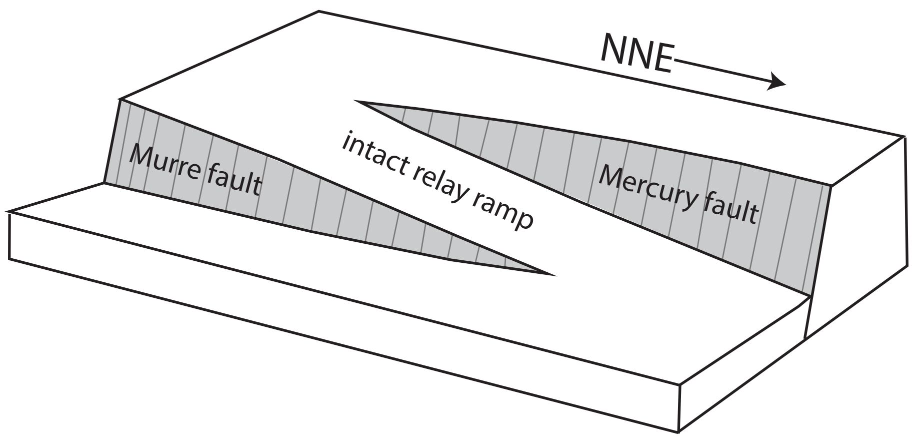

Figure 29. Relay ramp between the overlapping Mercury and Murre basin-bounding faults. a) Geologic map of part of the Jeanne d'Arc basin; see Figure 2 for a more complete map (modified from Withjack and Schlische, 2005; Sinclair, 1995). Black box shows area where relay ramp formed. b) Schematic illustration of relay ramp between the Mercury and Murre faults (modified from Whipp et al., 2015).

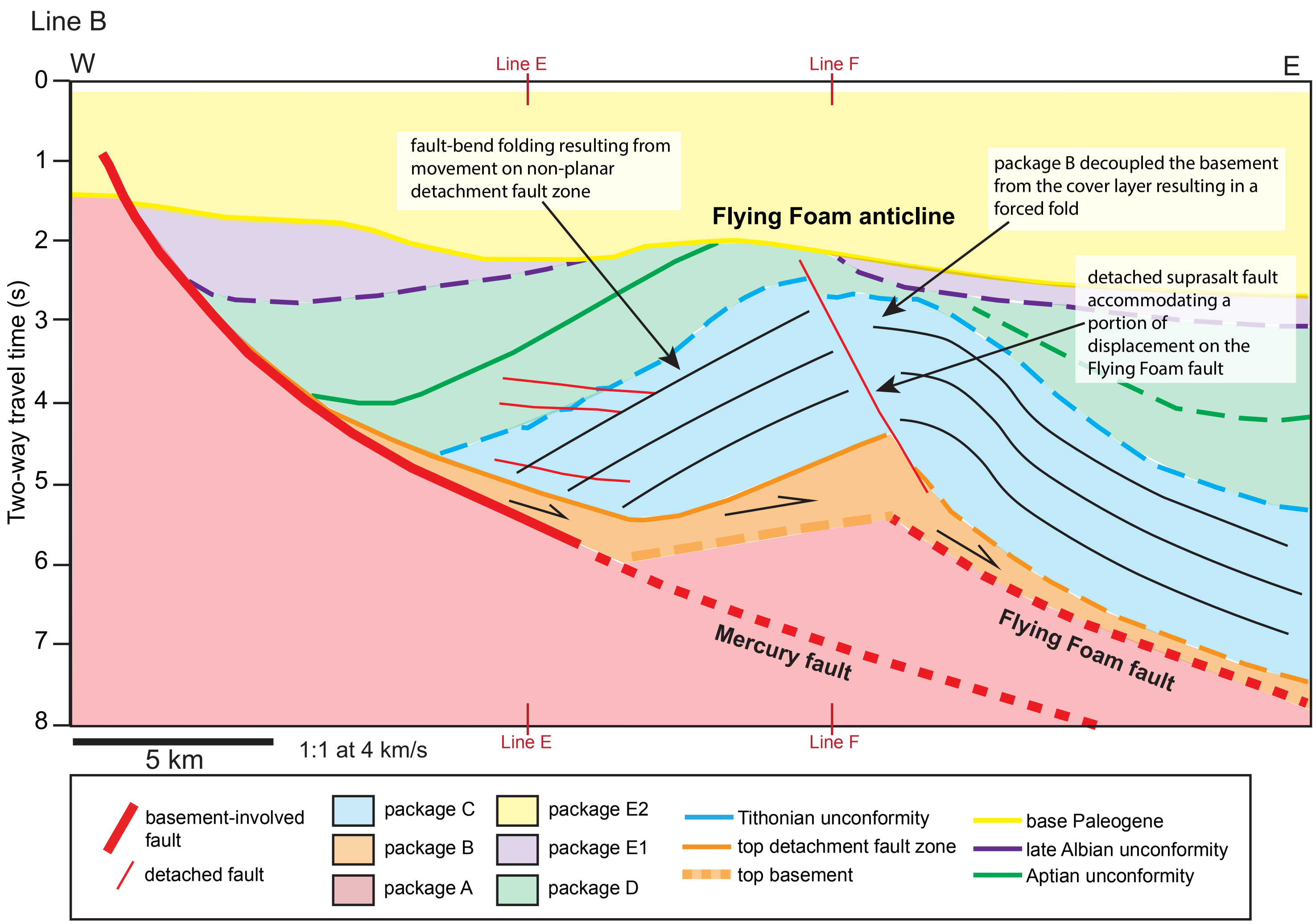

Figure 30. Line drawing of seismic line B showing a detailed analysis of the Flying Foam anticline. Black half arrows show the in-plane movement direction on the detachment fault zone during formation of the Flying Foam anticline. See line location in Figure 4b and uninterpreted line in Figure 12.

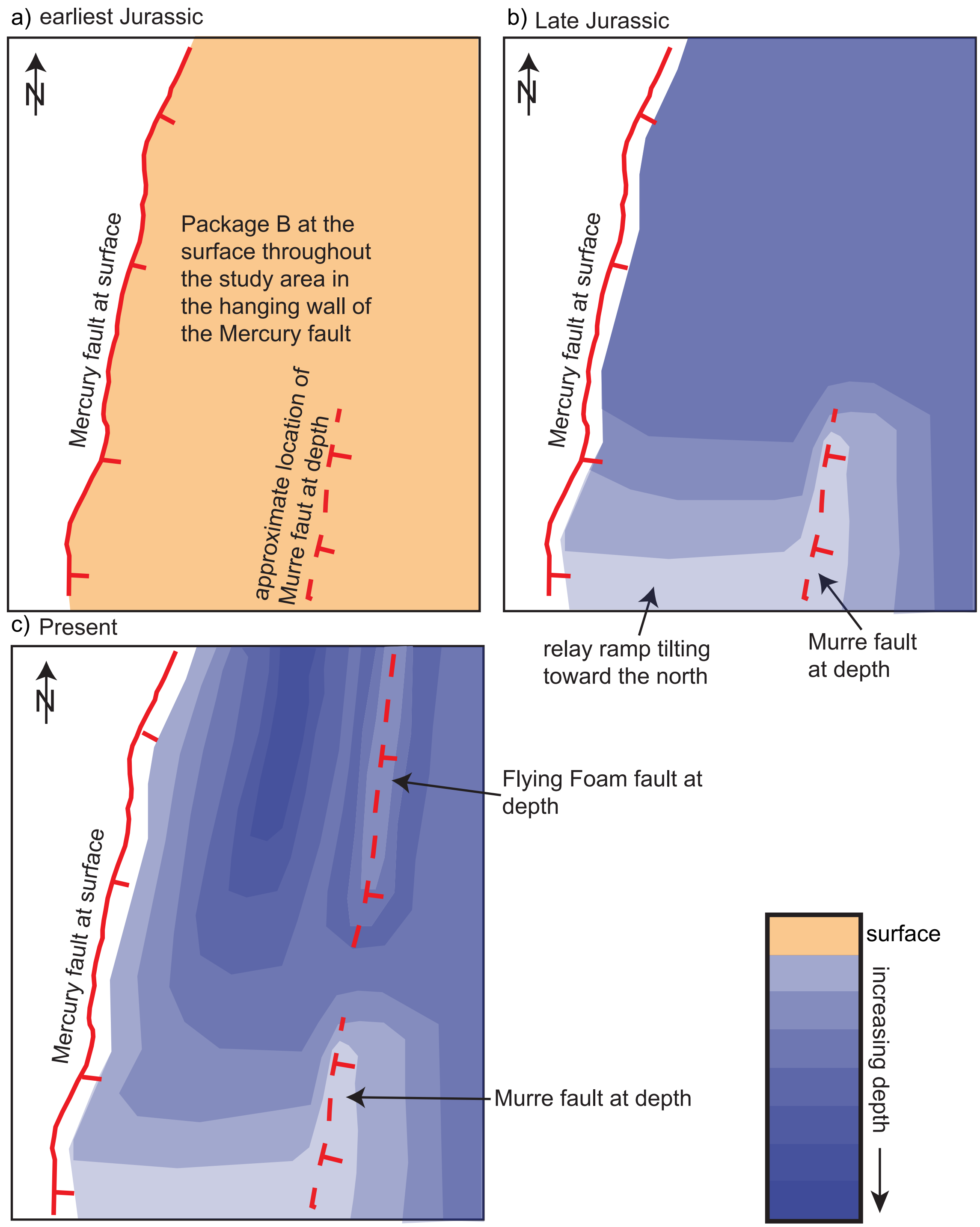

Figure 31. Schematic illustration showing evolution of the top of the detachment fault zone. a) At end of earliest Jurassic, package B was present at the surface in the hanging wall of the Mercury fault. b) Development of relay ramp in southern part of the study area between the Mercury and Murre faults during the second phase of rifting (Late Jurassic) resulted in a northward tilt of strata in the hanging wall of the Mercury fault. c) Development of Flying Foam anticline during the third phase of rifting (Early Cretaceous). Folding in the eastern part of the study area produced the current trough shape of the detachment fault zone.

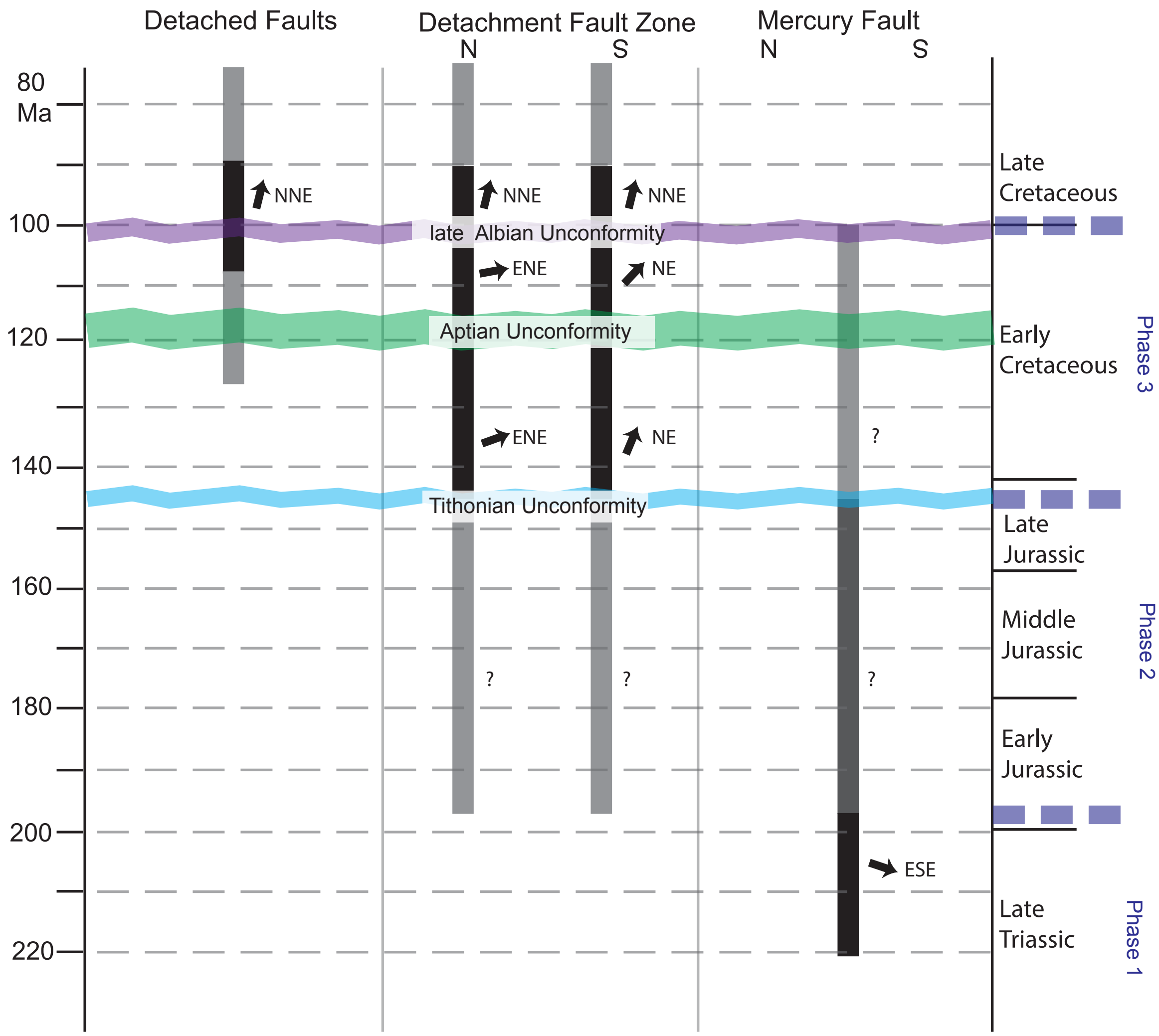

Figure 32. Timing of fault activity in the northern and southern sections of the Flying Foam region of the Jeanne d'Arc basin. Darker colors indicate more certainty about fault activity. Black arrows give inferred movement direction (in map view) during probable fault activity. Divisions between rift phases 1, 2, and 3 are based on published literature.

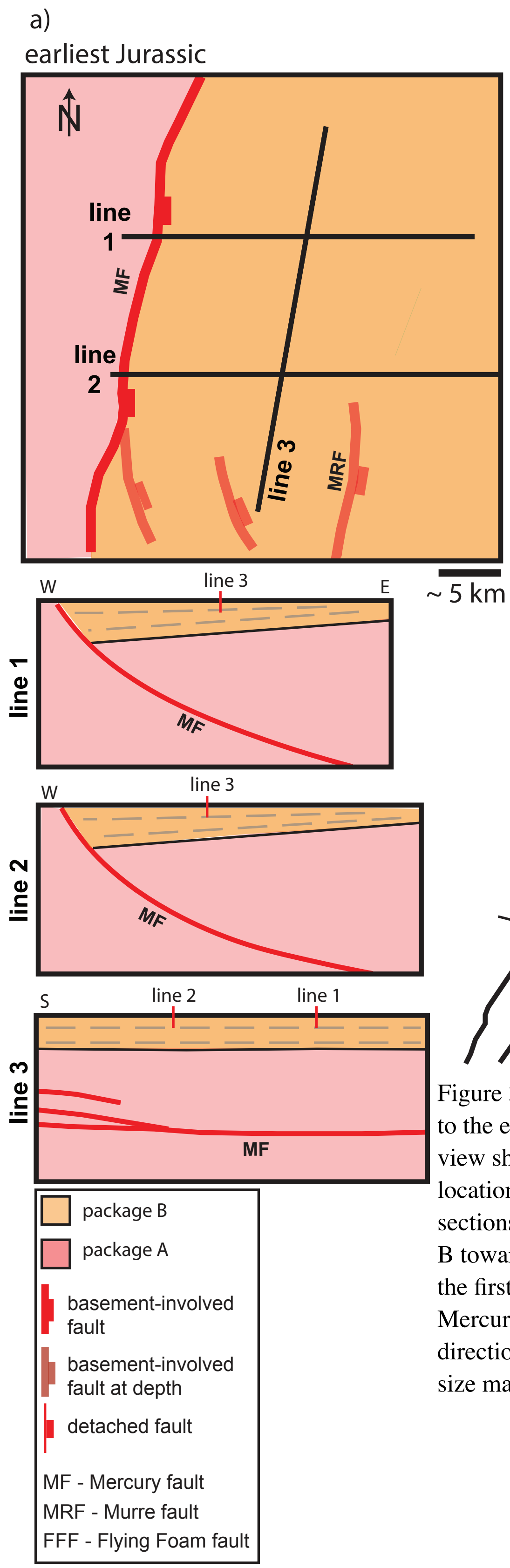

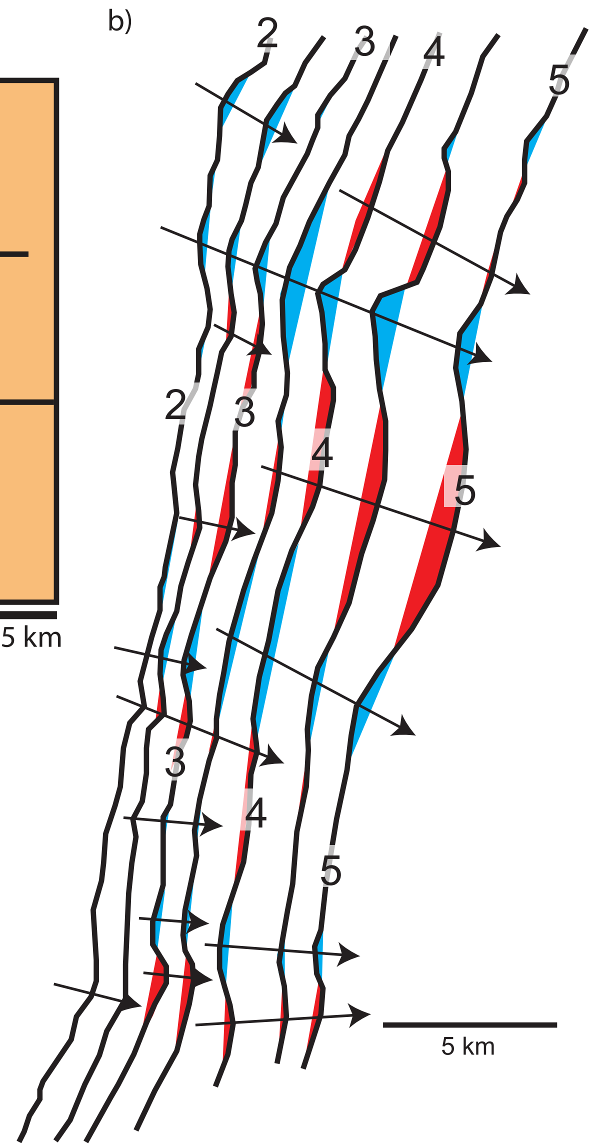

Figure 33. a) Schematic restoration of the Flying Foam region to the earliest Jurassic (end of the first phase of rifting). Map view shows surface geology during the specified time and the location of cross sections 1-3. Dashed lines within cross sections illustrate geometry of bedding. Thickening of package B toward the Mercury fault indicates syn-rift deposition during the first phase of rifting. b) Structure-contour map of the Mercury fault with corrugations indicating an ESE-movement direction on the fault during the first phase of rifting. See full-size map in Figure 20.

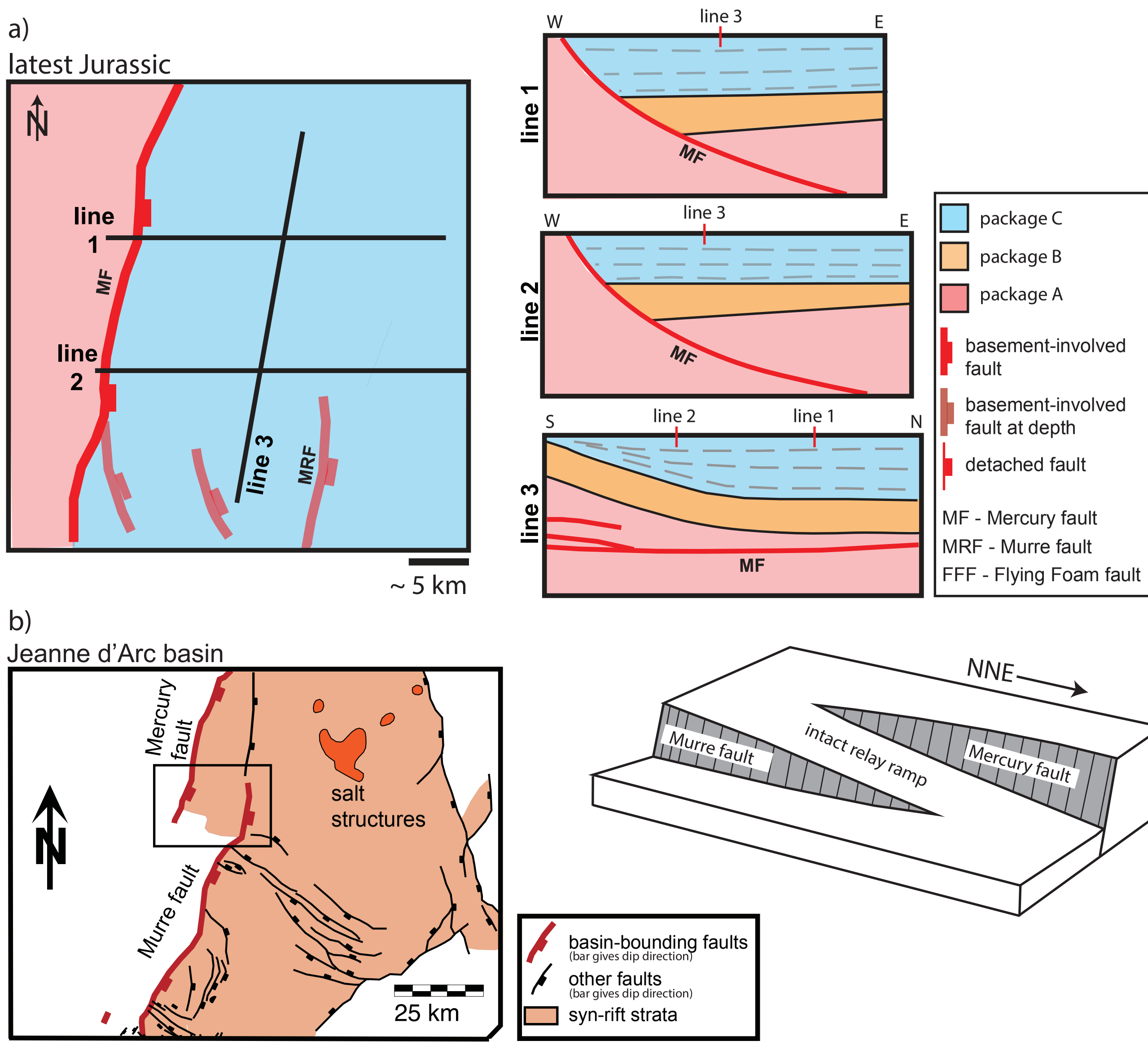

Figure 34. a) Schematic restoration of the Flying Foam region to the latest Jurassic (end of the second phase of rifting). Map view shows surface geology during the specified time and the location of cross sections 1-3. Dashed lines within cross sections illustrate geometry of bedding. During the second phase of rifting, formation of a relay ramp in the southern part of the study between the Mercury and Murre faults produced a northward tilt of strata in the hanging wall of the Mercury fault. b) Illustration of the relay ramp between the overlapping Mercury and Murre fault during the second phase of rifting (modified from Sinclair, 1995; Withjack and Schlische, 2005; Whipp et al., 2015). See Figure 29 for full size figure and explanation.

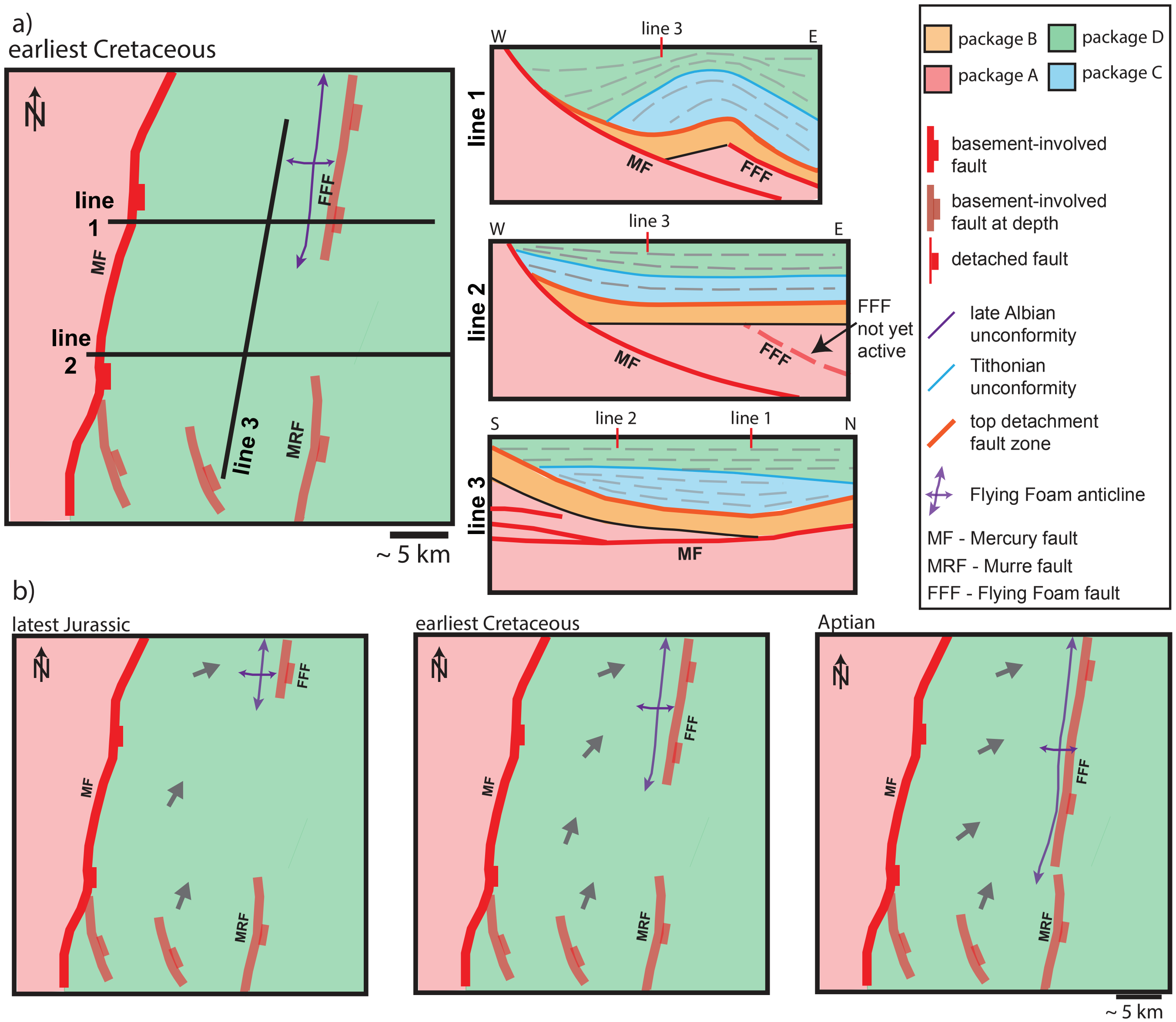

Figure 35. a) Schematic restoration of the Flying Foam region to the earliest Cretaceous (middle of the third phase of rifting). Map view shows surface geology during the specified time and the location of cross sections 1-3. Dashed lines within cross sections illustrate geometry of bedding. During the third phase of rifting, the Flying Foam fault began to propagate southward and the Flying Foam anticline formed above it. b) Schematic illustration of movement direction on the detachment fault zone during the third phase of rifting. Map view shows surface geology. Arrows are not meant to be exact, but illustrate the temporal and geographic change in the movement direction on the detachment fault zone.

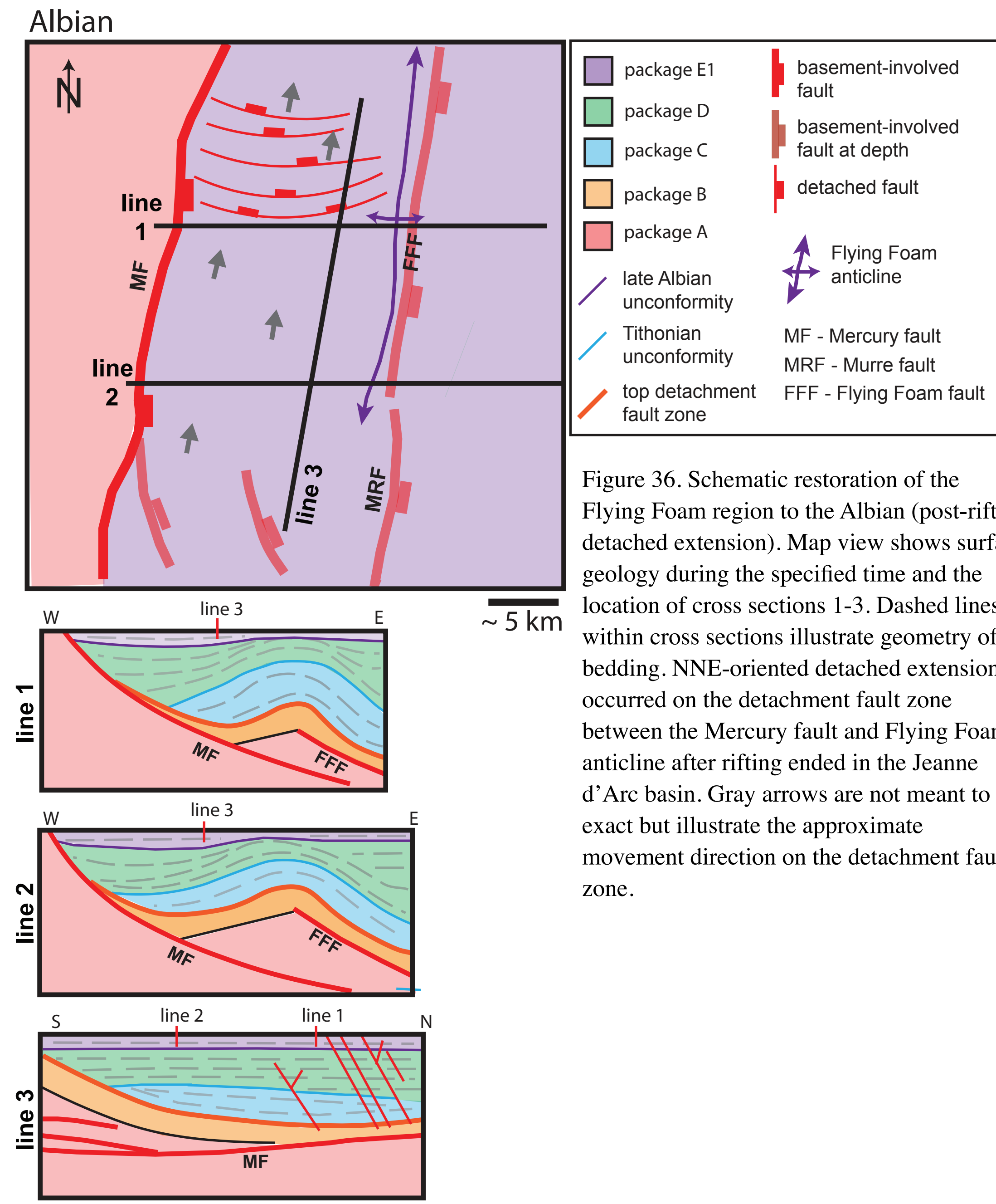

Figure 36. Schematic restoration of the Flying Foam region to the Albian (post-rift detached extension). Map view shows surface geology during the specified time and the location of cross sections 1-3. Dashed lines within cross sections illustrate geometry of bedding. NNE-oriented detached extension occurred on the detachment fault zone between the Mercury fault and Flying Foam anticline after rifting ended in the Jeanne d'Arc basin. Gray arrows are not meant to be exact but illustrate the approximate movement direction on the detachment fault zone.

APPENDIX 1

Schlumberger
Geco-Prakla

1995/6 Marine 3D Survey
Newfoundland Grand Banks
Final Processing Report
for
EXPLORATION SERVICES
Geco-Prakla

by

SCHLUMBERGER
GECO-PRAKLA
1325 South Dairy Ashford
Houston, Texas 77077

1. Introduction

This report summarizes the processing of the Marine 3D survey in GRAND BANKS area, Newfoundland, Canada, by Geco-Prakla, Houston, in 1996. The survey was shot east-west by M/V Geco Diamond. The survey spanned in-lines 11 to 1518 and cross-lines 320 to 2921.

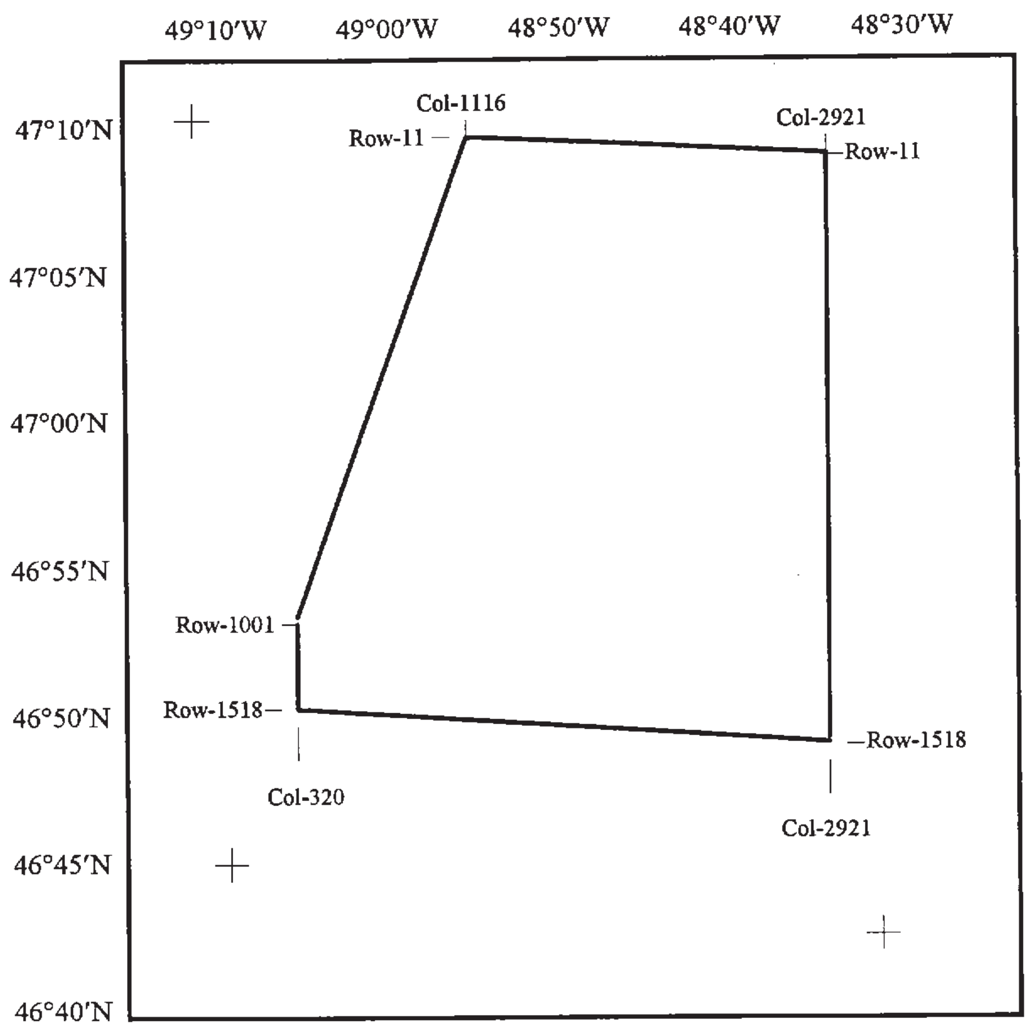

NEWFOUNDLAND GRAND BANKS

2. Acquisition Parameters

Shot by	Geco-Prakla Schlumberger July - September 1995
Boats	M/V Geco Diamond
Navigation	DGPS
Source	
Configuration	Triple Airgun Array Flip/Flop/Flap
Guns/Array	18, subdivided into 3 strings
Volume	5400 cubic inches per array
Pressure	2000 psi
Source Depth	6 meters
Source Separation	50 meters
Shot Interval	25 meters
Pop Interval	75 meters
Streamer	GECO HSSJ
Cable length	4 X 4800 meters
Streamer separation	150 meters
Group Interval	25 meters
Cable Depth	9 meters
Hydrophone per Group	40
Nominal Fold	32
Recording System	NESSIE III
Field Filters	
Low-cut	3 Hz 18 dB/octave slope
High-cut	125 Hz 70 dB/octave slope
Record Length	9.5 seconds
Sampling Interval	2 ms
Processing Record Length	9.0 seconds
Processing Sample Interval	4 ms

3. Processing Resources

3.1 Personnel

Processing Manager	Mark Bull
Processing Supervisor	Tony Johns
Group Supervisor	Catherine Tsai
Geophysicist	Indro Lawu, Mike Fagg

3.2 Software and Hardware

Software	Gecoseis System
Hardware	Fujitsu VPX240, Sun Workstation

4. Processing Parameters

4.1 Grid Orientation

Processing coordinates	
Base Angle	88.34 degrees
Side Angle	178.34 degrees
First in-line number on final migrated volume	1
In-line number increment	1
Distance between adjacent in-lines	25 meters
First cross-line number on final migrated volume	1
Cross-line number increment	1
Distance between adjacent cross-lines	12.5 meters
Spheroid	WGS-84
Projection	UTM
Scale factor on CM	0.9996
Central Meridian	-51.00 degrees
Grid System	TM
Grid Unit	Meters
False Northing	0.0
False Easting	500000
X-coordinate of in-line 1 cross-line 1	645410
Y-coordinate of in-line 1 cross-line 1	5226665

4.2 Processing sequence

4.2.1 Resample

Resample data from 2 ms to 4 ms with a 90 Hz 72 dB/octave high-cut filter.

4.2.2 Editing

Bad traces and/or shots flagged by Field Observers were deleted from the dataset.

4.2.3 Spherical Divergence Correction

Spherical divergence effects were removed by computing a scalar for each time sample from the following formula:

- $Scalar=T*(V_T/V_0)^2$
- T = seismic two-way time in seconds.
- V_0 = RMS velocity at time zero in meters/second.
- V_T = RMS velocity at time T in meters/second.

The following velocity function was used for the above calculation:

Time (sec)	Velocity (m/sec)
0.000	1472
0.500	1647
1.000	1813
1.500	2000
2.000	2221
2.500	2630
3.000	2990
3.500	3274
4.000	3548
4.500	3749
5.000	3920
5.500	4076
6.000	4218
6.500	4335
7.000	4450
7.500	4483
8.000	4509

4.2.4 Exponential Gain Correction

Exponential gain was applied to compensate for amplitude decay with time. The gain applied to the data for a sample at any time was determined by the following functions:

for $0.2 < T < 4.0$

$$Gain = e^{aT}$$

where,

a = (a user specified exponential gain value in dB/sec)*ln(10)/20. The user specified exponential gain value was +3 dB/sec.

$T = t - t_0$, where t is the sample time and t_0 is the start time for the gain function in seconds. The gain calculated at 4.0 seconds was applied to the end of the trace.

4.2.5 Source Signature and Instrument Compensation

An inverse filter was designed by Trilogy to convert the recorded source signature into a band limited minimum phase wavelet. The characteristics of this output wavelet were as follows :

```
Low  cut filter and slope :  6 Hz, 50 dB/octave
High cut filter and slope : 85 Hz, 90 dB/octave
```

This inverse filter was applied to the shot record data for removal of the known component of source wavelet before predictive deconvolution. See Section 12, *Figure 1*, for the production designature operator and *Figure 2* for the conditioned gun signature.

4.2.6 3-D XY Coordinate Merge

Cable position information from the processed navigation data was merged with the seismic data.

4.2.7 Prestack Predictive Deconvolution

Trace by trace predictive deconvolution was applied to further whiten the spectrum and to suppress reverberations. Based on the results of Trilogy testing, the following decon parameters were selected for production processing :

- Design window length: 6000 ms
- Operator length: 320 ms
- Gap length: 4 ms
- Prewhitening: 0.1 %

A job setup for the Deconvolution is attached in Sec. 11.1

4.2.8 Automatic Trace Editing

Data with anonymously large amplitude were edited prior to DMO stacking. From the tests performed, sample values above 10 could be identified as noise spikes for shot data. The near and far windows for this analysis were 1000-9000ms and 4500-9000ms, respectively. Whenever a sample above amplitude 10 was encountered in a window, a mute was applied from the previous sample to the end of the trace.

4.2.9 3-D Elastic Binning

The navigation information was extracted from the merged decon trace headers to generate coverage of the 3-D survey. The coordinates of each data trace were analyzed and each trace was assigned the following information:

- In-line bin number
- Cross-line bin number
- Micro-bin numbers (two values)
  Each bin was subdivided into a 100 X 100 grid. Micro-inline and micro-cross-line numbers were assigned from this micro-grid.
- Offset group (32 offset group numbers defined)
  Offset group 1 being the near, group 32 being the far.

Five values were used to uniquely defined a trace and tabulate binning statistics. From this information five tables were made.

- Total number of traces in each bin with All offset groups 1 - 32.
- Total number of traces in each bin with Nears offset groups 1 - 8.
- Total number of traces in each bin with MidNears offset groups 9 - 16.
- Total number of traces in each bin with MidFars offset groups 17 - 24.
- Total number of traces in each bin with Fars offset groups 25 - 32.

The coverage plots constructed from these tables reflect the actual live seismic data.

Because the binning was constructed from the merged decon trace headers, any missing and edited bad shots and traces were not included in the binning process. Elastic binning and redundancy editing trials were then performed. Each bin was searched in each offset group in an attempt to achieve a nominal 32-fold coverage throughout the survey, with maximum one trace contributing to each of the 32 allowed offset groups. If a particular bin contained more than one trace per offset group, the one trace closest to the bin center was accepted. If a particular bin and offset group contained no traces, adjacent bins were searched for traces in that offset group. If the traces found were within a user specified distance from the boundary of the primary bin, these traces were borrowed and allowed to stack into the bin. The user specified distances were expressed in terms of percentage of cross-line bin size. In this survey the cross-line bin size was 25 meters. A maximum of 2 traces per offset group were allowed in order to obtain nominal 32 fold.

Supergroups were used to describe groups of offset groups to be taken together for flexible redundancy editing. In this survey, the supergroups defined were: offsets 1-8, 9-16, 17-24, and 25-32 with each supergroup having a minimum fold requirement of 8. If normal flexing did not get enough traces in the supergroup to meet the minimum fold requirement, one additional trace from each group (1-32) which has surplus traces was accepted until the minimum fold was met.

Bin expansion tests were conducted at four parts of the survey area at 10, 20, 30 and 40 % respectively. The five coverage plots were once again generated and from these plots the following elastic binning parameters were chosen:

- For all offset groups: 40% bin expansion in cross-line direction. This expanded the cross-line bin size by 10 meters either side, from 25 meters to 45 meters.
- The five coverage plots were once again generated for the final binning table.

4.2.10 Normal Moveout

Normal Moveout was applied to the data using a fully interpolated 3-D velocity cube. See Sec. 10.1 "Stacking Velocity Field".

4.2.11 First Break Suppression

The data was muted in the following manner:

- Offsets up to 575 meters were not muted.
- Offset of 576 meters was muted at 500 ms.
- Offset of 5200 meters was muted at 4200 ms.

Mute times for offsets between the above offsets were calculated by linear interpolation.

4.2.12 3-D DMO and Stack with Elastic Binning

Common azimuth DMO was performed on the data. The procedures were as follows:

The final stack volume was allocated on disk. As traces were used, the DMO operator for each trace was calculated along the source to receiver azimuth.

The primary trace was stacked into the midpoint bin and stacking normalization information was recorded for that bin. The DMO energy traces were stacked into their proper bins but no normalization information was recorded.

As the traces were processed they were checked against the binning information. Redundant traces were discarded and flexed traces were copied if they were flagged as such by the binning information.

When all the data had gone through DMO/stacking procedure the normalization information was utilized to scale each sample of every trace by the inverse of the square root of the number of primary and flexed traces that contributed to the sample in question. This normalization scheme was used to scale down low fold areas that had poor signal to noise ratios. A job setup for 3-D DMO and stack with Elastic Binning is attached in Sec. 11.2.

4.2.13 In-line K-Filter

A k-filter was applied to remove aliased noise in the in-line direction caused by acquisition geometry. The filter was applied fully from 0.0 - 3.0 seconds and tapered off at 4.0 seconds. A job setup for In-line k-filter is attached in Sec. 11.3.

A sample of the Stack Timeslice at 2.0 sec is shown in Section 12, *Figure 3*.

4.2.14 3-D FXY-filter

3-D fxy-filter was applied to attenuate random noise. A job setup for 3-D fxy-filter is attached in Sec. 11.4.

A sample of the Stack Timeslice at 2.0 sec is shown in Section 12, *Figure 4*.

4.2.15 Datuming

A static shift of +12 ms was applied to the stacked data to compensate for the depth of source and the streamers below mean-sea-level.

4.2.16 One Pass Phase Shift Migration

Upon completion of various 2-D migration tests with different velocity reduction percentages of the RMS stacking velocities, the following parameters were used:

Time (seconds)	Percent
0.0	100
4.0	100
6.0	95
9.0	85

The following frequency and dip limits were used :

Time (seconds)	Max Frequency (Hz)
0.0	75

Time (seconds)	Max Dip (degrees)
0.0	60
3.0	60
6.0	40
9.0	10

After the parameters were picked on the 2-D tests, the southern half of the 3-D data-set, (in-line range 780-1532, cross-lines 1-3200), was migrated and provided as a preliminary deliverable to the underwriters on June 30th.

During the QC of the initial 3-D migrated volume there were some regions that were discovered to be slightly under-migrated.

Residual migration tests were performed using 103% and 106% of the above time-variant velocity reduction. These tests indicated that increasing the original reduction by 3% yielded improved imaging.

The following final velocity reductions of the RMS stacking velocities were used for the final 3D migration :

Time (seconds)	Percent
0.0	103
4.0	103
6.0	97.9
9.0	87.6

The phase shift migration uses a spatial operator, which allows accurate treatment of dips and gives a full 3-D operator. Since this operator must be laterally invariant, the data is stretched prior to the migration to accommodate lateral changes in velocity. The stretch function is computed by using a nonlinear optimization method developed at Geco-Prakla. Vertical velocity variations are handled exactly by the phase shift method without stretching.

A spatially and temporally smoothed interval velocity cube was used for input into this optimization algorithm. See Sec. 10.2 "Migration Velocity Field".

The phase shift migration was applied in the following 3 steps:

- The first step reads the unmigrated data by in-lines, stretches the data, and transforms the data into wave number domain over the in-line dimension, after padding to prevent wrap-around. A job setup for Step-I is attached in Sec. 11.5.
- The second step transforms the data in time and in the cross-line direction, performs the migration, and then inverse transforms the data over time and cross-line. A job setup for Step-II is attached in Sec. 11.6.
- The third step reads the data from Step-II by in-lines, inversely transforms the data over the in-line dimension and unstretches the data. A job setup for Step-III is attached in Sec. 11.7

See Section 12, *Figure 5* for the Quicklook cube Migration at 2.0 seconds.
See Section 12, *Figure 6* for the Final Migration timeslice at 2.0 seconds.

5. Final Products

5.1 Film displays

5.1.1 In-line AGC 3-D migration

Every 1500 meters (every 60th in-line) from in-line 61 to 1501 at 1:36,000 scale.

5.1.2 In-line RAP 3-D migration

Every 1500 meters (every 60th in-line) from in-line 61 to 1501 at 1:36,000 scale.

5.1.3 Cross-line AGC 3-D migration

Every 1500 meters (every 120th cross-line) from cross-line 360 to 2880 at 1:36,000 scale.

5.1.4 Cross-line RAP 3-D migration

Every 1500 meters (every 120th cross-line) from cross-line 360 to 2880 at 1:36,000 scale.

5.1.5 Timeslices

Every 200 ms of the final migrated volume from 0.2 - 6.0 sec. and every 1000 ms from 0.5 to 5.5 sec. at 1:48,000 scale.

5.2 Versatec displays

5.2.1 Binning/Index/Grid Plots

All, Nears, MidNears, MidFars, and Fars offset groups for edited and flexed index at 1:48,000 scale.

5.3 Deliverables on Tape

5.3.1 Decon SEGY Tapes

With navigation merge and designature filter applied.

5.3.2 Grid file SEGY Tapes

All, Nears, MidNears, MidFars, and Fars Offset groups from edited and flexed Index.

5.3.3 Binning/Index Offset groups FBKUP tapes

Edited and flexed index.

5.3.4 3-D Stack SEGY tapes

In-line ordered, with K-filter, 3D FXY-filter and +12 ms static shift applied.

5.3.5 3-D Migration SEGY tapes

In-line ordered.

5.3.6 3-D Migration SEGY tapes

Cross-line ordered.

5.3.7 3-D Migration SEGY film tapes

In-line ordered, every 60th in-line, from row 61 through to row 1501.

5.3.8 3-D Migration SEGY film tapes

Cross-line ordered, every 120th cross-line, from column 360 through to column 2880.

5.3.9 3-D DMO Gather SEGY tapes

Used in the velocity analysis for all 47 velocity lines.

5.3.10 Migration Timeslice Gather SEGY tapes.

Gathers are every 200ms from 0.200 - 6.000secs and every 1000ms from 0.500 - 5.500secs.

5.3.11 Migration Velocity Cube Timeslice SEGY tapes.

Every 200ms to 6.000secs.

5.3.12 Stack Velocity Cube Timeslice SEGY tapes.

Every 200ms to 6.000secs.

5.3.13 Following 8 mm velocity tapes:

- Navigation datasets in G2000 format.
- Stacking RMS velocity VBASE - ASCII format
- Stacking RMS velocity VCUBE 200*250 meter grid. i.e. every 8th row & every 20th column - ASCII format.
- Migration interval velocity VCUBE 200*250 meter grid. i.e. every 8th row & every 20th column - ASCII format.
- Migration interval velocity (with percentage reduction scheme applied) VCUBE 200*250 meter grid. i.e. every 8th row & every 20th column - ASCII format.
- Migration Interval velocity VBASE - ASCII format.
- Decon Reel dbase and Edit files.
- Spectra contour, CDP, and MVFS for all 47 velocity lines.

5.3.14 Floppy diskette.

Containing:

- source signature.
- designature operator used in the processing.

6. Line Statistics

Grand total mileage for the entire survey was 62643 kilometers.

```
System `A'
spint*grpint*noch*fcdp*
75.0  25.0   384  1
seq*punit*navn***rbi**fsp**rei**lsp**freel**lreel**nch*ns*nb*dpt*dir**nav**
040 a00    1p0101 1399 1399 2410 2410 D00345 D00348 384 2  1  11  088. 021
042 a01    1i0101 1399 1399 2410 2410 D00365 D00368 384 2  1  11  088. 041
034 a10    1p0113 1395 1395 2409 2409 D00305 D00308 384 2  1  11  088. 021
020 a20    1p0125 1391 1391 2409 2409 D00167 D00170 384 2  1   9  088. 001
032 a21    1i0125 1391 1391 2409 2409 D00285 D00288 384 2  1  11  088. 021
018 a30    1p0137 1387 1387 2410 2410 D00147 D00150 384 2  1   9  088. 001
008 a40    1p0149 1383 1383 2410 2410 D00070 D00073 384 2  1  11  088. 001
010 a50    1p0161 1379 1379 2409 2409 D00088 D00091 384 2  1  11  088. 001
016 a60    2p0173 1375 1375 2409 2409 D00127 D00130 384 2  1  11  088. 001
014 a70    1p0185 1372 1372 2410 2410 D00107 D00110 384 2  1  11  088. 001
024 a71    1i0185 1372 1372 2409 2410 D00205 D00208 384 2  1   9  088. 021
028 a80    1p0197 1368 1368 2409 2409 D00245 D00248 384 2  1  11  088. 021
038 a81    2i0197 1368 1368 2409 2409 D00325 D00329 384 2  1  11  088. 021
026 a90    1p0209 1364 1364 2409 2409 D00225 D00228 384 2  1   9  088. 021
022 b00    1p0221 1360 1360 2410 2410 000534 000558 384 2  1   9  088. 021
005 b10    1p0233 1356 1356 2409 2409 000113 000137 384 2  1   9  088. 001
003 b20    1p0245 1352 1352 2409 2409 000061 000085 384 2  1  11  088. 001
044 b30    1p0257 1348 1348 2409 2409 001105 001130 384 2  1  11  088. 041
047 b31    1i0257 1348 1348 2409 2409 001158 001182 384 2  1  11  088. 041
043 b40    1p0269 2300 2300 1236 1236 001078 001103 384 2  1  11  268. 041
049 b41    1i0269 1345 1345 1950 1950 001212 001226 384 2  1  11  088. 041
041 b50    1p0281 2301 2301 1232 1232 001027 001052 384 2  1  11  268. 041
033 b60    1p0293 2301 2301 1228 1228 000823 000848 384 2  1   9  268. 021
039 b61    1i0293 2301 2301 1228 1228 000977 001002 384 2  1  11  268. 021
031 b70    1p0305 2301 2301 1225 1224 000772 000797 384 2  1  11  268. 021
019 b80    1p0317 2301 2301 1220 1220 000454 000481 384 2  1   9  268. 001
013 b90    1p0329 2301 2301 1218 1216 000299 000324 384 2  1  11  268. 001
004 c00    1p0341 2260 2260 1212 1212 000088 000112 384 2  1   9  268. 001
050 c01    1r0341 2261 2261 2409 2409 001227 001230 384 2  1  11  088. 041
009 c10    1p0353 2301 2301 1209 1209 000197 000222 384 2  1   9  268. 001
011 c20    1p0365 2301 2301 1205 1205 000248 000273 384 2  1  11  268. 001
015 c30    1p0377 2300 2300 1201 1201 000350 000375 384 2  1  11  268. 001
017 c40    1p0389 2301 2301 1197 1197 000402 000427 384 2  1   9  268. 001
021 c50    1p0401 2301 2301 1193 1193 000507 000533 384 2  1   9  268. 021
027 c60    1p0413 2301 2301 1189 1189 000664 000690 384 2  1   9  268. 021
035 c61    1i0413 2301 2301 1189 1189 000873 000899 384 2  1  11  268. 021
023 c70    2p0425 2300 2300 1186 1185 000559 000585 384 2  1   9  268. 021
002 c80    1p0437 2301 2300 1183 1182 000034 000060 384 2  1  11  268. 001
007 c90    1p0449 2301 2301 1178 1178 000144 000171 384 2  1   9  268. 001
046 d00    3p0461 2300 2300 1174 1174 001131 001157 384 2  1  11  268. 041
048 d01    1i0461 2300 2300 1174 1174 001184 001211 384 2  1  11  268. 041
025 d10    1p0473 2300 2300 1170 1170 000611 000638 384 2  1   9  268. 021
030 d20    1p0485 1275 1275 2410 2410 000745 000771 384 2  1  11  088. 021
052 d30    1p0497 1271 1271 2409 2409 001260 001286 384 2  1  11  088. 041
059 d31    1i0497 1271 1271 2409 2409 001420 001446 384 2  1  11  088. 041
124 d32    2i0497 2064 2064 2248 2248 003303 003307 384 2  1  11  088. 121
054 d40    1p0509 1268 1268 2409 2409 001316 001342 384 2  1  11  088. 041
057 d50    1p0521 1264 1264 2410 2410 001374 001401 384 2  1  11  088. 041
061 d60    1p0533 1260 1260 2409 2409 001476 001502 384 2  1  11  088. 061
065 d70    1p0545 1256 1256 2407 2409 001590 001617 384 2  1  11  088. 061
069 d71    1i0545 1256 1256 2409 2409 001704 001731 384 2  1  11  088. 061
071 d72    2i0545 1317 1317 2409 2409 001761 001786 384 2  1  11  088. 061
073 d80    1p0557 1252 1252 2409 2409 001816 001843 384 2  1  11  088. 061
075 d90    1p0569 1248 1248 2380 2380 001874 001900 384 2  1  11  088. 061
081 d91    2p0569 1248 1248 2409 2409 002045 002072 384 2  1  11  088. 061
067 e00    1p0581 1244 1244 2407 2410 001647 001674 384 2  1  11  088. 061
063 e10    1p0593 1241 1241 2410 2410 001533 001560 384 2  1  11  088. 061
077 e20    1p0605 1237 1237 2410 2410 001931 001958 384 2  1  11  088. 061
079 e30    1p0617 1233 1233 2407 2410 001988 002015 384 2  1  11  088. 061
083 e40    1p0629 1229 1229 2410 2410 002101 002128 384 2  1   9  088. 082
082 e50    1p0641 2300 2300 1116 1116 002073 002100 384 2  1  11  268. 082
125 e51    1i0641 2300 2300 1230 1230 003308 003334 384 2  1  11  268. 121
080 e60    1p0653 2301 2301 1112 1112 002016 002043 384 2  1   9  268. 061
```

078	e70	1p0665	2301	2301	1108	1108	001959	001987	384	2	1	11	268. 061
062	e80	1p0677	2301	2301	1105	1105	001504	001532	384	2	1	11	268. 061
076	e81	1i0677	2301	2301	1105	1105	001902	001930	384	2	1	11	268. 061
051	e90	1p0689	2300	2300	1101	1101	001231	001259	384	2	1	11	268. 041
029	f00	1p0701	2301	2301	1099	1097	000716	000744	384	2	1	11	268. 021
053	f10	1p0713	2301	2301	1094	1093	001287	001315	384	2	1	11	268. 041
055	f20	1p0725	2300	2300	1800	1800	001343	001354	384	2	1	11	268. 041
058	f21	3p0725	1799	1799	1089	1089	001402	001418	384	2	1	11	268. 041
060	f30	1p0737	2301	2301	1086	1085	001447	001475	384	2	1	11	268. 060
064	f31	1i0737	2301	2301	1085	1085	001561	001589	384	2	1	11	268. 061
066	f40	1p0749	2301	2301	1081	1081	001618	001646	384	2	1	11	268. 061
068	f41	1i0749	2301	2301	1081	1081	001675	001703	384	2	1	11	268. 061
070	f50	1p0761	2300	2300	1078	1078	001732	001760	384	2	1	11	268. 061
072	f60	1p0773	2300	2300	1074	1074	001787	001815	384	2	1	11	268. 061
074	f70	1p0785	2301	2301	1070	1070	001844	001872	384	2	1	11	268. 061
129	f71	2i0785	2301	2301	1118	1118	003429	003457	384	2	1	11	268. 082
084	f80	1p0797	2300	2300	1066	1066	002129	002159	384	2	1	9	268. 082
088	f90	1p0809	2245	2245	1063	1062	002253	002281	384	2	1	9	268. 082
112	f91	2p0809	2300	2300	1062	1062	003008	003037	384	2	1	11	268. 101
090	g00	1p0821	2300	2300	1064	1058	002314	002343	384	2	1	9	268. 082
131	g01	1i0821	2005	2005	1058	1058	003491	003518	384	2	1	11	268. 121
098	g10	1p0833	2300	2300	1056	1054	002563	002592	384	2	1	9	268. 082
104	g20	1p0845	2300	2300	1052	1051	002751	002780	384	2	1	11	268. 101
107	g30	1p0857	1156	1156	2407	2409	002845	002876	384	2	1	9	088. 101
093	g40	1p0869	1152	1152	2409	2409	002406	002435	384	2	1	9	088. 082
116	g41	1i0869	1152	1152	2404	2409	003132	003163	384	2	1	11	088. 101
091	g50	1p0881	1148	1148	2409	2410	002344	002373	384	2	1	9	088. 082
087	g60	1p0893	1144	1144	2410	2410	002222	002251	384	2	1	9	088. 082
126	g61	1i0893	1580	1580	2410	2410	003336	003361	384	2	1	11	088. 121
001	g70	1p0905	1140	1140	2406	2410	000001	000032	384	2	1	11	088. 001
085	g80	1p0917	1136	1136	2410	2410	002160	002189	384	2	1	9	088. 082
118	g81	1i0917	1173	1173	2014	2015	003198	003219	384	2	1	11	088. 101
089	g90	1p0929	1133	1133	2410	2410	002282	002313	384	2	1	9	088. 082
095	h00	1p0941	1129	1129	2410	2410	002468	002499	384	2	1	11	088. 095
120	h01	1i0941	1166	1166	2124	2125	003233	003256	384	2	1	11	088. 101
097	h10	1p0953	1125	1125	2409	2410	002532	002562	384	2	1	9	088. 082
105	h20	1p0965	1121	1121	2410	2410	002781	002811	384	2	1	9	088. 101
113	h21	1i0965	1158	1158	2410	2410	003038	003068	384	2	1	11	088. 101
103	h30	1p0977	1117	1117	2410	2410	002720	002750	384	2	1	11	088. 101
101	h40	1p0989	1113	1113	2409	2409	002656	002686	384	2	1	9	088. 101
099	h50	1p1001	1109	1109	2410	2410	002593	002623	384	2	1	9	088. 082
109	h60	1p1013	1106	1106	2409	2410	002909	002940	384	2	1	9	088. 101
128	h61	2i1013	1143	1143	2409	2410	003395	003427	384	2	1	11	088. 121
111	h70	1p1025	1102	1102	2409	2409	002974	003007	384	2	1	11	088. 101
122	h71	1i1025	1380	1380	2408	2409	003270	003295	384	2	1	11	088. 121
130	h80	1p1037	1098	1098	2060	2060	003458	003484	384	2	1	11	088. 121
132	h81	1i1037	1098	1098	2409	2409	003519	003554	384	2	1	11	088. 121
186	h82	2i1037	1600	1600	2409	2409	005330	005349	384	2	1	11	088. 181
108	h90	1p1049	2301	2301	985	985	002877	002908	384	2	1	9	268. 101
086	i00	1p1061	2300	2300	983	981	002190	002221	384	2	1	9	268. 082
092	i10	1p1073	2300	2300	977	977	002374	002405	384	2	1	9	268. 082
188	i11	1i1073	1122	1122	2409	2409	005375	005413	384	2	1	11	088. 181
096	i20	1p1085	2301	2301	974	973	002500	002531	384	2	1	11	268. 082
100	i30	1p1097	2300	2300	970	970	002624	002655	384	2	1	9	268. 082
119	i31	1i1097	1450	1450	970	970	003220	003232	384	2	1	11	268. 101
187	i32	2i1097	2215	2215	1405	1405	005350	005372	384	2	1	11	268. 181
102	i40	1p1109	2300	2300	966	966	002687	002719	384	2	1	11	268. 101
127	i41	1i1109	2263	2263	966	966	003362	003394	384	2	1	11	268. 121
094	i50	1p1121	2300	2300	1451	1451	002436	002456	384	2	1	9	268. 082
121	i51	1r1121	1450	1450	962	962	003257	003269	384	2	1	11	268. 121
106	i60	1p1133	2300	2300	958	958	002812	002844	384	2	1	9	268. 101
110	i70	1p1145	2300	2300	954	954	002941	002973	384	2	1	9	268. 101
114	i80	1p1157	2300	2300	950	950	003069	003101	384	2	1	11	268. 101
117	i81	1i1157	2300	2300	950	950	003164	003197	384	2	1	11	268. 101
133	i90	1p1169	2301	2301	946	946	003555	003587	384	2	1	11	268. 121
137	j00	1p1181	2301	2301	943	943	003694	003728	384	2	1	11	268. 121
139	j01	1i1181	2301	2301	943	943	003765	003798	384	2	1	9	268. 121
145	j10	1p1193	2301	2301	939	939	003973	004006	384	2	1	11	268. 141
135	j20	1p1205	2301	2301	935	935	003622	003657	384	2	1	11	268. 121
151	j21	1i1205	2301	2301	1078	1078	004179	004209	384	2	1	11	268. 141
185	j22	2i1205	1753	1753	1354	1354	005320	005329	384	2	1	11	268. 181
141	j30	1p1217	2301	2301	931	931	003833	003867	384	2	1	9	268. 141
143	j40	1p1229	2301	2301	927	927	003904	003938	384	2	1	9	268. 141
147	j50	1p1241	2301	2301	924	923	004041	004074	384	2	1	11	268. 141
152	j51	1i1241	1032	1032	2410	2410	004210	004243	384	2	1	11	088. 141

148	j60	1p1253	1028	1028	2410	2410	004075	004109	384	2	1	11	088.	141
150	j61	1i1253	1028	1028	2410	2410	004144	004178	384	2	1	11	088.	141
146	j70	1p1265	1025	1025	2410	2410	004007	004040	384	2	1	11	088.	141
134	j80	1p1277	1021	1021	2410	2410	003588	003621	384	2	1	11	088.	121
136	j90	1p1289	1017	1017	2407	2409	003658	003693	384	2	1	11	088.	121
138	k00	1p1301	1013	1013	2410	2410	003729	003764	384	2	1	9	088.	121
140	k01	1i1301	1013	1013	2410	2410	003799	003832	384	2	1	9	088.	121
142	k10	1p1313	1009	1009	2410	2410	003868	003903	384	2	1	9	088.	141
144	k11	1i1313	1009	1009	2410	2410	003939	003972	384	2	1	11	088.	141
154	k20	1p1325	1005	1005	2409	2409	004282	004316	384	2	1	11	088.	141
156	k30	1p1337	1001	1001	2409	2409	004354	004391	384	2	1	11	088.	141
159	k40	1p1349	1001	1001	2409	2410	004470	004504	384	2	1	11	088.	141
161	k41	1i1349	1001	1001	2410	2410	004539	004577	384	2	1	11	088.	161
163	k50	1p1361	1001	1001	2409	2409	004612	004646	384	2	1	11	088.	161
165	k60	1p1373	1001	1001	2409	2409	004681	004714	384	2	1	11	088.	161
167	k70	1p1385	1001	1001	1674	1674	004749	004766	384	2	1	11	088.	161
168	k71	2p1385	1675	1675	2410	2410	004767	004784	384	2	1	11	088.	161
170	k80	1p1397	1001	1001	2409	2409	004821	004855	384	2	1	11	088.	161
172	k81	1i1397	1001	1001	2409	2409	004891	004926	384	2	1	11	088.	161
149	k90	1p1409	2300	2300	892	892	004110	004143	384	2	1	11	268.	141
184	k91	1i1409	1060	1060	1950	1950	005298	005319	384	2	1	11	088.	181
153	100	1p1421	2301	2301	893	892	004244	004281	384	2	1	11	268.	141
155	110	1p1433	2301	2301	892	892	004317	004353	384	2	1	11	268.	141
158	120	1p1445	2300	2300	893	892	004435	004468	384	2	1	11	268.	141
160	121	1i1445	2300	2300	892	892	004505	004538	384	2	1	11	268.	141
162	130	1p1457	2301	2301	892	892	004578	004611	384	2	1	11	268.	161
164	140	1p1469	2301	2301	893	892	004647	004680	384	2	1	11	268.	161
183	141	1i1469	2301	2301	1630	1630	005278	005297	384	2	1	11	268.	181
166	150	1p1481	2300	2300	892	892	004715	004748	384	2	1	11	268.	161
169	160	1p1493	2301	2301	892	892	004785	004820	384	2	1	11	268.	161
171	170	1p1505	2301	2301	892	892	004856	004890	384	2	1	11	268.	161
173	180	1p1517	2300	2300	892	892	004927	004960	384	2	1	11	268.	161
175	181	1i1517	2300	2300	892	892	005003	005036	384	2	1	11	268.	161
177	190	1p1529	2301	2301	892	892	005073	005106	384	2	1	11	268.	161
179	m00	1p1541	2301	2301	892	892	005145	005179	384	2	1	11	268.	161
181	m10	1p1553	2089	2089	892	892	005214	005242	384	2	1	11	268.	181
182	m11	1i1553	1001	1001	2409	2409	005243	005276	384	2	1	11	088.	181
176	m20	1p1565	1001	1001	2409	2409	005037	005072	384	2	1	11	088.	161
174	m30	1p1577	1001	1001	2410	2410	004961	005002	384	2	1	11	088.	161
178	m40	1p1589	1001	1001	2409	2409	005108	005143	384	2	1	11	088.	161
180	m50	1p1601	1001	1001	2409	2409	005180	005213	384	2	1	11	088.	161

System `B'

seq*punit*navn***ffil*fsp**lfil*lsp**freel**lreel**nch*ns*nb*dpt*dir**nav*

040	a00	1p0101	1399	1399	2410	2410	101003	101026	384	2	1	11	088.	021
042	a01	1i0101	1399	1399	2410	2410	101053	101076	384	2	1	11	088.	041
034	a10	1p0113	1395	1395	2409	2409	100849	100872	384	2	1	11	088.	021
020	a20	1p0125	1391	1391	2409	2409	100482	100505	384	2	1	9	088.	001
032	a21	1i0125	1391	1391	2409	2409	100798	100822	384	2	1	11	088.	021
018	a30	1p0137	1387	1387	2410	2410	100429	100453	384	2	1	9	088.	001
008	a40	1p0149	1383	1383	2410	2410	100172	100196	384	2	1	11	088.	001
010	a50	1p0161	1379	1379	2409	2409	100223	100247	384	2	1	11	088.	001
016	a60	2p0173	1375	1375	2409	2409	100377	100401	384	2	1	11	088.	001
014	a70	1p0185	1372	1372	2410	2410	100325	100349	384	2	1	11	088.	001
024	a71	1i0185	1372	1372	2409	2410	100586	100610	384	2	1	9	088.	021
028	a80	1p0197	1368	1368	2409	2409	100691	100715	384	2	1	11	088.	021
038	a81	2i0197	1368	1368	2409	2409	100952	100976	384	2	1	11	088.	021
026	a90	1p0209	1364	1364	2409	2409	100639	100663	384	2	1	9	088.	021
022	b00	1p0221	1360	1360	2410	2410	100534	100558	384	2	1	9	088.	021
005	b10	1p0233	1356	1356	2409	2409	100113	100137	384	2	1	9	088.	001
003	b20	1p0245	1352	1352	2409	2409	100061	100085	384	2	1	11	088.	001
044	b30	1p0257	1348	1348	2409	2409	101105	101130	384	2	1	11	088.	041
047	b31	1i0257	1348	1348	2409	2409	101158	101182	384	2	1	11	088.	041
043	b40	1p0269	2300	2300	1236	1236	101078	101103	384	2	1	11	268.	041
049	b41	1i0269	1345	1345	1950	1950	101212	101226	384	2	1	11	088.	041
041	b50	1p0281	2301	2301	1232	1232	101027	101052	384	2	1	11	268.	041
033	b60	1p0293	2301	2301	1229	1228	100823	100848	384	2	1	9	268.	021
039	b61	1i0293	2301	2301	1228	1228	100977	101002	384	2	1	11	268.	021
031	b70	1p0305	2301	2301	1225	1224	100772	100797	384	2	1	11	268.	001
019	b80	1p0317	2301	2301	1220	1220	100454	100481	384	2	1	9	268.	001
013	b90	1p0329	2301	2301	1218	1216	100299	100324	384	2	1	11	268.	001
004	c00	1p0341	2260	2260	1212	1212	100088	100112	384	2	1	9	268.	001
050	c01	1r0341	2261	2261	2409	2409	101227	101230	384	2	1	11	088.	041
009	c10	1p0353	2301	2301	1209	1209	100197	100222	384	2	1	9	268.	001
011	c20	1p0365	2301	2301	1205	1205	100248	100273	384	2	1	11	268.	001

015	c30	1p0377	2300	2300	1201	1201	100350	100375	384	2	1	11	268.	001
017	c40	1p0389	2301	2301	1197	1197	100402	100427	384	2	1	9	268.	001
021	c50	1p0401	2301	2301	1193	1193	100507	100533	384	2	1	9	268.	021
027	c60	1p0413	2301	2301	1189	1189	100664	100690	384	2	1	9	268.	021
035	c61	1i0413	2301	2301	1189	1189	100873	100899	384	2	1	11	268.	021
023	c70	2p0425	2300	2300	1186	1185	100559	100585	384	2	1	9	268.	021
002	c80	1p0437	2301	2300	1183	1182	D00015	D00019	384	2	1	11	268.	001
007	c90	1p0449	2301	2301	1178	1178	100144	100171	384	2	1	9	268.	001
046	d00	3p0461	2300	2300	1174	1174	101131	101157	384	2	1	11	268.	041
048	d01	1i0461	2300	2300	1174	1174	101184	101211	384	2	1	11	268.	041
025	d10	1p0473	2300	2300	1170	1170	100611	100638	384	2	1	9	268.	021
030	d20	1p0485	1275	1275	2410	2410	100745	100771	384	2	1	11	088.	021
052	d30	1p0497	1271	1271	2409	2409	101260	101286	384	2	1	11	088.	041
059	d31	1i0497	1271	1271	2409	2409	101420	101446	384	2	1	11	088.	041
124	d32	2i0497	2064	2064	2248	2248	103303	103307	384	2	1	11	088.	121
054	d40	1p0509	1268	1268	2409	2409	101316	101342	384	2	1	11	088.	041
057	d50	1p0521	1264	1264	2410	2410	101374	101401	384	2	1	11	088.	041
061	d60	1p0533	1260	1260	2409	2409	101476	101502	384	2	1	11	088.	061
065	d70	1p0545	1256	1256	2408	2409	101590	101617	384	2	1	11	088.	061
069	d71	1i0545	1256	1256	2409	2409	101704	101731	384	2	1	11	088.	061
071	d72	2i0545	1317	1317	2409	2409	101761	101786	384	2	1	11	088.	061
073	d80	1p0557	1252	1252	2409	2409	101816	101843	384	2	1	11	088.	061
075	d90	1p0569	1248	1248	2380	2380	101874	101900	384	2	1	11	088.	061
081	d91	2p0569	1248	1248	2409	2409	102045	102072	384	2	1	11	088.	061
067	e00	1p0581	1244	1244	2408	2410	101647	101674	384	2	1	11	088.	061
063	e10	1p0593	1241	1241	2410	2410	101533	101560	384	2	1	11	088.	061
077	e20	1p0605	1237	1237	2410	2410	101931	101958	384	2	1	11	088.	061
079	e30	1p0617	1233	1233	2408	2410	101988	102015	384	2	1	11	088.	061
083	e40	1p0629	1229	1229	2410	2410	102101	102128	384	2	1	9	088.	082
082	e50	1p0641	2300	2300	1116	1116	102073	102100	384	2	1	11	268.	082
125	e51	1i0641	2300	2300	1230	1230	103308	103334	384	2	1	11	268.	121
080	e60	1p0653	2301	2301	1112	1112	102016	102043	384	2	1	9	268.	061
078	e70	1p0665	2301	2301	1108	1108	101959	101987	384	2	1	11	268.	061
062	e80	1p0677	2301	2301	1105	1105	101504	101532	384	2	1	11	268.	061
076	e81	1i0677	2301	2301	1105	1105	101902	101930	384	2	1	11	268.	061
051	e90	1p0689	2300	2300	1101	1101	101231	101259	384	2	1	11	268.	041
029	f00	1p0701	2301	2301	1099	1097	100716	100744	384	2	1	11	268.	021
053	f10	1p0713	2301	2301	1094	1093	101287	101315	384	2	1	11	268.	041
055	f20	1p0725	2300	2300	1800	1800	101343	101354	384	2	1	11	268.	041
058	f21	3p0725	1799	1799	1089	1089	101402	101418	384	2	1	11	268.	041
060	f30	1p0737	2301	2301	1085	1085	101447	101475	384	2	1	11	268.	060
064	f31	1i0737	2301	2301	1085	1085	101561	101589	384	2	1	11	268.	061
066	f40	1p0749	2301	2301	1081	1081	101618	101646	384	2	1	11	268.	061
068	f41	1i0749	2301	2301	1081	1081	101675	101703	384	2	1	11	268.	061
070	f50	1p0761	2300	2300	1078	1078	101732	101760	384	2	1	11	268.	061
072	f60	1p0773	2300	2300	1074	1074	101787	101815	384	2	1	11	268.	061
074	f70	1p0785	2301	2301	1070	1070	101844	101872	384	2	1	11	268.	061
129	f71	2i0785	2301	2301	1118	1118	103429	103457	384	2	1	11	268.	121
084	f80	1p0797	2300	2300	1066	1066	102129	102159	384	2	1	9	268.	082
088	f90	1p0809	2257	2245	1075	1062	102253	102281	384	2	1	9	268.	082
112	f91	2p0809	2300	2300	1062	1062	103008	103037	384	2	1	11	268.	101
090	g00	1p0821	2300	2300	1065	1058	102314	102343	384	2	1	9	268.	082
131	g01	1i0821	2005	2005	1058	1058	103491	103518	384	2	1	11	268.	121
098	g10	1p0833	2300	2300	1056	1054	102563	102592	384	2	1	9	268.	082
104	g20	1p0845	2300	2300	1052	1051	102751	102780	384	2	1	11	268.	101
107	g30	1p0857	1156	1156	2407	2409	102845	102876	384	2	1	9	088.	101
093	g40	1p0869	1152	1152	2409	2409	102406	102435	384	2	1	9	088.	082
116	g41	1i0869	1152	1152	2409	2409	103132	103163	384	2	1	11	088.	101
091	g50	1p0881	1148	1148	2410	2410	102344	102373	384	2	1	9	088.	082
087	g60	1p0893	1144	1144	2410	2410	102222	102251	384	2	1	9	088.	082
126	g61	1i0893	1580	1580	2410	2410	103336	103361	384	2	1	11	088.	121
001	g70	1p0905	1140	1140	2407	2410	100001	100032	384	2	1	11	088.	001
085	g80	1p0917	1136	1136	2410	2410	102160	102189	384	2	1	9	088.	082
118	g81	1i0917	1173	1173	2014	2015	103198	103218	384	2	1	11	088.	101
089	g90	1p0929	1133	1133	2410	2410	102282	102313	384	2	1	9	088.	082
095	h00	1p0941	1129	1129	2410	2410	102468	102499	384	2	1	11	088.	095
120	h01	1i0941	1166	1166	2124	2125	103233	103256	384	2	1	11	088.	101
097	h10	1p0953	1125	1125	2410	2410	102532	102562	384	2	1	9	088.	082
105	h20	1p0965	1121	1121	2410	2410	102781	102811	384	2	1	9	088.	101
113	h21	1i0965	1158	1158	2410	2410	103038	103068	384	2	1	11	088.	101
103	h30	1p0977	1117	1117	2410	2410	102720	102750	384	2	1	11	088.	101
101	h40	1p0989	1113	1113	2409	2409	102656	102686	384	2	1	9	088.	101
099	h50	1p1001	1109	1109	2410	2410	102593	102623	384	2	1	9	088.	082
109	h60	1p1013	1106	1106	2409	2410	102909	102940	384	2	1	9	088.	101
128	h61	2i1013	1143	1143	2410	2410	103395	103428	384	2	1	11	088.	121

111	h70	1p1025	1102	1102	2409	2409	102974	103007	384	2	1	11	088.	101
122	h71	1i1025	1380	1380	2408	2409	103270	103295	384	2	1	11	088.	121
130	h80	1p1037	1098	1098	2060	2060	103458	103484	384	2	1	11	088.	121
132	h81	1i1037	1098	1098	2409	2409	103519	103554	384	2	1	11	088.	121
186	h82	2i1037	1600	1600	2409	2409	105330	105349	384	2	1	11	088.	181
108	h90	1p1049	2301	2301	985	985	102877	102908	384	2	1	9	268.	101
086	i00	1p1061	2300	2300	982	981	102190	102221	384	2	1	9	268.	082
092	i10	1p1073	2300	2300	977	977	102374	102405	384	2	1	9	268.	082
188	i11	1i1073	1122	1122	2409	2409	105374	105413	384	2	1	11	088.	181
096	i20	1p1085	2301	2301	974	973	102500	102531	384	2	1	11	268.	082
100	i30	1p1097	2300	2300	970	970	102624	102655	384	2	1	9	268.	082
119	i31	1i1097	1450	1450	970	970	103220	103232	384	2	1	11	268.	101
187	i32	2i1097	2215	2215	1405	1405	105350	105372	384	2	1	11	268.	181
102	i40	1p1109	2300	2300	966	966	102687	102719	384	2	1	11	268.	101
127	i41	1i1109	2263	2263	966	966	103362	103394	384	2	1	11	268.	121
094	i50	1p1121	2300	2300	1451	1451	102436	102456	384	2	1	9	268.	082
121	i51	1r1121	1450	1450	962	962	103257	103269	384	2	1	11	268.	121
106	i60	1p1133	2300	2300	958	958	102812	102844	384	2	1	9	268.	101
110	i70	1p1145	2300	2300	954	954	102941	102973	384	2	1	9	268.	101
114	i80	1p1157	2300	2300	950	950	103069	103101	384	2	1	11	268.	101
117	i81	1i1157	2300	2300	950	950	103164	103197	384	2	1	11	268.	101
133	i90	1p1169	2301	2301	946	946	103555	103587	384	2	1	11	268.	121
137	j00	1p1181	2301	2301	943	943	103694	103728	384	2	1	11	268.	121
139	j01	1i1181	2301	2301	943	943	103765	103798	384	2	1	9	268.	121
145	j10	1p1193	2301	2301	939	939	103973	104006	384	2	1	11	268.	141
135	j20	1p1205	2301	2301	935	935	103622	103657	384	2	1	11	268.	121
151	j21	1i1205	2301	2301	1078	1078	104179	104209	384	2	1	11	268.	141
185	j22	2i1205	1753	1753	1354	1354	105320	105329	384	2	1	11	268.	181
141	j30	1p1217	2301	2301	931	931	103833	103867	384	2	1	9	268.	141
143	j40	1p1229	2301	2301	927	927	103904	103938	384	2	1	9	268.	141
147	j50	1p1241	2301	2301	924	923	104041	104074	384	2	1	11	268.	141
152	j51	1i1241	1032	1032	2410	2410	104210	104243	384	2	1	11	088.	141
148	j60	1p1253	1028	1028	2410	2410	104075	104109	384	2	1	11	088.	141
150	j61	1i1253	1028	1028	2410	2410	104144	104178	384	2	1	11	088.	141
146	j70	1p1265	1025	1025	2410	2410	104007	104040	384	2	1	11	088.	141
134	j80	1p1277	1021	1021	2410	2410	103588	103621	384	2	1	11	088.	121
136	j90	1p1289	1017	1017	2408	2409	103658	103693	384	2	1	11	088.	121
138	k00	1p1301	1013	1013	2410	2410	103729	103764	384	2	1	9	088.	121
140	k01	1i1301	1013	1013	2410	2410	103799	103832	384	2	1	9	088.	121
142	k10	1p1313	1009	1009	2410	2410	103868	103903	384	2	1	9	088.	141
144	k11	1i1313	1009	1009	2410	2410	103939	103972	384	2	1	11	088.	141
154	k20	1p1325	1005	1005	2409	2409	104282	104316	384	2	1	11	088.	141
156	k30	1p1337	1001	1001	2409	2409	104354	104391	384	2	1	11	088.	141
159	k40	1p1349	1001	1001	2409	2410	104470	104504	384	2	1	11	088.	141
161	k41	1i1349	1001	1001	2410	2410	104539	104577	384	2	1	11	088.	161
163	k50	1p1361	1001	1001	2409	2409	104612	104646	384	2	1	11	088.	161
165	k60	1p1373	1001	1001	2409	2409	104681	104714	384	2	1	11	088.	161
167	k70	1p1385	1001	1001	1674	1674	104749	104766	384	2	1	11	088.	161
168	k71	2p1385	1675	1675	2410	2410	104767	104784	384	2	1	11	088.	161
170	k80	1p1397	1001	1001	2409	2409	104821	104855	384	2	1	11	088.	161
172	k81	1i1397	1001	1001	2409	2409	104891	104926	384	2	1	11	088.	161
149	k90	1p1409	2300	2300	892	892	104110	104143	384	2	1	11	268.	141
184	k91	1i1409	1060	1060	1950	1950	105298	105319	384	2	1	11	088.	181
153	l00	1p1421	2301	2301	893	892	104244	104281	384	2	1	11	268.	141
155	l10	1p1433	2301	2301	892	892	104317	104353	384	2	1	11	268.	141
158	l20	1p1445	2300	2300	893	892	104435	104468	384	2	1	11	268.	141
160	l21	1i1445	2300	2300	892	892	104505	104538	384	2	1	11	268.	141
162	l30	1p1457	2301	2301	892	892	104578	104611	384	2	1	11	268.	161
164	l40	1p1469	2301	2301	893	892	104647	104680	384	2	1	11	268.	161
183	l41	1i1469	2301	2301	1630	1630	105278	105297	384	2	1	11	268.	181
166	l50	1p1481	2300	2300	892	892	104715	104748	384	2	1	11	268.	161
169	l60	1p1493	2301	2301	892	892	104785	104820	384	2	1	11	268.	161
171	l70	1p1505	2301	2301	892	892	104856	104890	384	2	1	11	268.	161
173	l80	1p1517	2300	2300	892	892	104927	104960	384	2	1	11	268.	161
175	l81	1i1517	2300	2300	892	892	105003	105036	384	2	1	11	268.	161
177	l90	1p1529	2301	2301	892	892	005073	005106	384	2	1	11	268.	161
179	m00	1p1541	2301	2301	892	892	105145	105179	384	2	1	11	268.	161
181	m10	1p1553	2089	2089	892	892	105214	105242	384	2	1	11	268.	181
182	m11	1i1553	1001	1001	2409	2409	105243	105276	384	2	1	11	088.	181
176	m20	1p1565	1001	1001	2409	2409	105037	105072	384	2	1	11	088.	161
174	m30	1p1577	1001	1001	2410	2410	104961	105002	384	2	1	11	088.	161
178	m40	1p1589	1001	1001	2409	2409	105108	105144	384	2	1	11	088.	161
180	m50	1p1601	1001	1001	2409	2409	105180	105213	384	2	1	11	088.	161

7. Processing Time Line

Decon	August-December 1995
Elastic Binning	April - May 1996
Velocity	January - April 1996
DMO Stack	May - June 1996
Migration	July 1996

8. Notable Processing Problems and Solutions

The benefits from the decision to rebuild the Index from seismic headers instead of using the G2000 navigation files delivered from the Calgary center were not realised until stack production. After 34% of the southern priority area was stacked, it was discovered that the 'dpr' files generated from the G2000 did not agree with the seismic trace headers which created the index file. This discrepancy caused a significant amount of traces to be dropped from the stack. After discussing the problem with the DP support group, stack production resumed by using a processor `dmbgf' which circumvented the input of dpr files. As a consequence, an initial delay of 1 week was encountered, but was later recovered from the assignment of additional cpu resources.

9. Conclusion

Houston DP inherited this project from the Calgary DP Center in late March 1996 when the original deadline was due. After reviewing the previous processing, it soon became obvious that the Index had to be rebuilt from scratch and the velocities had to be partially re-run and completely re-picked. However, with the support of the DP management and from the great effort of the processing group, we were able to deliver the Migrated Volume of the Southern priority area of the survey on June 30, while continuing to stack the Northern half. Finally, by the end of July 1996, as promised, the final migration of the entire volume was delivered.

Due to the wide spread deployment of the four streamer and triple source array, the shallow data was heavily contaminated by aliased noise. In fact, the data volume as a whole had a relatively poor signal/noise ratio. It was deemed necessary to apply, post-stack, a shallow in-line K-filter in conjunction with a 3-D FXY noise attenuation filter over the entire record length.

Figures 3 & 4 in Section 12 illustrate the results with and without the 3-D FXY noise attenuation filter.

Also shown in Section 12, Figures 5 and 6 are the timeslices from the QuickLook Cube migration (QLC) and the Final migrated volume, respectively. These timeslices are both at 2.0secs and clearly demonstrate the improvements attained from the final processing sequence.

10. 3-D Velocity Fields

10.1 Stacking Velocity Field

The 3-D stacking velocity field was generated using velocities derived by performing 3-D velocity analysis at selected in-line locations on the 3-D grid. The velocities were to be calculated on an 800 X 800 meter grid. Since the data was acquired with a subsurface line spacing of 25 meters, this required that every 32nd row location be processed in 3-D mode as a velocity line, starting with row 25. The following is a list of the velocity lines that were used for this survey.

> Rows 25, 57, 89, 121, 153, 185, 217, 249, 281, 313, 345, 377, 409, 441, 473, 505, 537, 569, 601, 633, 665, 697, 729, 761, 793, 825, 857, 889, 921, 953, 985, 1017, 1049, 1081, 1113, 1145, 1177, 1209, 1241, 1273, 1305, 1337, 1369, 1401, 1433, 1465, and 1497.

The DMO gathers were created on Fujitsu for above velocity lines and transferred to the Geco-Prakla Sun Workstation for velocity analysis. Finally, 2-D DMO stacks were generated to verify velocity interpretation. The stacks were created by using data acquired closest to the velocity row location, merging data with navigation and then stacking into 3-D grid which was allocated with wide bins.

Once all the velocities analyses had been interpreted and approved, a 3-D velocity database was constructed. According to the grid definition, the in-line position and the cross-line position, each velocity location was assigned the proper X, Y coordinate. In order for our program to properly build a velocity cube, the input grid of velocity cube completely covered the survey, the rectangular grid was defined to cover cross-line 1 through 3200 and in-line 1 through 1532. The first and last functions for each velocity line were repeated to cover this area. Once this velocity database was built, velocities were interpolated in time and space.

Temporal resampling to a regular time increment was done first, such that each function now had 76 velocity picks (i.e. 76 velocity timeslices). Each timeslice was then interpolated to fill in all intermediate points. Interpolation of the timeslices was done in the following manner:

1. Calculate the midpoint bin number of the four velocities on the regular rectangle bounded input velocities $V_{i,j}$ $V_{i+1,j}$ $V_{i,j+1}$ $V_{i+1,j+1}$, where i is the in-line number and j is the cross-line number.
2. Calculate the average velocity of these four velocities weighted by the inverse of the distance to the midpoints.
3. Linearly interpolate between known input points in the in-line direction.
4. Linearly interpolate between known input points in the cross-line direction.
5. Linearly interpolate the midpoints calculated in step 2 in the in-line direction.
6. Linearly interpolate the midpoints calculated in step 2 in the cross-line direction.
7. Linearly interpolate points along every 64 cross-line.
8. Linearly interpolate remaining points in the in-line direction.

10.2 Migration Velocity Field

The migration velocity field was constructed in a similar fashion. This procedure started with the temporally resampled database that was used for the stacking velocity cube. Before spatial interpolation of the functions, the velocities were converted to interval velocities. In addition, these interval velocity functions were temporally smoothed by fitting the time velocity points to a ninth order polynomial. This ensured that there were no unreasonably large temporal velocity changes in the interval velocity functions. These smoothed interval velocity functions were then spatially interpolated as above. After spatial interpolation, a four-pass recursive smoothing filter was applied to the velocity cube. This recursive filter operated in the following manner:

1. Each bin was summed with the previous bin in the cross-line direction with the following weights: 0.1 for the current bin and 0.9 for the previous bin. The resultant velocity was immediately written back to the current location. This procedure was repeated at next location and continued until all bins were mixed. The direction of mixing was from highest in-line number to lowest in-line number.
2. Same as in 1, but done from lowest in-line number to highest in-line number.
3. Same as 1, but in the in-line direction from highest cross-line number to lowest cross-line number.
4. Same as 3, but from lowest cross-line number to highest cross-line number.

11. Job Setups for Main Processing Steps

11.1 A job setup for Deconvolution

```
/job      acct '7263 nf1p0557 explserv segystbd'
          trdcntl '/proj/nav/cntl/g2s0731.cntl'

/seisin   format segd datafmt 8015
          data 1 9000 2 384 0
          dens hc
          exthdr 12
          extprint
          errtyp 2
          nodummy conskip 999999 totskip 999999
          reel 1816
          reel 1817
          reel 1818
          reel 1819
          reel 1820
          reel 1821
          reel 1822
          reel 1823
          reel 1824
          reel 1825
          reel 1826
          reel 1827
          reel 1828
          reel 1829
          reel 1830
          reel 1831
          reel 1832
          reel 1833
          reel 1834
          reel 1835
          reel 1836
          reel 1837
          reel 1838
          reel 1839
          reel 1840
          reel 1841
          reel 1842
          reel 1843
          bi 1252 ei 2409
          (revfiles
          device 'rmt1'
          ftraces d9,200,1 d201,392,1
(port          ftraces d1,192,1 d201,392,1
          reseq 1

/deadset

/filter   butterwo lowpass minimum filt 90 72 nfpts 121
/resamp   sro 4 noalias

(@zero
/zero ftraces 208
```

```
/zero ffiles 1278 1353 2219
(         1         2         3         4         5         6
(234567890123456789012345678901234567890123456789012345678901234567890
(nf-1p0557     FSP       LSP        1.0  FTR  LTR
(nf-1p0557                               200  200
(nf-1p0557     1278      1278       1.0
(nf-1p0557     1353      1353       1.0
(nf-1p0557     2219      2219       1.0
(234567890123456789012345678901234567890123456789012345678901234567890

( add 384 to port cable only to match p190s and make each kfldtn unique:
/glmod    add kfldtn -8 0
(port /glmod    ftraces d201,392,1 add kfldtn -8 0
(port /glmod    add kfldtn 384 0
/sphdiv   vel
            1.  1472.   500.  1647.  1000.  1813.  1500.  2000.
         2000.  2221.  2500.  2630.  3000.  2990.  3500.  3274.
         4000.  3548.  4500.  3749.  5000.  3920.  5500.  4076.
         6000.  4218.  6500.  4335.  7000.  4450.  7500.  4483.
         8000.  4509.  8500.  4509.  9000.  4509
          tstop 8000

/expgain  begtime 1 200 9999 200 endtime 1 4000 9999 4000 expfunc +3.0
/filter   filename '/data11/desig/designature'

/merg3d   mxtrskip 300000
          detnum   768
          usefldtr
          navshots 1252 2409
          mxspskip 999
          mxsptdlt 30
          timediff 2
          todmerge
          (sidfmt '(i8,2x)'
          line 'nf_1p0557     ' (these blank spaces are needed to make it
work..

/preddcon zone 1
          operator    1 6000 320    4
          operator 9999
          design      1 260 400  5050 4700
          design   9999
          apply      1 260 0  5050 0
          apply    9999
          prewhite 0.1
          byfile

/glmod set kgrrow 0557,0
/glmod setlid nf1p kgrrow
(this is optional to stop /output putting all reel numbers as "SCRTCH":
/hdrsegy  cardnum 3
 contents 'C 3 REEL NO 1p0557  DAY_START OF REEL     YEAR      OBSERVER'
/output   lname '1p0557' dens hc segyhead gecostrd
          device rmt2
          segyhist '/proj/gss/jobs/segy/newf_template'
          noreseq
/eoj
```

11.2 A job setup for 3-D DMO and Stack with Elastic Binning

```
/job        acct      '0489 g30a nfgb   dms'
            (runcode 0
            (system  vpx220
            (division  f
            (region 84 Mb
/jobtick    submitby 'group11'
            runtime   5.0
            inreel 'D00987'
            inreel 'D00988'
            inreel 'D00989'
            inreel 'D00990'
            inreel 'D00991'
            process 'dmbtd'
            userinst '**** NEW FOUNDLAND **'
            userinst '                    '
            userinst 'RUN ONE JOB AT A TIME'
            userinst '*** dmo stack *******'
            dsn '/prod/dmstk/b4dmstkg30a.s'
/trdfile    use stack  ctrlname '/SDP248/grp11/p489/stack.cntl'
            use index  ctrlname '/SDP366/grp11/p489/index.cntlall'
            jobrows    759  797
            jobcols    1    3200
/seisin     data 5 9000 4 384  0
            eofcount 2
            dens silo
            reel D00987
            reel D00988
            reel D00989
            reel D00990
            reel D00991
            byfield
            reseq 1
/deadset
/grdit      getrwcl
            xorigin   645410   yorigin   5226665
            basangle   88.34   sidangle   178.34
            rowsize     25.0   colsize     12.50
            nombinsx     100   nombinsy      100
            maxgrdcl    3200
            setcdp             setsta
/dmbgf      contfile '/SDP213/grp11/p489/dmbtd.cntl'
            xorigin   645410   yorigin   5226665
            basangle   88.34   sidangle   178.34
            rowsize     25.0   colsize     12.50
            newline '1p0857 A  '
            print  30
/dmbcd      contfile '/SDP213/grp11/p489/dmbtd.cntl'
            mappedtr 1200
            firstrow  763
            lastrow   793
            firstcol    1
            lastcol  3200
            xorigin   645410   yorigin   5226665
            basangle   88.34   sidangle   178.34
            rowsize     25.0   colsize     12.50
```

```
/tranalys
               offset        265 5040 thres 10.0 firstspk
               nearwind     1000 9000
               farwind      4500 9000
               taper         200
/zvelocit      threed
               rmsvels
               notintrp
               rdthreed    0 100 9000 100
               maxrow      1532
               maxcol      3200
               vcubenam 'dsn=/SDP238/grp11/p489/vcub489.cntl;'
/nmo
/mute         fmute        1  0+0 575+0 576+500  5200+4200
              fmute 9999999  0+0 575+0 576+500  5200+4200
              taper 20
/deadset      useglcom
              (fmute and tmute in headers applied to trace samples
/dmbtd
              stkcntl  '/SDP248/grp11/p489/stack.cntl'
              contfile '/SDP213/grp11/p489/dmbtd.cntl'
              filetype stack
              (restart
              boundary  1  1  1532  1 1532  3200  1 3200
                        1  1
              firstrow  763
              lastrow   793
              firstcol  1
              lastcol   3200
              feather    200
              numbins   5500
              unnorm
              (printbnd   use for first dmo run only
/eoj
```

11.3 A job setup for In-line k-filter

```
/job        acct '0489 norm nfgb    dms'
            (runcode 0
            (system  vpx220
            (priority  8
            (division  e
/jobtick    submitby 'cathy'
            runtime  3.5
            process  'norm'
            userinst '*** NEW FOUNDLAND**'
            userinst ' DMO STACK      '
            userinst ' NORMALIZE CUBE'
            userinst ' row 001-200       '
            userinst '*******************'
            dsn      'gss/jobs/prod/norm/b1normala.s'
/trdfile    use stack
            ctrlname  '/SDP248/grp11/p489/stack.cntl'
            jobrows  001 200
            jobcols  1   3200
/stkin      data 4 9000 4 1 0
            rows 1  200 1
            cols 1 3200 1
            use  stack
            root
            xorigin  645410    yorigin   5226665
            basangle  88.34    sidangle  178.34
            rowsize      25    colsize   12.5

/deadset
/glmod      set kcdp 1  1

/filtwod
            nxfilt 25 ntfilt 1
            timegate 0 0 3000 4000
            kfilt  -43  -38  -28  -23
            reject  costaper
/filtwod
            nxfilt 25 ntfilt 1
            timegate 0 0 3000 4000
            kfilt  -76  -71  -61  -56
            reject  costaper
/filtwod
            nxfilt 25 ntfilt 1
            timegate 0 0 3000 4000
            kfilt  -110  -105  -95  -90
            reject  costaper

/deadset    useglcom
/stkout     client 'exp services'
            area   'n foundland'
            use stack
            firstrow  1       lastrow  779
            firstcol  1       lastcol  3200

/eoj
```

11.4 A job setup for 3-D FXY-filter

```
/job       acct '0489 rowqc nfgb dms' plotevry 1
           (runcode 0
           (system  vpx220
           (division e
           (priority 8
           (region 60 Mb
/jobtick   submitby 'indro'
           runtime  1.30
           process  'fxy'
           userinst '***newfoundland***'
           userinst 'fxy dcn            '
           userinst '******************'
           dsn      'gss/jobs/test/b0fxy1.s'
/trdfile   use stack
           ctrlname  '/SDP248/grp11/p489/stack.cntl'
           jobrows 211    278
           jobcols 1533   3200
/stkin     data 4 9000 4 1 0
           rows  211    278  1    (insert correct row range
           cols  1533   3200 1
           root
           bycol
           xorigin  645410    yorigin   5226665
           basangle  88.34    sidangle  178.34
           rowsize    25      colsize   12.5

/deadset
/renumber  firstcdp  1

/fxyfilt
           ilwind 20
           xlwind 20
           lenfil 5 (default 3 ,recomm
           ilovlp 10
           xlovlp 10
           lowfreq  0
           highfreq 75
           nscalwin 10
           bycol

/deadset useglcom
/stkout    client 'exp services'
           area   'n foundland'
           use stack
           firstrow   1       lastrow  1532
           firstcol   1       lastcol  3200
/eoj
```

11.5 A job setup for Migration Step-I

```
/job       acct '0489 1225 nfgb mig'
     (runcode 0
           (system   vpx220
           (priority 8
           (region 110Mb
           (division E
/jobtick   submitby 'nicholas'
           runtime   5.00
           inreel   'disk'
           outreel  'no/op'
           process  'mig'
           userinst '******nfgb*****'
           userinst 'migration step 1        '
           userinst '!!! check memory before'
           userinst 'starting job!!          '
           userinst '******nfgb*****'
           dsn      'N/A'
/trdfile   use mig
           ctrlname '/SDP248/grp11/p489/mig.cntl'
           jobrows 1051 1225 (reading in 175 in-lines
           jobcols 1 3750 (full range including padded zone
/stkin     data 4 9000 6 1 0 (without stretch
           use mig
           rows 1051 1225 1 (reading in 175 inlines
           cols 1 3200 1 (full range excluding padded zone
/renumber  firstcdp 1
/deadset
/mgtda     qc
           unit     '3380  '
           volser   'SDP388'
           resfile  '/SDP388/grp11/p489/mgtdap1_1225.log'
           wrkfile  '/SDP388/grp11/p489/mgtdap1_1225.wrk'
           hdrfile  '/SDP388/grp11/p489/mgtdap1_1225.hdr'
           atap      20 (default is 30
           vmax      0  (0 for steps 1 and 3 otherwise 5000.0
           use mig
           flagtd
           byrows             (byrows or bycols
           firstrow  1051     (first row forjob
           lastrow   1225     (last row forjob
           firstcol  1
           lastcol   3200     (excluding padding
           delrow    25.0
           delcol    12.5
           anone     0.5
           antwo     1.5
           anthree   65
           (anfour    75 2.0 70 4.0 50 6.0 40 9.0 30
           anfour    75
           angm      60 3.0 60 6.0 40 9.0 10
           (bmem      0.4
           padt      2.0
           interval
           fracv     3.0
           dtrms     200
           ivpt      1        (step number 1 2 or 3
```

```
            nrows      1532     (total rows
            ncols      3200     (total, excluding padding
            ncolsb     3750     (total, including padding
            knsmpa     1501     (based on 9000ms same for all 3 steps
            knsmpb     1617     (based on 9700ms same for all 3 steps
            minrow     1
            mincol     1
            oppam      0 4 4 4
            opcoef
2.6885530025518318e-12
-1.5643384297873967e-10
2.1290515836198131e-09
9.8991836409524095e-10
-3.1765299123544911e-10
1.7937876643132595e-08
-2.5513263531331779e-07
5.8315702273087551e-07
6.5697373079858209e-09
-3.7729275820553167e-07
5.7157588556168815e-06
-2.9293642775904404e-05
-1.9393565181001961e-08
1.5356500315522706e-06
-3.0044565226616910e-05
2.0466111784319987e-04
-4.6059397877277321e-11
2.2498468580708324e-09
-2.0560394654967973e-08
-1.1887344421262180e-07
5.0196558319867309e-09
-2.6580428720523643e-07
3.2847062992355365e-06
-7.8541951852597136e-07
-1.0053347633009887e-07
5.6454287584597702e-06
-8.0992933789517047e-05
3.4944739663473836e-04
2.3097712487347025e-07
-2.1946018446472336e-05
4.3855936018693099e-04
-1.5231606720904691e-03
1.9308953322115055e-10
-6.0785162295568208e-09
-3.9673038335757044e-08
1.5050571147391096e-06
-1.9009562222806280e-08
8.3932435472912061e-07
-5.7555177273305824e-06
-8.2047805427580000e-05
3.3276832198055027e-07
-1.7517174728528716e-05
2.2245527911552334e-04
-4.8666418329775061e-04
8.7828068061426891e-09
4.8522394112172528e-05
-1.2590824440579876e-03
5.6091735027792361e-04
2.9426077435090765e-11
-7.1375725480455047e-09
2.4061149572508669e-07
```

```
-8.3096238541784616e-07
2.0173669271152617e-09
1.2334199172536735e-07
-8.4742999246973462e-06
1.0141919557191004e-04
-7.0234471937942906e-10
-9.0518773823712036e-07
1.2399309386829978e-05
-4.6301647641408615e-04
-1.0515828579203047e-06
3.3027604263354205e-05
1.4688985990807825e-04
1.8936469985501221e-02
(pilot interval velocities follow
vpilot (reduced pilot velocity function
1561.48 ( at 0.00000000e+00  milliseconds
1591.35 ( at 199.99992  milliseconds
1701.56 ( at 399.99976  milliseconds
1849.88 ( at 599.99976  milliseconds
1992.02 ( at 799.99976  milliseconds
2135.19 ( at 999.99976  milliseconds
2314.41 ( at 1199.9998  milliseconds
2520.41 ( at 1399.9995  milliseconds
2755.25 ( at 1599.9993  milliseconds
3005.54 ( at 1799.9990  milliseconds
3257.89 ( at 1999.9990  milliseconds
3504.06 ( at 2199.9998  milliseconds
3735.81 ( at 2399.9995  milliseconds
3953.14 ( at 2599.9993  milliseconds
4163.26 ( at 2799.9990  milliseconds
4332.18 ( at 2999.9990  milliseconds
4475.35 ( at 3199.9988  milliseconds
4617.49 ( at 3399.9995  milliseconds
4724.61 ( at 3599.9993  milliseconds
4818.34 ( at 3799.9990  milliseconds
4916.19 ( at 3999.9990  milliseconds
4727.63 ( at 4199.9961  milliseconds
4775.36 ( at 4399.9961  milliseconds
4828.32 ( at 4599.9961  milliseconds
4890.72 ( at 4799.9961  milliseconds
4930.20 ( at 4999.9961  milliseconds
4994.20 ( at 5199.9961  milliseconds
5043.84 ( at 5399.9961  milliseconds
5064.38 ( at 5599.9961  milliseconds
5100.93 ( at 5799.9961  milliseconds
5110.71 ( at 5999.9961  milliseconds
4915.52 ( at 6199.9961  milliseconds
4882.66 ( at 6399.9961  milliseconds
4838.82 ( at 6599.9961  milliseconds
4757.56 ( at 6799.9961  milliseconds
4663.44 ( at 6999.9961  milliseconds
4574.28 ( at 7199.9961  milliseconds
4454.18 ( at 7399.9961  milliseconds
4353.84 ( at 7599.9961  milliseconds
4260.69 ( at 7799.9961  milliseconds
4190.87 ( at 7999.9961  milliseconds
4106.28 ( at 8199.9961  milliseconds
4021.91 ( at 8399.9961  milliseconds
3930.85 ( at 8599.9961  milliseconds
3838.66 ( at 8799.9961  milliseconds
```

```
 3746.56 ( at 8999.9961  milliseconds
 3746.56 (repeat last velocity for stretch
 3746.56 (9400 milliseconds
 3746.56 (9600 milliseconds
 3746.56 (9800 milliseconds
/stkout   use mig
          client 'expl'
          area 'nfgb'
          firstrow 1051 lastrow 1225
          firstcol 1 lastcol 3750 (including padding
/eoj
```

11.6 A job setup for Migration Step-II

```
/job        acct '0489 3000 nfgb mig'
            (runcode 0
            (system   vpx220
            (priority 8
            (region 110Mb
            (division G
/jobtick    submitby 'nicholas'
            runtime   6.00
            inreel    'disk'
            outreel   'no/op'
            process   'mig'
            userinst  '******nfgb*****'
            userinst  'migration step 2       '
            userinst  '!!! check memory before'
            userinst  'starting job!!         '
            userinst  '******nfgb*****'
            dsn       'N/A'
/trdfile    use mig
            ctrlname '/SDP248/grp11/p489/mig.cntl'
            jobrows 1 1532 (reading in 1532 inlines
            jobcols 2851 3000 (150 cols, last job includes padded zone
/syndata    sr 6 msi 9700 ntr 1 nrecs 1 datatype shot type 5
/mgtda      qc
            unit      '3380  '
            volser    'SDP388'
            resfile   '/SDP388/grp11/p489/mgtdap2_3000.log'
            wrkfile   '/SDP388/grp11/p489/mgtdap2_3000.wrk'
            hdrfile   '/SDP388/grp11/p489/mgtdap2_3000.hdr'
            atap      20 (default is 30
            vmax      5200  (0 for steps 1 and 3 otherwise 5200.0
            use mig
            flagtd
            bycols              (byrows or bycols
            firstrow  1         (first row forjob
            lastrow   1532      (last row forjob
            firstcol  2851      (first col for job
            lastcol   3000      (last job includes padding
            delrow    25.0
            delcol    12.5
            anone     0.5
            antwo     1.5
            anthree   65
            anfour    75
            angm      60 3.0 60 6.0 40 9.0 10
            (bmem      0.4
            padt      2.0
            interval
            fracv     3.0
            dtrms     200
            ivpt      2          (step number 1 2 or 3
            nrows     1532       (total rows
            ncols     3200       (total, excluding padding
            ncolsb    3750       (total, including padding
            knsmpa    1501       (based on 9000ms same for all 3 steps
            knsmpb    1617       (based on 9700ms same for all 3 steps
```

```
            minrow    1
            mincol    1
            oppam     0 4 4 4
            opcoef
2.6885530025518318e-12
-1.5643384297873967e-10
2.1290515836198131e-09
9.8991836409524095e-10
-3.1765299123544911e-10
1.7937876643132595e-08
-2.5513263531331779e-07
5.8315702273087551e-07
6.5697373079858209e-09
-3.7729275820553167e-07
5.7157588556168815e-06
-2.9293642775904404e-05
-1.9393565181001961e-08
1.5356500315522706e-06
-3.0044565226616910e-05
2.0466111784319987e-04
-4.6059397877277321e-11
2.2498468580708324e-09
-2.0560394654967973e-08
-1.1887344421262180e-07
5.0196558319867309e-09
-2.6580428720523643e-07
3.2847062992355365e-06
-7.8541951852597136e-07
-1.0053347633009887e-07
5.6454287584597702e-06
-8.0992933789517047e-05
3.4944739663473836e-04
2.3097712487347025e-07
-2.1946018446472336e-05
4.3855936018693099e-04
-1.5231606720904691e-03
1.9308953322115055e-10
-6.0785162295568208e-09
-3.9673038335757044e-08
1.5050571147391096e-06
-1.9009562222806280e-08
8.3932435472912061e-07
-5.7555177273305824e-06
-8.2047805427580000e-05
3.3276832198055027e-07
-1.7517174728528716e-05
2.2245527911552334e-04
-4.8666418329775061e-04
8.7828068061426891e-09
4.8522394112172528e-05
-1.2590824440579876e-03
5.6091735027792361e-04
2.9426077435090765e-11
-7.1375725480455047e-09
2.4061149572508669e-07
-8.3096238541784616e-07
2.0173669271152617e-09
1.2334199172536735e-07
-8.4742999246973462e-06
1.0141919557191004e-04
```

```
 -7.0234471937942906e-10
 -9.0518773823712036e-07
 1.2399309386829978e-05
 -4.6301647641408615e-04
 -1.0515828579203047e-06
 3.3027604263354205e-05
 1.4688985990807825e-04
 1.8936469985501221e-02
 (pilot interval velocities follow
 vpilot (reduced pilot velocity function
 1561.48 ( at 0.00000000e+00  milliseconds
 1591.35 ( at 199.99992  milliseconds
 1701.56 ( at 399.99976  milliseconds
 1849.88 ( at 599.99976  milliseconds
 1992.02 ( at 799.99976  milliseconds
 2135.19 ( at 999.99976  milliseconds
 2314.41 ( at 1199.9998  milliseconds
 2520.41 ( at 1399.9995  milliseconds
 2755.25 ( at 1599.9993  milliseconds
 3005.54 ( at 1799.9990  milliseconds
 3257.89 ( at 1999.9990  milliseconds
 3504.06 ( at 2199.9998  milliseconds
 3735.81 ( at 2399.9995  milliseconds
 3953.14 ( at 2599.9993  milliseconds
 4163.26 ( at 2799.9990  milliseconds
 4332.18 ( at 2999.9990  milliseconds
 4475.35 ( at 3199.9988  milliseconds
 4617.49 ( at 3399.9995  milliseconds
 4724.61 ( at 3599.9993  milliseconds
 4818.34 ( at 3799.9990  milliseconds
 4916.19 ( at 3999.9990  milliseconds
 4727.63 ( at 4199.9961  milliseconds
 4775.36 ( at 4399.9961  milliseconds
 4828.32 ( at 4599.9961  milliseconds
 4890.72 ( at 4799.9961  milliseconds
 4930.20 ( at 4999.9961  milliseconds
 4994.20 ( at 5199.9961  milliseconds
 5043.84 ( at 5399.9961  milliseconds
 5064.38 ( at 5599.9961  milliseconds
 5100.93 ( at 5799.9961  milliseconds
 5110.71 ( at 5999.9961  milliseconds
 4915.52 ( at 6199.9961  milliseconds
 4882.66 ( at 6399.9961  milliseconds
 4838.82 ( at 6599.9961  milliseconds
 4757.56 ( at 6799.9961  milliseconds
 4663.44 ( at 6999.9961  milliseconds
 4574.28 ( at 7199.9961  milliseconds
 4454.18 ( at 7399.9961  milliseconds
 4353.84 ( at 7599.9961  milliseconds
 4260.69 ( at 7799.9961  milliseconds
 4190.87 ( at 7999.9961  milliseconds
 4106.28 ( at 8199.9961  milliseconds
 4021.91 ( at 8399.9961  milliseconds
 3930.85 ( at 8599.9961  milliseconds
 3838.66 ( at 8799.9961  milliseconds
 3746.56 ( at 8999.9961  milliseconds
 3746.56 (repeat last velocity for stretch
 3746.56 (9400 milliseconds
 3746.56 (9600 milliseconds
/eoj
```

11.7 A job setup for Migration Step-III

```
/job        acct '0489 1225 nfgb mig'
            (runcode 0
            (system   vpx220
            (priority 8
            (region 110Mb
            (division E
/jobtick    submitby 'nicholas'
            runtime   6.00
            inreel    'disk'
            outreel   'no/op'
            process   'mig'
            userinst  '******nfgb*****'
            userinst  'migration step 3       '
            userinst  '!!! check memory before'
            userinst  'starting job!!         '
            userinst  '******nfgb*****'
            dsn       'N/A'
/trdfile    use mig
            ctrlname '/SDP248/grp11/p489/mig.cntl'
            jobrows 1051 1225 (reading in 175 inlines
            jobcols 1 3750 (full range including padded zone
/stkin      data 4 9700 6 1 0 (with stretch
            use mig
            rows 1051 1225 1 (reading in 175 inlines
            cols 1 3750 1 (full range including padded zone
/renumber   firstcdp 1
/mgtda      qc
            unit      '3380  '
            volser    'SDP388'
            resfile   '/SDP388/grp11/p489/mgtdap3_1225.log'
            wrkfile   '/SDP388/grp11/p489/mgtdap3_1225.wrk'
            hdrfile   '/SDP388/grp11/p489/mgtdap3_1225.hdr'
            atap       20 (default is 30
            vmax       0  (0 for steps 1 and 3 otherwise 5000.0
            use mig
            flagtd
            byrows              (byrows or bycols
            firstrow  1051      (first row forjob
            lastrow   1225      (last row forjob
            firstcol  1
            lastcol   3750      (including padding
            delrow    25.0
            delcol    12.5
            anone     0.5
            antwo     1.5
            anthree   65
            (anfour    75 2.0 70 4.0 50 6.0 40 9.0 30
            anfour    75
            angm      60 3.0 60 6.0 40 9.0 10
            (bmem      0.4
            padt      2.0
            interval
            fracv     3.0
            dtrms     200
            ivpt      3         (step number 1 2 or 3
```

```
nrows     1532    (total rows
ncols     3200    (total, excluding padding
ncolsb    3750    (total, including padding
knsmpa    1501    (based on 9000ms same for all 3 steps
knsmpb    1617    (based on 9700ms same for all 3 steps
minrow    1
mincol    1
oppam     0 4 4 4
opcoef
2.6885530025518318e-12
-1.5643384297873967e-10
2.1290515836198131e-09
9.8991836409524095e-10
-3.1765299123544911e-10
1.7937876643132595e-08
-2.5513263531331779e-07
5.8315702273087551e-07
6.5697373079858209e-09
-3.7729275820553167e-07
5.7157588556168815e-06
-2.9293642775904404e-05
-1.9393565181001961e-08
1.5356500315522706e-06
-3.0044565226616910e-05
2.0466111784319987e-04
-4.6059397877277321e-11
2.2498468580708324e-09
-2.0560394654967973e-08
-1.1887344421262180e-07
5.0196558319867309e-09
-2.6580428720523643e-07
3.2847062992355365e-06
-7.8541951852597136e-07
-1.0053347633009887e-07
5.6454287584597702e-06
-8.0992933789517047e-05
3.4944739663473836e-04
2.3097712487347025e-07
-2.1946018446472336e-05
4.3855936018693099e-04
-1.5231606720904691e-03
1.9308953322115055e-10
-6.0785162295568208e-09
-3.9673038335757044e-08
1.5050571147391096e-06
-1.9009562222806280e-08
8.3932435472912061e-07
-5.7555177273305824e-06
-8.2047805427580000e-05
3.3276832198055027e-07
-1.7517174728528716e-05
2.2245527911552334e-04
-4.8666418329775061e-04
8.7828068061426891e-09
4.8522394112172528e-05
-1.2590824440579876e-03
5.6091735027792361e-04
2.9426077435090765e-11
-7.1375725480455047e-09
2.4061149572508669e-07
```

```
-8.3096238541784616e-07
2.0173669271152617e-09
1.2334199172536735e-07
-8.4742999246973462e-06
1.0141919557191004e-04
-7.0234471937942906e-10
-9.0518773823712036e-07
1.2399309386829978e-05
-4.6301647641408615e-04
-1.0515828579203047e-06
3.3027604263354205e-05
1.4688985990807825e-04
1.8936469985501221e-02
(pilot interval velocities follow
vpilot (reduced pilot velocity function
1561.48 ( at 0.00000000e+00  milliseconds
1591.35 ( at 199.99992  milliseconds
1701.56 ( at 399.99976  milliseconds
1849.88 ( at 599.99976  milliseconds
1992.02 ( at 799.99976  milliseconds
2135.19 ( at 999.99976  milliseconds
2314.41 ( at 1199.9998  milliseconds
2520.41 ( at 1399.9995  milliseconds
2755.25 ( at 1599.9993  milliseconds
3005.54 ( at 1799.9990  milliseconds
3257.89 ( at 1999.9990  milliseconds
3504.06 ( at 2199.9998  milliseconds
3735.81 ( at 2399.9995  milliseconds
3953.14 ( at 2599.9993  milliseconds
4163.26 ( at 2799.9990  milliseconds
4332.18 ( at 2999.9990  milliseconds
4475.35 ( at 3199.9988  milliseconds
4617.49 ( at 3399.9995  milliseconds
4724.61 ( at 3599.9993  milliseconds
4818.34 ( at 3799.9990  milliseconds
4916.19 ( at 3999.9990  milliseconds
4727.63 ( at 4199.9961  milliseconds
4775.36 ( at 4399.9961  milliseconds
4828.32 ( at 4599.9961  milliseconds
4890.72 ( at 4799.9961  milliseconds
4930.20 ( at 4999.9961  milliseconds
4994.20 ( at 5199.9961  milliseconds
5043.84 ( at 5399.9961  milliseconds
5064.38 ( at 5599.9961  milliseconds
5100.93 ( at 5799.9961  milliseconds
5110.71 ( at 5999.9961  milliseconds
4915.52 ( at 6199.9961  milliseconds
4882.66 ( at 6399.9961  milliseconds
4838.82 ( at 6599.9961  milliseconds
4757.56 ( at 6799.9961  milliseconds
4663.44 ( at 6999.9961  milliseconds
4574.28 ( at 7199.9961  milliseconds
4454.18 ( at 7399.9961  milliseconds
4353.84 ( at 7599.9961  milliseconds
4260.69 ( at 7799.9961  milliseconds
4190.87 ( at 7999.9961  milliseconds
4106.28 ( at 8199.9961  milliseconds
4021.91 ( at 8399.9961  milliseconds
3930.85 ( at 8599.9961  milliseconds
3838.66 ( at 8799.9961  milliseconds
```

```
 3746.56 ( at 8999.9961  milliseconds
 3746.56 (repeat last velocity for stretch
 3746.56 (9400 milliseconds
 3746.56 (9600 milliseconds
 3746.56 (9800 milliseconds
/renumber firstcdp 1
/glcom    grrows 1051 1225
/expgain  begtime 1 5000 999999 5000
          endtime 1 9000 999999 9000
          expfunc +2.0
/stkout   use mig
          client 'expl'
          area 'nfgb'
          firstrow 1051 lastrow 1225
          firstcol 1 lastcol 3200 (excluding padding
/eoj
```

12. Figures

- **Figure 1 :** GRAND BANKS production designature operator
- **Figure 2 :** GRAND BANKS conditioned gun signature
- **Figure 3 :** K-Filter Stack Timeslice 2.0 sec
- **Figure 4 :** 3D FXYFILT Stack Timeslice 2.0 sec
- **Figure 5 :** Quick Look Cube Migration Timeslice 2.0 sec
- **Figure 6 :** Final Migration Timeslice 2.0 sec

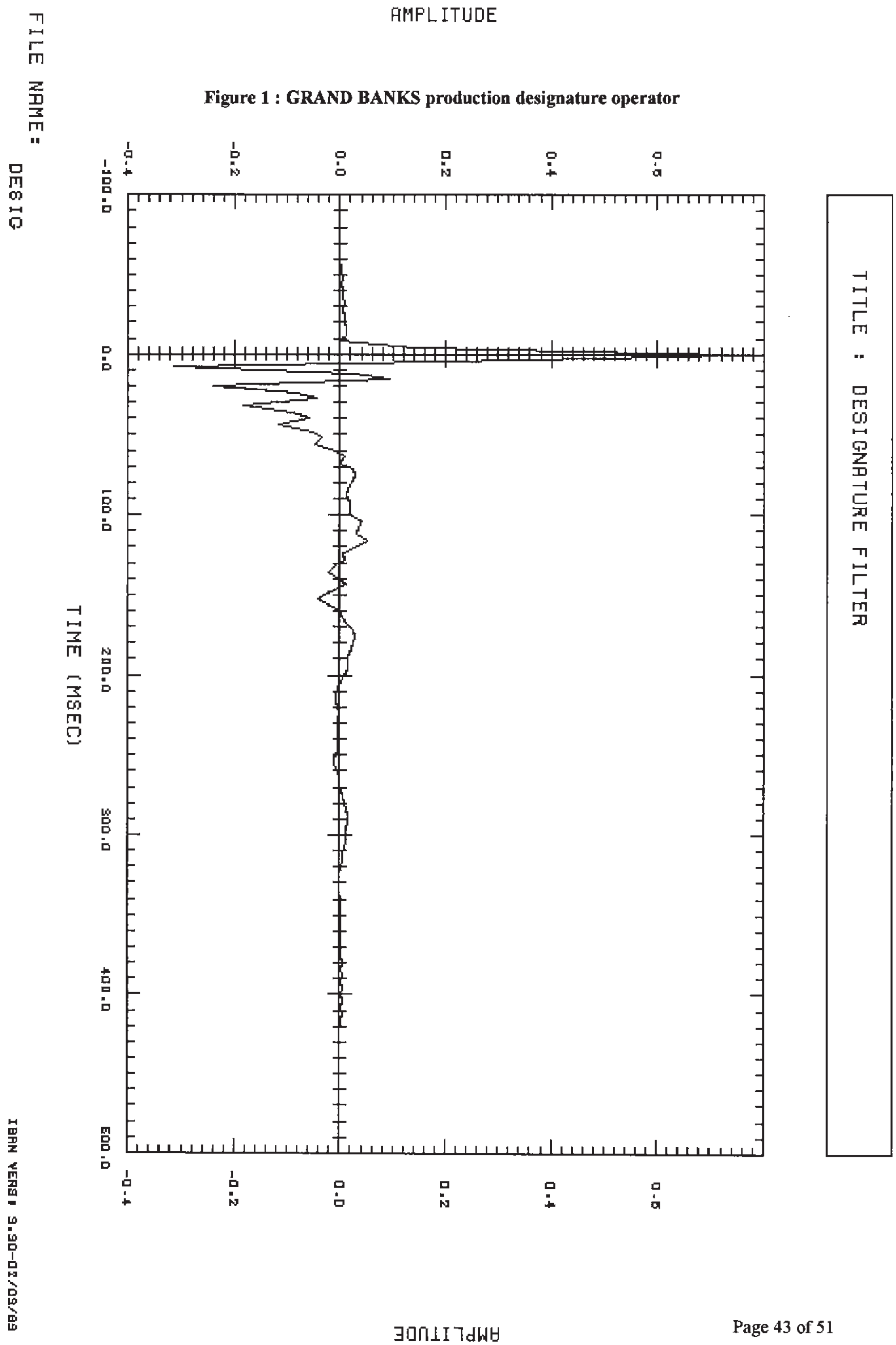

Figure 1 : GRAND BANKS production designature operator

Figure 2 : GRAND BANKS conditioned gun signature

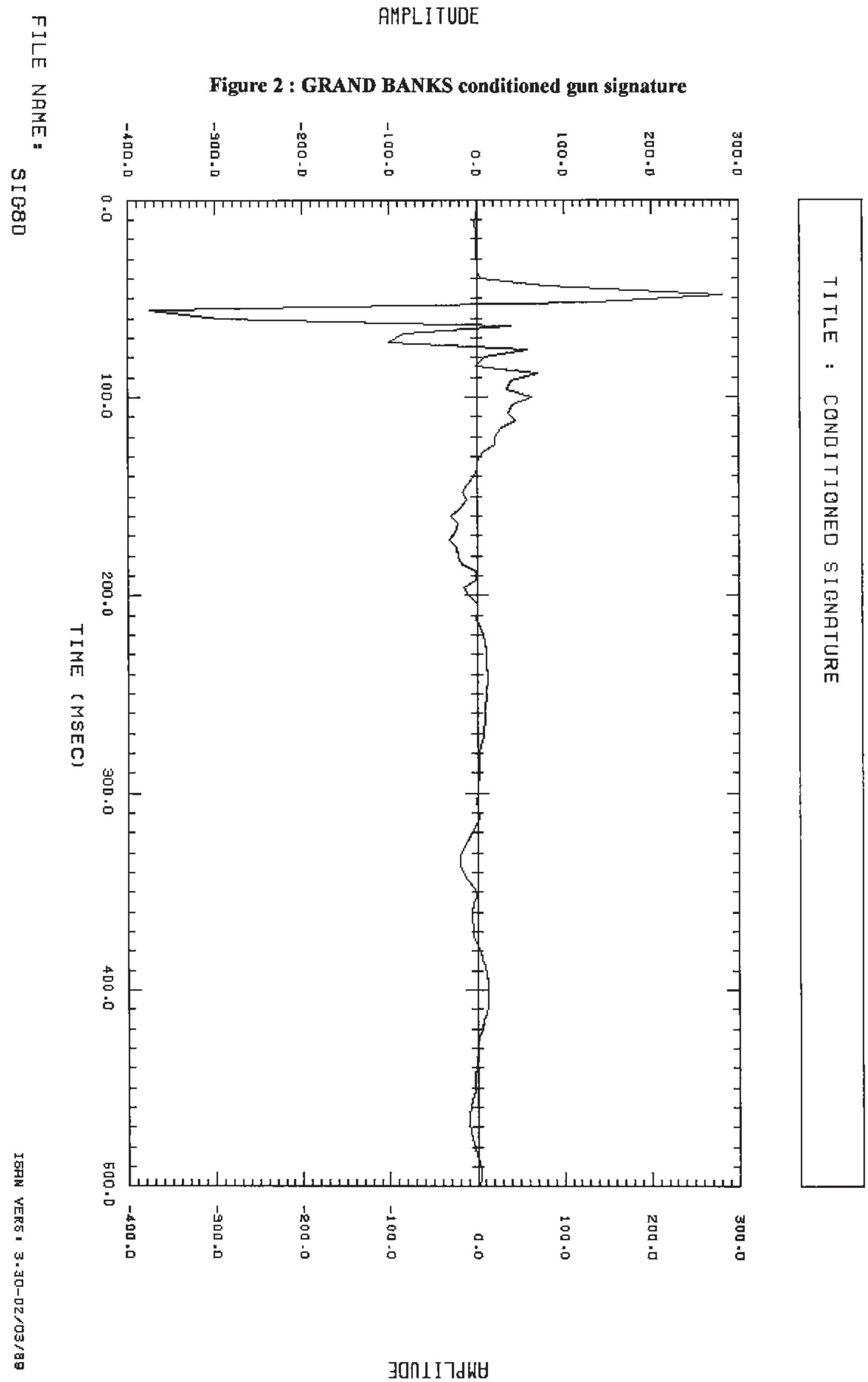

Figure 3 : K-Filter Stack Timeslice 2.0 sec

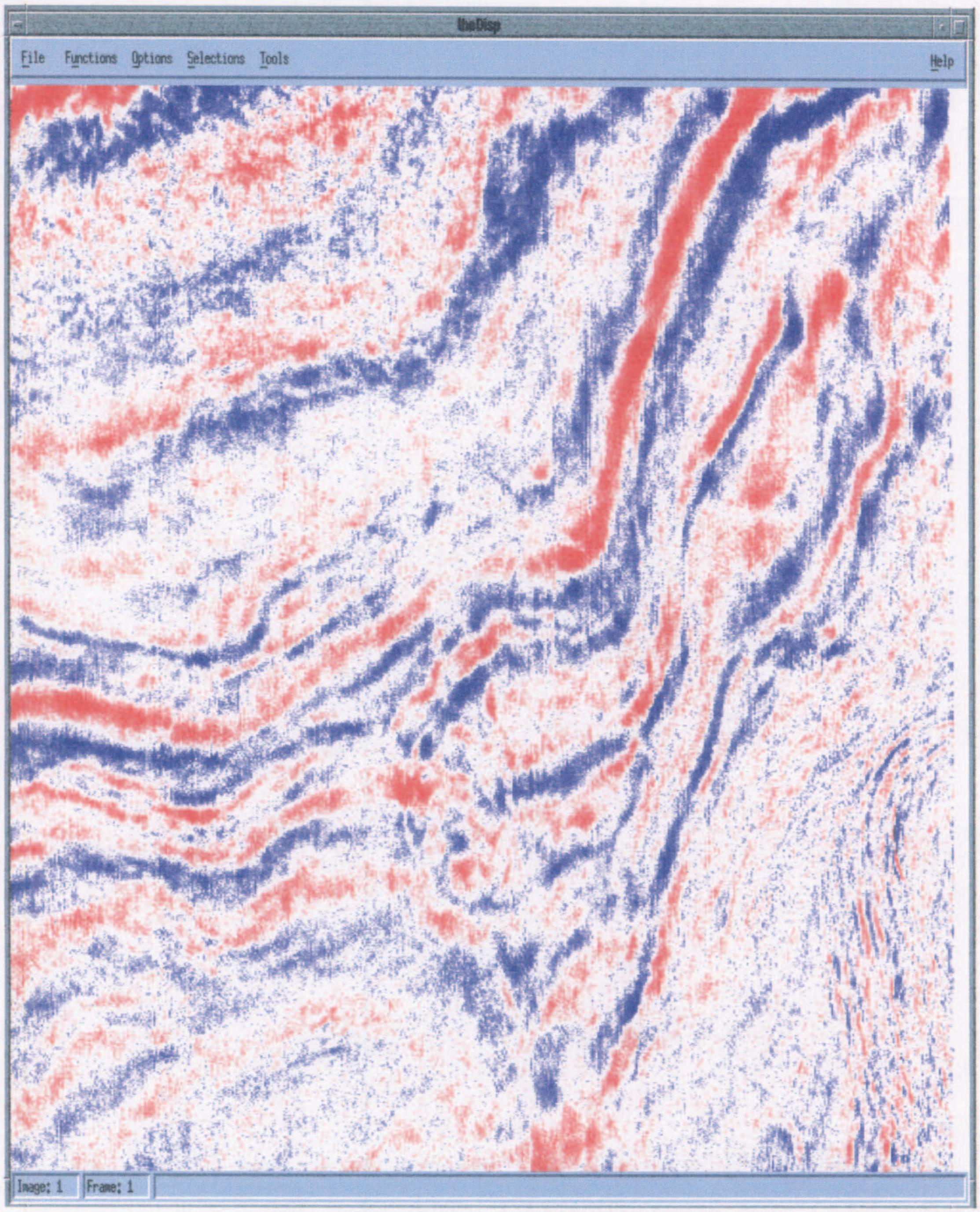

Figure 4 : 3D FXYFILT Stack Timeslice 2.0 sec

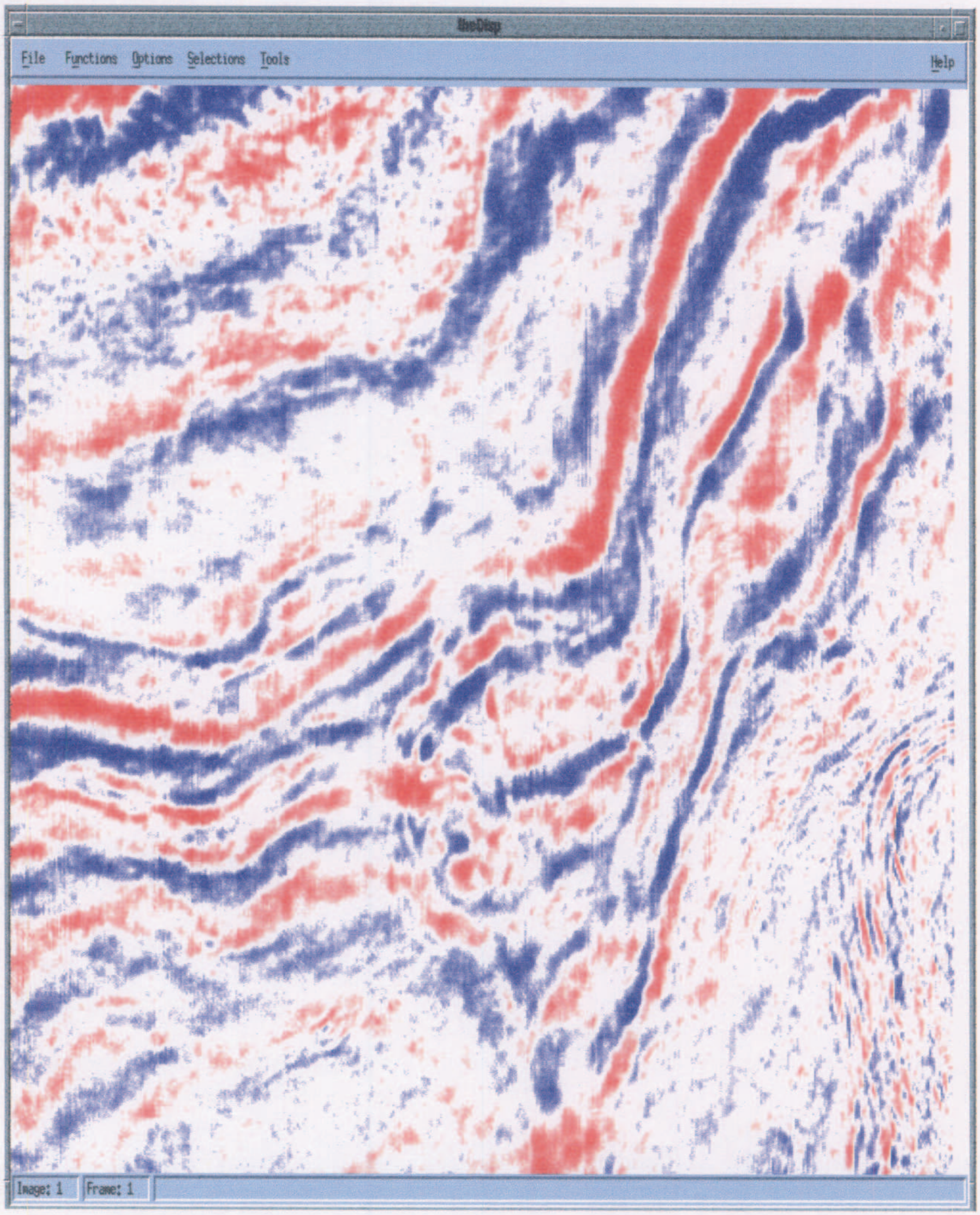

Figure 5 : Quick Look Cube Migration Timeslice 2.0 sec

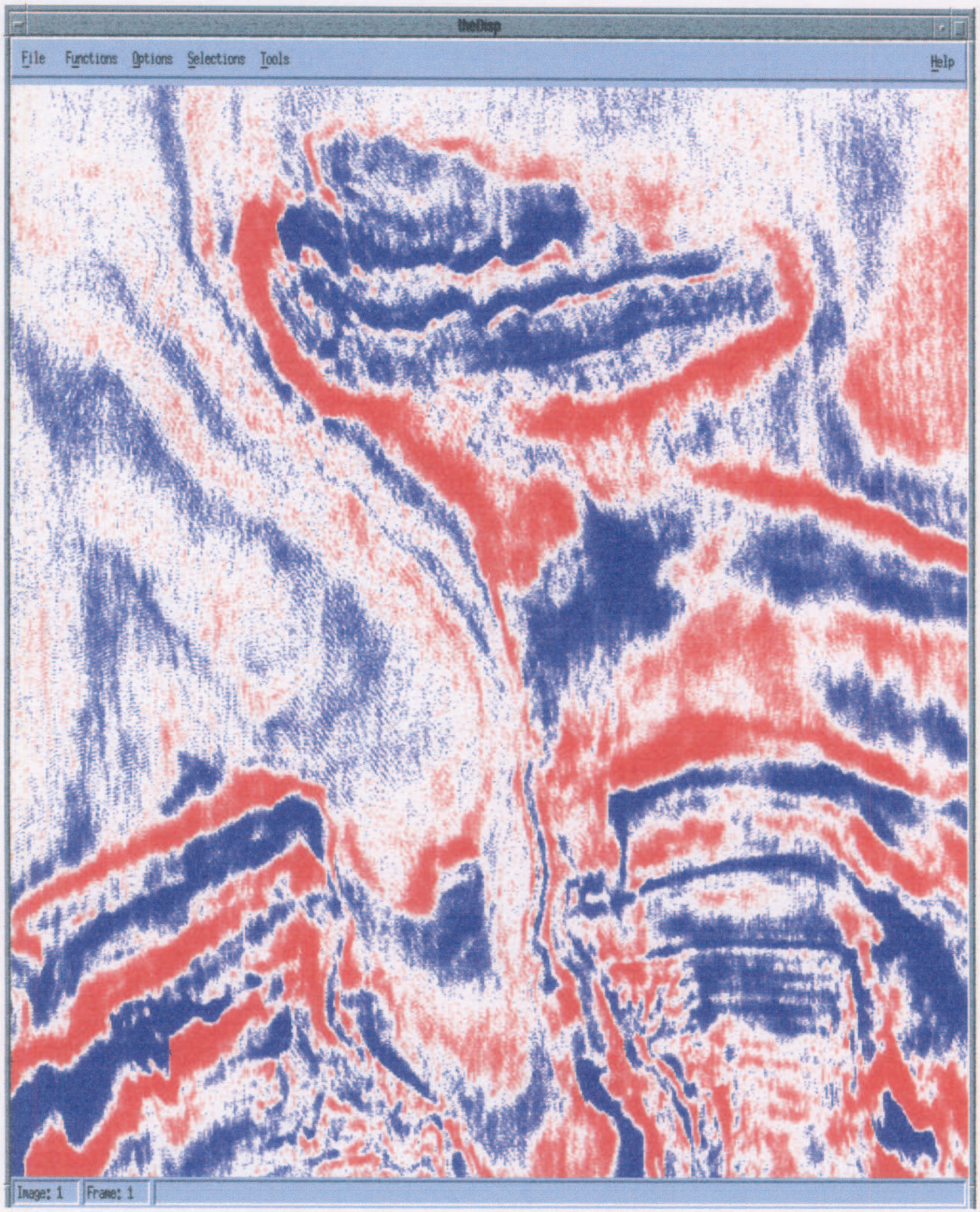

Figure 6 : Final Migration Timeslice 2.0 sec

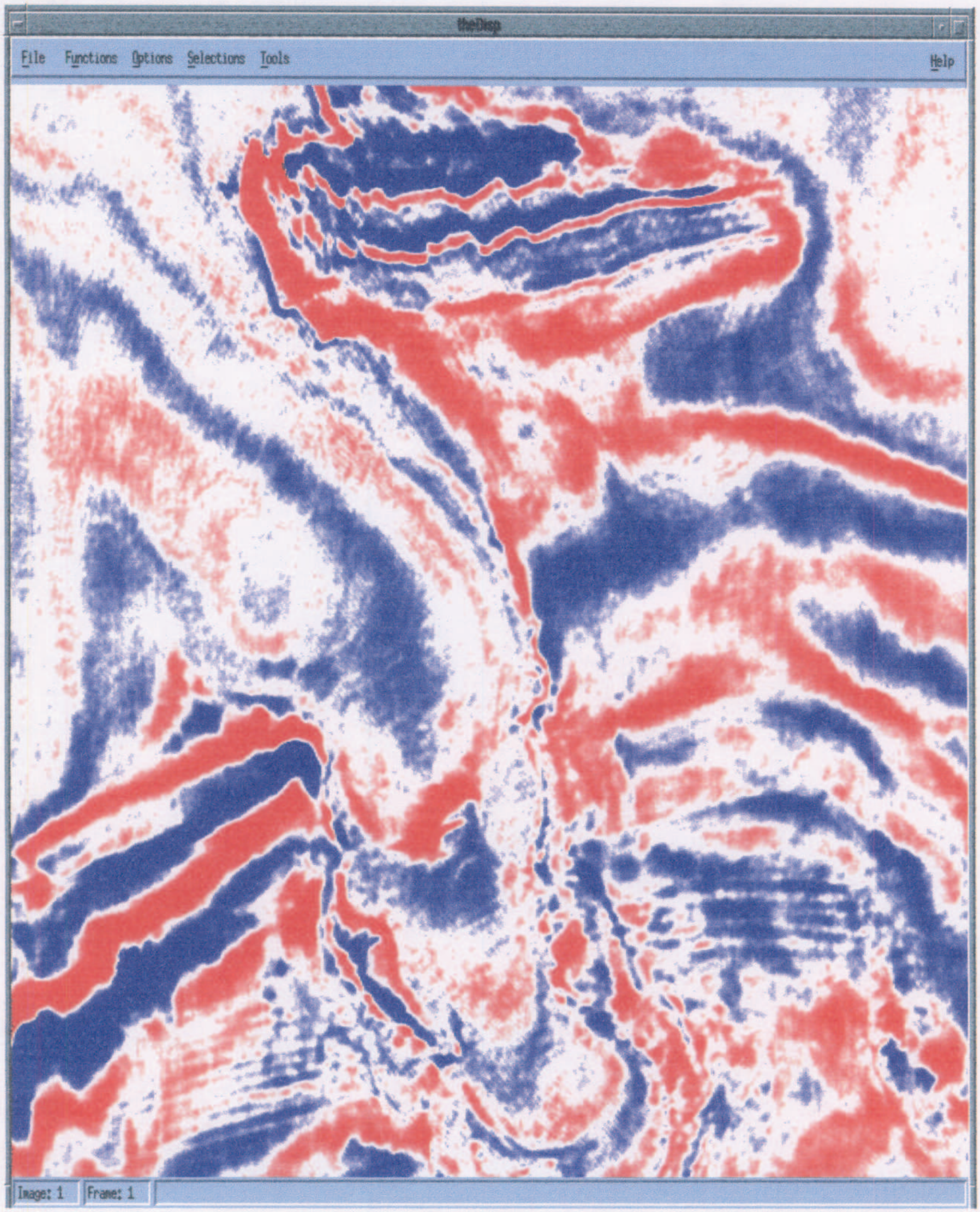

13. Appendix

13.1 Average Amplitude Report

```
after  10 traces. mn/av/mx -2.9757  0.24983   5.1008 samp 1: 1501
after  20 traces. mn/av/mx -2.9757  0.26086   5.6896 samp 1: 1501
after  30 traces. mn/av/mx -3.5370  0.27447   5.8874 samp 1: 1501
after  40 traces. mn/av/mx -3.8205  0.28321   5.8874 samp 1: 1501
after  50 traces. mn/av/mx -3.8205  0.28813   5.8874 samp 1: 1501
                        cdp   51
after  60 traces. mn/av/mx -3.8205  0.29130   5.8874 samp 1: 1501
after  70 traces. mn/av/mx -3.8205  0.29214   5.8874 samp 1: 1501
after  80 traces. mn/av/mx -3.8205  0.29232   5.8874 samp 1: 1501
after  90 traces. mn/av/mx -3.8205  0.29432   5.8874 samp 1: 1501
after 100 traces. mn/av/mx -3.8205  0.29570   5.8874 samp 1: 1501
                        cdp  101
after 110 traces. mn/av/mx -3.8205  0.29648   5.8874 samp 1: 1501
after 120 traces. mn/av/mx -3.8205  0.30070   5.8874 samp 1: 1501
after 130 traces. mn/av/mx -3.8205  0.30416   5.8874 samp 1: 1501
after 140 traces. mn/av/mx -3.8205  0.30628   5.8874 samp 1: 1501
after 150 traces. mn/av/mx -3.8205  0.30971   5.8874 samp 1: 1501
                        cdp  151
after 160 traces. mn/av/mx -3.8205  0.31184   5.8874 samp 1: 1501
after 170 traces. mn/av/mx -3.8205  0.31369   5.8874 samp 1: 1501
after 180 traces. mn/av/mx -3.8205  0.31572   6.5053 samp 1: 1501
after 190 traces. mn/av/mx -3.8205  0.31695   6.5053 samp 1: 1501
after 200 traces. mn/av/mx -3.8205  0.31682   6.5053 samp 1: 1501
                        cdp  201
after 210 traces. mn/av/mx -3.8205  0.31812   6.5053 samp 1: 1501
after 220 traces. mn/av/mx -3.8205  0.31883   6.5053 samp 1: 1501
after 230 traces. mn/av/mx -3.8205  0.31920   6.5053 samp 1: 1501
after 240 traces. mn/av/mx -3.8205  0.32017   6.5053 samp 1: 1501
after 250 traces. mn/av/mx -4.2455  0.32153   6.5053 samp 1: 1501
                        cdp  251
after 260 traces. mn/av/mx -4.4773  0.32264   6.5053 samp 1: 1501
after 270 traces. mn/av/mx -4.4773  0.32424   6.5053 samp 1: 1501
after 280 traces. mn/av/mx -4.4773  0.32576   6.5053 samp 1: 1501
after 290 traces. mn/av/mx -4.4773  0.32604   6.5053 samp 1: 1501
after 300 traces. mn/av/mx -4.4773  0.32712   6.5053 samp 1: 1501
                        cdp  301
after 310 traces. mn/av/mx -4.4773  0.32850   6.5053 samp 1: 1501
after 320 traces. mn/av/mx -4.4773  0.32981   6.5053 samp 1: 1501
after 330 traces. mn/av/mx -4.4773  0.33099   6.5053 samp 1: 1501
after 340 traces. mn/av/mx -4.4773  0.33178   6.5053 samp 1: 1501
after 350 traces. mn/av/mx -4.4773  0.33398   6.5053 samp 1: 1501
                        cdp  351
after 360 traces. mn/av/mx -4.5997  0.33540   6.5053 samp 1: 1501
after 370 traces. mn/av/mx -4.5997  0.33567   6.5053 samp 1: 1501
after 380 traces. mn/av/mx -5.7632  0.33632   6.5053 samp 1: 1501
after 390 traces. mn/av/mx -5.7707  0.33718   6.5053 samp 1: 1501
after 400 traces. mn/av/mx -5.7707  0.33747   6.5053 samp 1: 1501
                        cdp  401
```

```
after 410 traces. mn/av/mx -5.7707  0.33797  6.5053 samp 1: 1501
after 420 traces. mn/av/mx -5.7707  0.33795  6.5053 samp 1: 1501
after 430 traces. mn/av/mx -5.7707  0.33767  6.5053 samp 1: 1501
after 440 traces. mn/av/mx -5.7707  0.33741  6.5053 samp 1: 1501
after 450 traces. mn/av/mx -5.7707  0.33730  6.5053 samp 1: 1501
                         cdp 451
after 460 traces. mn/av/mx -5.7707  0.33782  6.5053 samp 1: 1501
after 470 traces. mn/av/mx -5.7707  0.33875  6.5053 samp 1: 1501
after 480 traces. mn/av/mx -5.7707  0.33930  6.5053 samp 1: 1501
after 490 traces. mn/av/mx -5.7707  0.33936  6.5053 samp 1: 1501
after 500 traces. mn/av/mx -5.7707  0.33927  6.5053 samp 1: 1501
                         cdp 501
after 510 traces. mn/av/mx -5.7707  0.33911  6.5053 samp 1: 1501
after 520 traces. mn/av/mx -5.7707  0.33853  6.5053 samp 1: 1501
after 530 traces. mn/av/mx -5.7707  0.33766  6.5053 samp 1: 1501
after 540 traces. mn/av/mx -5.7707  0.33762  6.5053 samp 1: 1501
after 550 traces. mn/av/mx -5.7707  0.33778  6.5053 samp 1: 1501
                         cdp 551
after 560 traces. mn/av/mx -5.7707  0.33742  6.5053 samp 1: 1501
after 570 traces. mn/av/mx -5.7707  0.33710  6.5053 samp 1: 1501
after 580 traces. mn/av/mx -5.7707  0.33672  6.5053 samp 1: 1501
after 590 traces. mn/av/mx -5.7707  0.33622  6.5053 samp 1: 1501
after 600 traces. mn/av/mx -5.7707  0.33583  6.5053 samp 1: 1501
                         cdp 601
after 610 traces. mn/av/mx -5.7707  0.33600  6.5053 samp 1: 1501
after 620 traces. mn/av/mx -5.7707  0.33583  6.5053 samp 1: 1501
after 630 traces. mn/av/mx -5.7707  0.33555  6.5053 samp 1: 1501
after 640 traces. mn/av/mx -5.7707  0.33525  6.5053 samp 1: 1501
after 650 traces. mn/av/mx -5.7707  0.33538  6.5053 samp 1: 1501
                         cdp 651
after 660 traces. mn/av/mx -5.7707  0.33537  6.5053 samp 1: 1501
after 670 traces. mn/av/mx -5.7707  0.33523  6.5053 samp 1: 1501
after 680 traces. mn/av/mx -5.7707  0.33487  6.5053 samp 1: 1501
after 690 traces. mn/av/mx -5.7707  0.33463  6.5053 samp 1: 1501
after 700 traces. mn/av/mx -5.7707  0.33426  6.5053 samp 1: 1501
                         cdp 701
after 710 traces. mn/av/mx -5.7707  0.33394  6.5053 samp 1: 1501
after 720 traces. mn/av/mx -5.7707  0.33353  6.5053 samp 1: 1501
after 730 traces. mn/av/mx -5.7707  0.33315  6.5053 samp 1: 1501
after 740 traces. mn/av/mx -5.7707  0.33284  6.5053 samp 1: 1501
after 750 traces. mn/av/mx -5.7707  0.33280  6.5053 samp 1: 1501
                         cdp 751
after 760 traces. mn/av/mx -5.7707  0.33277  6.5053 samp 1: 1501
after 770 traces. mn/av/mx -5.7707  0.33304  6.5053 samp 1: 1501
after 780 traces. mn/av/mx -5.7707  0.33307  6.5053 samp 1: 1501
after 790 traces. mn/av/mx -5.7707  0.33335  6.5053 samp 1: 1501
after 800 traces. mn/av/mx -5.7707  0.33374  6.5053 samp 1: 1501
                         cdp 801
after 810 traces. mn/av/mx -5.7707  0.33397  6.5053 samp 1: 1501
after 820 traces. mn/av/mx -5.7707  0.33403  6.5053 samp 1: 1501
after 830 traces. mn/av/mx -5.7707  0.33422  6.5053 samp 1: 1501
after 840 traces. mn/av/mx -5.7707  0.33427  6.5053 samp 1: 1501
after 850 traces. mn/av/mx -5.7707  0.33418  6.5053 samp 1: 1501
                         cdp 851
```

```
after  860 traces. mn/av/mx -5.7707   0.33428   6.5053  samp  1: 1501
after  870 traces. mn/av/mx -5.7707   0.33446   6.5053  samp  1: 1501
after  880 traces. mn/av/mx -5.7707   0.33474   6.5053  samp  1: 1501
after  890 traces. mn/av/mx -5.7707   0.33478   6.5053  samp  1: 1501
after  900 traces. mn/av/mx -5.7707   0.33467   6.5053  samp  1: 1501
                             cdp  901
after  910 traces. mn/av/mx -5.7707   0.33460   6.5053  samp  1: 1501
after  920 traces. mn/av/mx -5.7707   0.33458   6.5053  samp  1: 1501
after  930 traces. mn/av/mx -5.7707   0.33454   6.5053  samp  1: 1501
after  940 traces. mn/av/mx -5.7707   0.33467   6.5053  samp  1: 1501
after  950 traces. mn/av/mx -5.7707   0.33474   6.5053  samp  1: 1501
                             cdp  951
after  960 traces. mn/av/mx -5.7707   0.33498   6.5053  samp  1: 1501
after  970 traces. mn/av/mx -5.7707   0.33529   6.5053  samp  1: 1501
after  980 traces. mn/av/mx -5.7707   0.33540   6.5053  samp  1: 1501
after  990 traces. mn/av/mx -5.7707   0.33574   6.5053  samp  1: 1501
after 1000 traces. mn/av/mx -5.7707   0.33608   6.5053  samp  1: 1501
```

after a total of 1000 traces with live data between samples 1 and 1501 **avg = 0.3360797**

-

APPENDIX 2

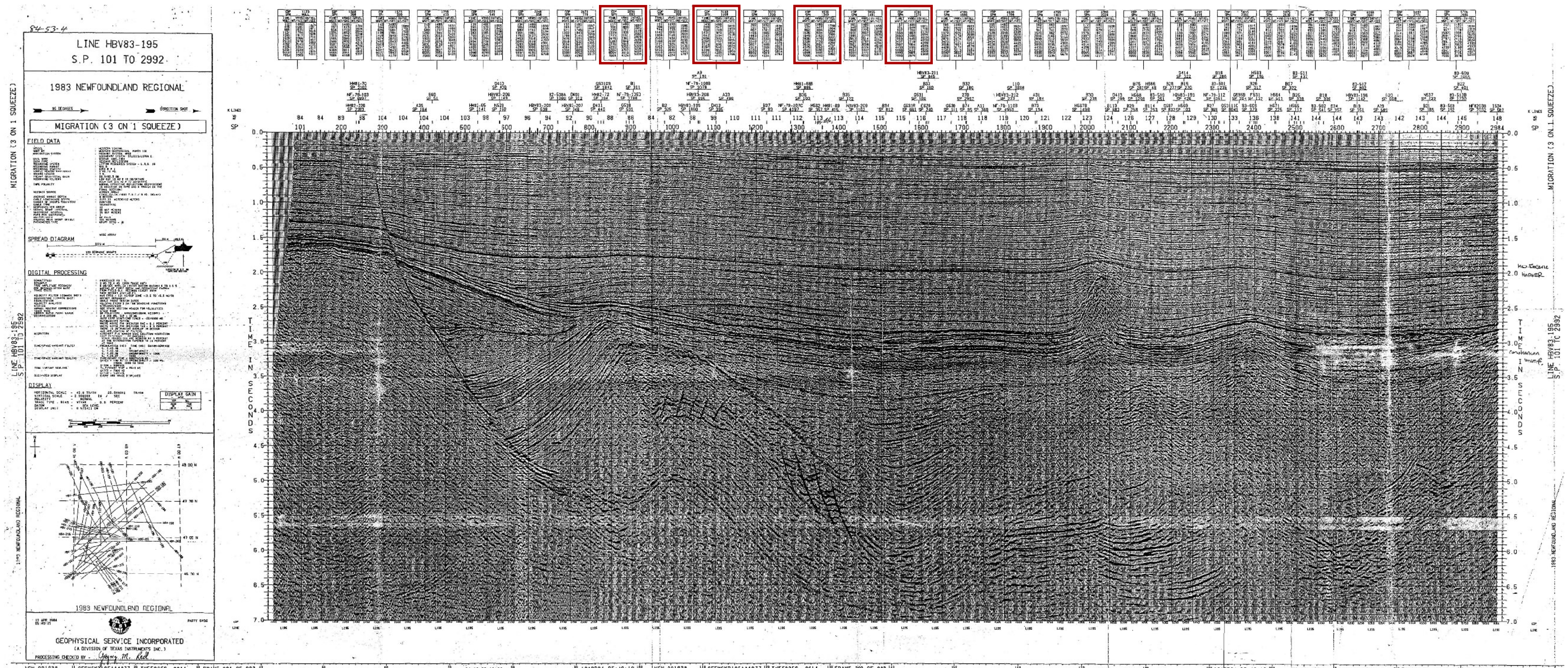

2D seismic line HBV83-195. Red rectangles highlight velocity survey selected by Serrano Suarez (2013) to calculate the average velocity of the sedimentary section (appendix 3).

APPENDIX 3

Root mean square velocities (V_{RMS}) from some velocity surveys from line HBV83-195 used to calculate the average velocity of the sedimentary section.

Velocity survey	Time (ms)	V_{RMS} (m/s)
CDP 2698	6005	3910
CDP 3148	6012	4289
CDP 3630	5998	3899
CDP 4080	5999	3689
	Average	3946 (~4.0 km/s)

CDP: 2698		
Time (ms)	V_{RMS} (m/s)	Vint (m/s)
117	1480	1687
300	1609	1885
735	1777	2118
1319	1935	2682
1773	2151	2823
2476	2361	3489
3166	2648	4004
3776	2910	5320
4222	3250	5236
5204	3707	5034
6005	3910	5233
7000	4124	

CDP: 3148		
Time (ms)	V_{RMS} (m/s)	Vint (m/s)
143	1480	1606
299	1547	1859
802	1749	2221
1431	1970	2516
1842	2104	2977
2606	2393	3895
3252	2757	4854
3714	3096	5623
4297	3546	5217
5126	3955	5859
6012	4289	5796
7000	4532	

CDP: 3630		
Time (ms)	V_{RMS} (m/s)	Vint (m/s)
167	1480	1730
327	1607	1916
862	1805	2298
1526	2034	2580
1940	2162	3032
2836	2470	3948
3328	2739	4293
3874	3007	4737
4375	3252	4959
4941	3490	5416
5998	3899	5882
7000	4240	

CDP: 4080		
Time (ms)	V_{RMS} (m/s)	Vint (m/s)
157	1480	1601
351	1548	1796
907	1704	2132
1550	1893	2694
2000	2100	3039
2963	2445	4030
3437	2719	4299
3907	2954	4593
4439	3195	4632
5088	3412	4960
5999	3689	5380
7000	3975	

(Serrano Suarez, 2013)

APPENDIX 4

List of formation tops from available wells. Depths are in meters and measured depths. From the BASIN database website (http://basin.gdr.nrcan.gc.ca/wells/index_e.php) (2012)

Well Flying Foam I-13

Year	Author	Depth Type	Top	Bottom	Units	Formation
2007	CNLOPB	MD		2115.5	M	BANQUEREAU FM
2007			744	768	M	(OLIGOCENE SANDSTONE - UPPER)
2007			940.5	948	M	(OLIGOCENE SANDSTONE - LOWER)
2007			2115.5	2115.5	M	(BASE TERTIARY UNCONFORMITY)
2007			2115.5	2487	M	WHITEROSE FM
2007			2115.5	2467	M	CATALINA
2007			2467	2487	M	"B" MARKER MB
2007			2487	3114	M	HIBERNIA FM
2007			2487	2847	M	SHALE EQUIV OF HIBERNIA UPPER ZONE
2007			2847	3114	M	HIBERNIA LOWER ZONE
2007			3114	3268	M	FORTUNE BAY FM
2007			3268	3268	M	(TITHONIAN UNCONFORMITY)
2007			3268	3683.2	M	RANKIN FM
2007			3281	3353	M	EGRET MB
2007			3592.5	3683.2	M	PORT AU PORT MB
1989	MCALPINE,K.D.			2116	M	BANQUEREAU FM
1989			2116	2116	M	(UNCONFORMITY)
1989			2116	2467	M	CATALINA FM
1989			2467	2487	M	("B" MARKER)
1989			2487	2847	M	WHITEROSE SHALE (LOWER)
1989			2847	3114	M	HIBERNIA FM
1989			3114	3194	M	FORTUNE BAY SHALE
1989			3194	3269	M	JEANNE D'ARC FM
1989			3269	3269	M	(UNCONFORMITY)
1989			3269	3683	M	RANKIN FM
1989			3281	3353	M	EGRET MB
1987	WADE,J.A. & SHERWIN,D.F.				FT	BANQUEREAU FM
1987			6941	6941		(AVALON UNCONFORMITY)
1987			6941	8170		MISSISAUGA EQUIV
1987			8170	10488		VERRILL CANYON FM ?
1987			10488	12084		ABENAKI/MIC MAC ?
1985	MCALPINE,K.D.					(SEE UPDATED REPORT)
1980	WADE,J.A.					(SEE MCALPINE REPORT)

Well West Flying Foam L-23

Year	Author	Depth Type	Top	Bottom	Units	Formation
2007	CNLOPB	MD		2496	M	BANQUEREAU FM
2007			755	780	M	(OLIGOCENE SANDSTONE - UPPER)
2007			962	968	M	(OLIGOCENE SANDSTONE - LOWER)
2007			2464	2496	M	SOUTH MARA MB
2007			2483	2490	M	(LIMESTONE)
2007			2496	2496	M	(BASE TERTIARY UNCONFORMITY)
2007			2496	3430	M	NAUTILUS FM
2007			3430	3471	M	BEN NEVIS FM
2007			3471	3471	M	(APTIAN UNCONFORMITY)
2007			3471	3580	M	AVALON FM
2007			3493	3564	M	(SHALE TONGUE)
2007			3564	3580	M	"A" MARKER MB
2007			3580	3760	M	WHITEROSE FM
2007			3760	4292	M	CATALINA FM
2007			4167	4292	M	"B" MARKER MB
2007			4292	4553.8	M	HIBERNIA FM
2007			4292	4553.8	M	SHALE EQUIV OF HIBERNIA UPPER ZONE
1989	MCALPINE,K.D.			2496	M	BANQUEREAU FM
1989			2407	2407	M	(UNCONFORMITY)
1989			2407	2496	M	SOUTH MARA UNIT
1989			2496	2496	M	(UNCONFORMITY)
1989			2496	2516	M	DAWSON CANYON FM
1989			2516	3090	M	NAUTILUS SHALE
1989			2570	2570	M	(UNCONFORMITY)
1989			3090	3090	M	
1989			3090	3189	M	AVALON FM
1989			3189	3189	M	(UNCONFORMITY)
1989			3189	3760	M	WHITEROSE SHALE
1989			3760	4554	M	CATALINA FM
1987	WADE,J.A. & SHERWIN,D.F.		2293		M	(UPPER CRETACEOUS "K" MARKER)
1987			2483		M	(PETREL LIMESTONE MARKER)
1987			2517	2517	M	(MIDDLE CRETACEOUS UNCONFORMITY)
1985	MCALPINE,K.D.					(SEE UPDATED REPORT)
1982	MOBIL OIL CANADA LTD		2292.8		M	("K" MARKER)
1982			2482.8		M	(PETREL LIMESTONE "P" MARKER)
1982			2516.8		M	(UNCONFORMITY)
1982			2746.8		M	